Fall 12-16-2016

Bone Loss Quantification Following Extraction in Rats: A Foundation for Grafting and Regenerative Studies

Emily Willett
University of Nebraska Medical Center

BONE LOSS QUANTIFICATION FOLLOWING EXTRACTION IN RATS:

A FOUNDATION FOR GRAFTING AND REGENERATIVE STUDIES

by

Emily S. Willett, D.D.S.

A THESIS

Presented to the Faculty of

the University of Nebraska Graduate College

in Partial Fulfillment of the Requirements

for the Degree of Master of Science

Medical Sciences Interdepartmental Area Graduate Program
(Oral Biology)

Under the Supervision of Professor Richard A. Reinhardt

University of Nebraska Medical Center
Omaha, Nebraska

August, 2016

Advisory Committee

Peter J. Giannini, D.D.S., M.S.

J. Bruce Bavitz, D.M.D.

Ali Nawshad, Ph. D.

Sundaralingam Premaraj, M.S., Ph.D.

ACKNOLWEDGEMENTS

I would like to express my immense gratitude to my committee chair and thesis advisor, Dr. Richard Reinhardt, who is one of the finest educators with whom I have had the honor of working. I am so appreciative for your patience, expertise, and encouragement. I consider it a true privilege to have learned from you and I am thankful to join the ranks of numerous other students who have benefitted from the evidence of your commitment to dental education and dental research.

Thank you to the members of my committee, Drs. S. Prem Premaraj, Ali Nawshad, Peter J. Giannini, and J. Bruce Bavitz, who have kindly given of their time and talents in the pursuit of this thesis.

I am also thankful to Mrs. Marian Schmid and Jingpeng Liu for their assistance and time in managing the specimens, performing the surgical procedures, and providing instruction during data collection; it was greatly appreciated.

To Dr. Dong Wang and Xiobei Wang, thank you for your drug-graft conjugate preparation and assistance with the protocol for μCT imaging.

Thank you also to the members of the UNMC Regenerative Medicine Group for their support, intellectual contributions, and funding.

I would also like to acknowledge Dr. Fang Yu and Kaeli Samson for their expertise in preparing the statistical analyses for this study.

The time and expertise of Kim Theesen is greatly appreciated in the preparation of the graphs and figures used in this paper.

I owe special thanks to my family for their encouragement and I owe my deepest gratitude to my husband, Ryan, for his constant support through all of my pursuits. I appreciate the hours on evenings and during weekends you spent with me and supporting me while I was collecting and analyzing data, and I want you to know your love and encouragement made it possible for me to accomplish my goals. Our shared faith in God has been the most important influence in my life and in this academic pursuit and I want to give Him the credit and thanks for this achievement.

BONE LOSS QUANTIFICATION FOLLOWING EXTRACTION IN RATS:

A FOUNDATION FOR GRAFTING AND REGENERATIVE STUDIES

Emily S. Willett, D.D.S., M.S.

University of Nebraska Medical Center, 2016

Advisor: Richard A. Reinhardt, D.D.S., Ph. D.

Background: Loss of the alveolar ridge width and height following extraction is well-documented and several techniques, including grafting, have been proposed to reduce bone loss. **Purpose**: To characterize the pattern of bone turnover and inflammation after extraction and to initiate a study of the effect of grafting and local administration of simvastatin (SIM). **Methods**: Thirty-two retired-breeder rats underwent extraction of the right maxillary first molar and standard surgical defect creation under inhalation anesthesia. The left side of each animal served as the unmanipulated control. Comparison of groups (n=8, ANOVA) was done at days 0, 7, 14, and 28 for alveolar bone height and width and for markers of inflammation and bone turnover by micro-computed tomography (μCT) and histology/ELISA. Seventeen additional specimens had the defects grafted with either bone mineral matrix (BMM) or a BMM+SIM conjugate. **Results**: μCT and histologic analysis demonstrated extraction-induced bone loss is most evident on the palatal ($p < 0.001$) and interproximal ($p < 0.05$) aspects of the socket. After the first week, a more intense inflammatory reaction corresponded to a reduction in alveolar bone height in the interproximal areas and alveolar bone height and width on the palatal aspect ($p < 0.05$). Increased numbers of osteoblasts were evident at the periphery of the socket at later time periods, particularly in the grafted specimens. BMM+SIM also reduced inflammation at 28 days ($p < 0.001$) and enhanced ridge width ($p < 0.001$). **Conclusions**: The standard defect used in the current study paralleled human post-extraction alveolar bone loss and defect grafting partially preserved bone.

TABLE OF CONTENTS

LIST OF TABLES

LIST OF FIGURES

LIST OF ABBREVIATIONS

µCT	micro-computed tomography
UNMC	University of Nebraska Medical Center
IACUC	Institutional Animal Care and Use Committee
CEJ	cementoenamel junction
ABC	alveolar bone crest
M1	maxillary first molar
M2	maxillary second molar
M3	maxillary third molar
BMM	bone mineral matrix
SIM	simvastatin
g	gram
PPi	inorganic pyrophosphate
ml	milliliter
mg	milligram
rpm	revolutions per minute
UV	ultraviolet
nm	nanometer
DFDBA	demineralized freeze-dried bone allografts
PG	prostaglandin
PGE_2	prostaglandin E2
LPS	lipopolysaccharide
PLGA	polylactic glycolic acid
NSAID	nonsteroidal anti-inflammatory drug

DXA	dual-energy X-ray absorptiometry
ROI	region of interest
BMD	bone mineral density
BV	bone volume
TV	trabecular volume
BS	bone surface
BSD	bone surface density
H&E	hematoxylin and eosin
ANOVA	analysis of variance
ICC	intra-class correlation coefficient
CI	confidence interval
SD	standard deviation
SE	standard error
SEM	scanning electron microscopy

INTRODUCTION

The field of dentistry has historically been concerned with the lasting effects of tooth loss, and increasingly so considering advancements in surgical and non-surgical procedures to replace the missing structures. Extraction of teeth routinely involves creation of a bony defect and associated bony and soft tissue changes. Alveolar bone is a tooth-dependent structure and extraction of teeth results in compensatory fill of the extraction site as well as a well-documented dimensional change of the alveolar ridge in width and height (Van der Weijden et al. 2009). After tooth extraction, there is a progressive and substantial reduction in the height and width of the bone in the immediate area of the extraction socket (Sun et al. 2013; Sadeghi et al. 2016). All of this occurs in an environment laden with bacteria capable of inducing variable amounts of inflammation. Many fields of dentistry are heavily invested in the field of research to preserve and enhance the alveolar bone and associated periodontal structures.

Tooth extraction is a frequent occurrence and consistently leads to conformational and bone quality changes in the tooth socket and surrounding alveolar bone (Van der Weijden et al. 2009). Specialists and general dentists alike are faced with the challenges that alveolar defects present in achieving a stable and esthetic result following compensatory tooth movement or prosthetic replacement. While post-extraction changes in alveolar bone are well described, cost-effective models to dissect the impact of inflammation and grafting or pharmacological interventions are lacking. Understanding the healing process of bony contour changes and molecular and cellular responses of extraction sites will better enable clinicians to predict and modify the biologic response during healing. Refining a model to better define the role of inflammation on the process of healing following extractions will strengthen the foundation of knowledge and will provide a basis for future studies of modifications of the process using pharmacologic interventions.

The current study was designed to evaluate alveolar bone dimensions and bone quality changes after extraction in rats both with and without post-extraction grafting procedures. There were two parts to the current study. Part I involved extraction of a maxillary right molar and creation of a standard-sized defect, then prospective evaluation of the healing pattern over a four week period. Part 2 involved extraction of the maxillary right molar and a subsequent grafting of the site using the bovine non-antigenic, porous bone mineral matrix (BMM) (BioOss®, Geistlich Pharma North America, Inc.) both alone, and infused with simvastatin. Grafting was done with the benefit of filling the defect and providing a scaffold for eventual bone fill with the proven effect of decreasing the loss of the alveolar ridge following extraction (Wood & Mealey 2012). The local administration of simvastatin has the effect of stimulating local bone formation (Thylin et al. 2002; Stein et al. 2005). The hypotheses were that analysis by micro-computed tomography (μCT) would demonstrate a significant reduction in alveolar bone dimensions and volume following extraction, and that analysis by histological sections and ELISA would indicate a concurrent inflammatory process correlated with loss of alveolar bone. In a proof-of-principal study, the hypothesis was that addition of mineral matrix to the socket will preserve alveolar bone and serve as a method to test future grafting compounds and pharmacological interventions.

LITERATURE REVIEW

Tooth Extraction

Many studies have been conducted concerning extraction healing and various pharmaceutical and chemical applications to modulate the bone and soft tissue response (Araujo & Lindhe 2005; Tan et al. 2012; Tomlin et al. 2014). Extractions are among the most routine dental procedures (Van der Weijden et al. 2009; Tan et al. 2012) and are commonly prescribed in a variety of clinical scenarios like fracture, non-restorable decay, failed root canal treatments, and advanced periodontitis. Many fields of dentistry are heavily invested in the field of research to preserve and enhance the alveolar bone and associated periodontal structures. Millions of teeth are extracted annually, and most without regard for alveolar ridge maintenance (Moya-Villaescusa & Sanchez-Perez 2010). Alveolar bone is a tooth-dependent structure and its shape and volume are determined by dental influences like morphology of the teeth and tooth position upon eruption (Araujo & Lindhe 2005; Avila-Ortiz et al. 2014). It has been well-documented that with the removal of teeth, the adjacent alveolar bone undergoes significant atrophy. There are significant dimensional changes that occur in the early phases of healing, particularly in the first three months (Ashman 2000; Schropp & Isidor 2008; Tomlin et al. 2014). Bone loss of alveolar ridges after extraction complicate the treatment options following extraction. It is essential to have sufficient alveolar bone volume and adequate tissue contours for a functional and esthetic restoration (Avila-Ortiz et al. 2014; Tomlin et al. 2014). Appropriate pre-extraction and pre-prosthetic planning is essential to maintain the alveolar ridge to an adequate degree for replacement of the tooth by implant or other prosthetic intervention (Seibert & Salama 1996). Grafting of the extraction site immediately following the removal of the tooth has been proven in humans to reduce the amount of bone loss in the area as compared to ungrafted control sites (Araujo & Lindhe 2005; Nevins et al. 2006).

Normal Healing Response/Alveolar Bone Changes

The removal of a tooth from its alveolar housing triggers a distinctive cascade of anatomical and physiological events that typically result in significant anatomic changes and decreases in the contours of the alveolar bone (Van der Weijden et al. 2009; Kuroshima et al. 2014; Tomlin et al. 2014). After tooth extraction, there is generally a lack of soft tissue to cover the socket and any associated defect, thus the area must heal by secondary intention (Tan et al. 2012). The initial stages of healing are marked by an increase in soft tissue volume by cell proliferation and a soft tissue covering will develop to close off the surgical area (Tan et al. 2012). The process of healing following extraction in humans proceeds in a predictable pattern, involving both cellular and tissues changes (Tomlin et al. 2014). Moya-Villaescusa and Sanchez-Perez (2010) described a process involving the following: immediately post-extraction the socket fills with blood as a result of vessel ruptures from the surrounding periodontal ligament and a severing of the blood supply to the tooth directly. In the first 24 hours, the collection of damaged cells and proteins from the wound initiate a series of cellular events leading to the formation of a fibrin network that traps platelets, establishing a clot. The clot is subsequently replaced within one week with granulation tissue (Pagni et al. 2012). There are additional biological events that characterize the healing of the extraction socket, namely the healing process called “corticalization”, where a bridge of hard tissue will cover the margins of the extraction socket and proliferative and resorptive events will lead to the development of a wall of cortical bone, although with reduced height and width (Moya-Villaescusa & Sanchez-Perez 2010). It has been shown that osteoclasts emerge from the remaining crestal bone to resorb damaged bone, reducing the inflammatory reaction in the socket, which is required to progress through the wound healing process (Kuroshima et al. 2014). Socket healing is characterized by the migration of epithelium over the inflammatory granulation tissue to effectively cover the

wound and protect the clot. The granulation tissue is progressively replaced with connective tissue which becomes the provisional matrix of densely packed mesenchymal cells with fibers, blood vessels and woven bone (Trombelli et al. 2008; Pagni et al. 2012). The immature woven bone is then progressively replaced by lamellar bone and corresponding marrow spaces by progressive mineralization, demonstrating modeling of the extraction socket (Trombelli et al. 2008). The hard and soft tissue changes continue in parallel processes with the changes in the alveolar ridge dimensions as modeling occurs, but remodeling of the socket continues after de novo bone formation in the extraction socket and bony defect areas (Madden & Caton 1994).

The most significant dimensional changes are recognized in the early phase after extraction, with marked osteoclastic activity to resorb the crestal region of the alveolar bone, most notably in the buccal crestal bone (Araujo & Lindhe 2005; Sun et al. 2013). Tan et al. demonstrated a pattern of alveolar bone changes in vertical and horizontal dimensions that are most rapid in the initial six months after extraction, with a gradual reduction thereafter for up to five years. It has been concluded that the alveolar bone around the extraction site is resorbed in two overlapping phases: Phase 1 is marked by the resorption of the bundle bone that has a role in surrounding the teeth and its replacement with woven bone, demonstrated by a marked reduction in crestal height. Phase 2 includes resorption on the outer surfaces of the alveolar process, resulting in a reduction of bone width (Araujo & Lindhe 2005; Pagni et al. 2012). A systematic review of the studies of the alveolar dimensional changes post-extraction found the greatest change in the clinical loss of width (Van der Weijden et al. 2009). Human and animal studies have demonstrated that the buccal plate is resorbed to a greater degree than the palatal or lingual aspects because it is generally thinner (Huynh-Ba et al. 2010; Sun et al. 2013). The normal healing response is characterized by a significant decrease in the quality and quantity of alveolar bone and by a collapse in the surrounding gingival architecture (Steiner et al. 2008).

There is vertical and horizontal bone loss associated with the extraction-induced alveolar bone loss. Loss of the buccal plate in humans is the most dramatic post-extraction alveolar change because it is comprised of bundle bone and is thinner than the palatal or lingual plate (Jamjoom & Cohen 2015).

Relevant Animal Models for Study

According to previous studies, small animals (e.g. rats, hamsters, rabbits) are excellent models for the evaluation of extraction healing and various interventions. The physiology of such small animals is not as similar to humans as larger animals, but there is a larger ethical concern and a significantly greater cost to canines and non-human primates (Madden & Caton 1994; Struillou et al. 2010). Evaluation of alveolar bone healing following extractions and various manipulations has been done in various animals, including non-human primates, canines, ferrets, rabbits, and rats (Bodner et al. 1991; Devlin 2000). Using rats provides a more cost-effective method with advantages for ease of housing and handling, making it possible to carry out studies with numbers necessary for statistical analysis (Struillou et al. 2010). Rats are the most extensively-studied rodent for research regarding the periodontium and various surgical techniques (Bodner et al. 1991; Struillou et al. 2010). Retired-breeder Sprague-Dawley rats were chosen for the current study to eliminate the potential for growth to influence the results. Sprague-Dawley rats were used to roughly standardize the size and metabolic activities of the specimens, and because of the extensive use of Sprague-Dawley rats in dental research (Struillou et al. 2010; Yang et al. 2015).

The rat model of post-extraction bone modeling has shown general similarities to the human model from a physiologic perspective, but, in general, rats have a faster regeneration of oral tissues than humans (Schropp et al. 2003; Wu et al. 2008). Previous studies have indicated that there can be as much as 50% loss in the bucco-lingual dimension occurring after 12 months

in humans (Madden & Caton 1994; Schropp et al. 2003; Pagni et al. 2012). A radiographic and histologic study of the healing extraction site in rats demonstrated that no changes were observed in the socket between the 28 and 60 day observation points, thus a 28 day period was chosen for the current study (Bodner et al. 1993). In humans, the most rapid alveolar resorption occurs in the first six months following extraction and continues throughout life at a rate of 0.5-1.0% (Pagni et al. 2012). Comparable studies on the timing and percentage of alveolar bone loss following extraction in rats have not been done. Other studies evaluating alveolar bone dimensions using a rat model had evaluation time points of significantly less time, with the greatest reported time period being 12 weeks (Wu et al. 2008; Yang et al. 2015). In addition, extraction of the largest rat tooth (the maxillary first molar), leaves five small sockets corresponding to the five roots of the tooth of irregular shape. Creation of a single larger socket would be more clinically relevant and can be done by manipulation of the socket after extraction using a dental hand piece and round bur, as was done by Hile et al. (2005) to create a standardized defect.

A 2008 study by Wu et al. evaluated the effect of simvastatin (SIM) on the alveolar bone following extraction and found that on the non-intervention side, a measurable loss of bone occurred over the 12 weeks of evaluation. This study evaluated the bone level by capturing a 2D image to evaluate interproximal bone and measurements were obtained between two standardized points. Bone mineral density was also measured in this study and was obtained by dual-energy X-ray absorptiometry (DXA) measurements and Lexxos (DMS, France) software. The four week animals demonstrated a gradual reduction in relative (no units of measure published) alveolar bone height measured on 2D radiographs from 0.996±0.004 ($p=0.304$) at week 1 to 0.987±0.004 ($p=0.017$) at week 2 to 0.906±0.034 at week 4 (Wu et al. 2008). This study also reported the bone mineral density changes for the unmanipulated side that served as the

control over time as a gradual increase: 6.775±0.042 (p=0.106) at week 1, 7.053±0.032 (p=0.076) at week 2, and 7.101±0.014 (p=0.039) at week 4 following extraction of a mandibular tooth. DXA is considered the gold standard for BMD measurements and BMD an important parameter to evaluate the amount of bone formation and degree of calcification of the newly formed bone (Adams 1997; Wu et al. 2008).

Fine et al. (2009) also measured alveolar bone level changes in rats, but focused on induced periodontitis. Their method for measuring bone level changes involved 2D radiographs to measure from the CEJ to the alveolar bone crest to determine area of bone loss, linear bone loss, and bone loss by a direct visual measurement of the interproximal region after a 12 week study period. To calculate the total area and linear measurements for this study, six regions were traced from the CEJ to the alveolar bone crest to include the furcation areas and interproximal areas between M1, M2, and M3. The investigators (Fine et al. 2009) for this study did additional research to determine baseline bone loss but the bone loss was cumulative across six measurement sites and thus cannot be applied to the current study (Schreiner et al. 2011).

Interventions and Grafting Methods

Acknowledging the prevalence of tooth extractions in dentistry and their pattern of alveolar bone contour changes and loss of dimension, it is important to focus on the options available to minimize the destruction that occurs. Several surgical techniques have been proposed to reduce the loss of alveolar bone (Pagni et al. 2012). After the extraction of teeth, the periodontium (gingiva, connective tissue, cementum, periodontal ligament, alveolar bone) undergoes significant changes, most clinically significant of which is the loss of alveolar bone by bone modeling (Tomlin et al. 2014). More posterior teeth, or larger teeth, and more traumatic extractions result in more bone loss (Tomlin et al. 2014). A bone substitute is ideally biocompatible and is gradually replaced by new bone (Su-Gwan et al. 2001). Knowing that there

are significant dimensional changes that occur, particularly in the early phase after extraction (Araujo & Lindhe 2005), dentistry has become interested in various mechanisms of bone preservation. Such methods include the following: atraumatic extraction techniques, various bone grafting materials and methods, and tissue engineering methods. Although autogenous grafting material is the gold standard for bone grafting because of the osteogenic potential and no risk of graft rejection, there is significant site morbidity (Darby et al. 2008). There are many options when choosing a graft material, including the following: autogenous bone, demineralized freeze-dried bone allografts (DFDBA), xenografts like Bio-Oss, bioactive glass, hydroxyapatite and calcium sulfate (Darby et al. 2008). Utilizing bone grafts and bone substitutes provide the clinical advantages of filling the defect and providing a scaffold for eventual bone fill with the proven effect of decreasing the loss of the alveolar ridge following extraction (Wood & Mealey 2012).

Clinicians prefer graft materials that can be easily manipulated (Kim et al. 2016). Deproteinized bovine bone (DBB) material, commonly known as bone mineralized matrix (BMM) or its brand name, Bio-Oss, is the most commonly used xenograft (Tomlin et al. 2014). BMM can be hydrated to form a slurry or a gel prior to use. It has been found that hydration of graft materials like Bio-Oss promotes the environment of the graft site (Pietrzak 2006). BMM is a popular graft material due to its biocompatibility and osteoconductive properties (Jensen et al. 1996; Skoglund et al. 1997; Su-Gwan et al. 2001). The composition of BMM is the spongiosa of bovine bone cleansed of organic matrix, or deproteinized, and denatured so that is it biologically compatible to serve as a xenogenic bone graft (Pinholt et al. 1991). A study of BMM implanted in male rats concluded that an inflammatory reaction occurs with implantation subcutaneously and in the maxilla (Pinholt et al. 1991), while a previous study identified the BMM graft demonstrated the best bone formation and organization of the graft itself as compared with

particulate dentin and plaster in various combinations (Su-Gwan et al. 2001). A human study evaluating BMM as graft material identified that the graft material is slowly degraded rather than resorbed and the new bone was present close to the implant particles and ossification centers were identified centrally (Skoglund et al. 1997).

Role and Interaction of Inflammation in Healing

Many studies have documented the significance inflammation plays during the wound healing process and the inflammatory reaction has been described as the second of four distinct wound healing phases (Guo & Dipietro 2010). Inflammation is a critical and normal part of the healing process and the cells of the inflammatory process are critical in removing contaminants and micro-organisms (Guo & Dipietro 2010).

In the inflammatory process, the cellular products, like prostaglandins (PG), and the pathways they mediate play a critical role in the physiological response for wound healing. Prostaglandins are lipid mediators that act in autocrine and paracrine functions and can mediate a number of physiological and pathological conditions, both stimulatory and resorptive (Pountos et al. 2012). Key markers of inflammation include PGE_2, which is one of the most abundant prostaglandins in the body (Funk 2001). PGE_2 is ubiquitously produced and is constantly present at low levels, but the PGE_2 level increases immediately in acute inflammation to act as a chemoattractant for leukocytes and other immune cells (Ricciotti & FitzGerald 2011). Heavily involved in the classical signs of inflammation, including redness, swelling, and pain, PGE_2 acts to mediate the inflammatory process (Funk 2001).

Bone healing is one of the most complex physiological cascades of events, with local and systemic cytokines and other mediators directing the outcome (Pountos et al. 2012). Considering the influence of inflammation on healing, specific important mediators of inflammation, like PGE_2, can be quantified at various time points to determine the relative

degree of inflammatory response. PGE_2 serves many important physiologic functions, depending on its level in tissues. Depending on levels, PGE_2 is involved in bone resorption at high levels and bone formation at lower and intermittent levels (Pountos et al. 2012). Since PGE_2 is a product of the COX-2 pathway, inhibition of that pathway by pharmaceutical interventions may have an effect on the physiological outcome of PGE_2 pathways (Bradley et al. 2007; Lee et al. 2011). Following grafting procedures, an inflammatory response is stimulated and preliminary studies demonstrated that there is a potential negative effect for graft survival if the mediators of inflammation are inhibited (Preston et al. 2007). Many animal studies, but very few human studies, have been conducted to evaluate the role of nonsteroidal anti-inflammatory drug (NSAID) use and suppression of the inflammatory response and the results of the animal studies are somewhat mixed (Pountos et al. 2012). It has been hypothesized that in patients taking anti-inflammatory medicines like NSAIDs after bone grafting procedures will have less successful clinical outcomes, as compared to individuals who do not inhibit the inflammatory response, based on the significance of prostaglandins, and specifically PGE_2, in the healing process (Pountos et al. 2012).

The bone healing response has been evaluated in light of the concurrent administration of simvastatin, which has demonstrated bone anabolic properties based on the ability of the statin to stimulate endogenous BMP-2 for osteogenesis (Mundy et al. 1999). Other studies have further evaluated this link between statins and bone formation and have confirmed that the local administration does stimulate bone growth in rodent populations (Thylin et al. 2002; Stein et al. 2005). Those studies reported local inflammation around injection sites and thus interventions to reduce the swelling by administration of the NSAID indomethacin and, therefore, interruption of the COX and PG pathways resulted in nearly eliminating the statin-induced new bone growth. Rodent studies have demonstrated that NSAIDs that inhibit PGE_2

interrupt both bone healing and normal bone growth (Yugoshi et al. 2002). Another study that evaluated the role of the PG pathway with simvastatin-induced oral bone growth in rats found that higher levels of PGE2 in the first week enhanced the bone growth (Lee et al. 2011). Bradley et al. (2007) demonstrated in a rat model that locally administered SIM stimulates bone formation, but that effect is diminished when inflammation is inhibited pharmacologically.

Evaluation Methods

I. µCT

Micro-computed tomography (µCT) is a valuable research and clinical tool to evaluate mineralized tissues by two-dimensional and three-dimensional parameters. Linear measurements of alveolar height and width as well as volumetric measurements of bone quality and quantity, like bone density and trabecular separation, can be accomplished with µCT. A 2007 study of mature Sprague-Dawley rats evaluated the linear and volumetric parameters of alveolar bone by µCT (Park et al. 2007). In this study, they were able to develop methods to accurately and reproducibly quantify alveolar bone as a way to standardize bone measurements in scenarios of disease progression or regeneration attempts. Park et al. (2007) utilized an experimental bone loss model to validate the use of µCT for bone imaging. Linear and volumetric measurements were obtained in this study for the clinical models of disease, trauma, and regeneration, but the results were not reported for bone level. The methods for obtaining the linear measurements were to measure in the interdental regions of M1-M2 and M2-M3 from the CEJ to ABC and orienting the image to view the CEJ and root apices (Park et al. 2007). Bone volume, bone mineral density, and bone volume fraction were volumetric measurements obtained from the ROI captured, although the baseline values were not reported (Park et al. 2007). Linear measurements are typically taken on 2D radiographs, but the 3D images can be manipulated in such a way as to standardize their projection and linear measurements can be

obtained. This study split the rats into two groups: a bone loss group which received *Porphyromonas gingivalis* LPS injections, and a regeneration group received surgical osteotomies that were then covered with seeded PLGA scaffolds, described previously by Jin et al. (2004). Comparing baseline to 8 weeks of the LPS-injected group, the interdental bone regions demonstrated significant differences in cementoenamel junction (CEJ) to alveolar bone crest (ABC) distance, concurrent with periodontal disease-induced bone loss. There was no difference between baseline and 8 weeks with the control group with no disease. In the regenerative therapy group, exposure of the tooth root with a cell-seeded PLGA barrier resulted in less root exposure by bone loss than the control group. In all groups, the amount of bone changes were evident on both 2D and 3D images, and volumetric measurements of bone volume, bone mineral content, and bone mineral density were obtainable. There was high reliability and reproducibility and, thus, the authors felt the proposed method of 3D μCT was valuable to assess periodontal osseous changes over time.

There is a paucity of studies that have evaluated the changes in rat alveolar bone following extraction using μCT. A 2014 study of rats comparing bisphosphonate and parathyroid hormone treatments using μCT demonstrated the usefulness of the technology and also measured the vertical alveolar bone loss after extraction, but did not report the baseline bone loss values prior to pharmacologic intervention (Kuroshima et al. 2014). This study evaluated the sockets at 10 days following extraction because of the pattern of healing in rats that demonstrates epithelial coverage of the wound and woven bone filling the bottom half of the socket.

II. Histological Analysis

The distinct pattern of wound healing can be characterized by histologic analysis of the process at distinct time points. The characterization of the healing process has been well

described in various studies and is consistent across species (Kim et al. 2012). The normal healing process generally progresses through a series of distinctive phases, and the inflammatory infiltrate and bone surface response has been characterized in a rat model (Kim et al. 2012). From the sections, inflammatory infiltrate area, cell types and bone surface osteoblast and osteoclast surfaces were measured at the periphery of the healing wound. After the initial blood clot formation, the inflammatory infiltration was rapid and the cells of an acute inflammatory reaction were present but diminish after about 10 days, coinciding with indications of bone turnover and new bone forming in the socket (Kim et al. 2012). Healing can be assessed histologically by looking at the quality (acute, mixed, or chronic inflammatory infiltrate) or the quantity (mild, moderate, or severe inflammation) of the inflammatory response in the area of interest. By evaluating the cells present in the inflammatory infiltrate, the inflammation can be characterized as acute with a predominantly neutrophilic infiltrate, chronic with a predominantly a lymphocytic infiltrate, or mixed with both a neutrophilic and lymphocytic infiltrate. The relative severity of the inflammatory response can be characterized using a numerical scale based on the histologic presentation (Kristensen et al. 2008).

In addition to the inflammatory reaction, the histological sections can reveal the relative bone surface activity and relative amount of bone turnover. The development of new bone on the periosteal aspect during healing has been seen in previous rat studies (Pietrokovski & Massler 1967; Todo 1968). By evaluating the bone surface for activity and quantifying the proportion of surface lined by osteoblasts or osteoclasts, relative surface activity or quiescence of the bone can be determined. The active bone cells can be identified histologically and microscopically. Osteoblasts are bone forming cells that contain one nucleus and are plump cells found in a single layer on the surface of the bone (Clarke 2008). On the other hand, osteoclasts are the only cells that resorb bone and they can be microscopically identified based on their

multinuclear appearance and their presence on the surface of bone accompanied by their resorptive area or Howship's lacunae (Clarke 2008). Any area of the bony surface not occupied by an active osteoblast or osteoclast is said to be in a stage of quiescence and is not actively undergoing formation or resorption.

In the first month of healing following extraction, the normal histological sequence of wound healing is expected to progress without incident. A previous study of the bone density and histological changes following extraction in rats demonstrated distinctive phases of healing (Bodner et al. 1993). Bodner et al. (1993) identified a bone formation phase occurring at the 7 and 14 day time periods and a bone remodeling phase with maturation of the young bone and modeling of the alveolar ridge at the 28 day periods.

A study of maxillary molar extraction sockets in ovariectomized rats evaluated the healing process at various time periods with SEM and light microscopic histologic analysis (Shimizu et al. 1998). The 7 day and 30 day time periods of the above study aligned with the current study. At 7 days after extraction, the SEM analysis revealed Howship's lacunae of resorptive areas mainly on the buccal aspect, but also on the palatal aspect, and commonly in the deeper regions of the extraction socket. The study also demonstrated subtle areas of bone formation and thin lamellar bone was evident. At 30 days following extraction, the extraction sockets were filled with lamellar bone, but there were significant resorptive areas on the palatal aspect (Shimizu et al. 1998). In this study, bone resorption was more evident on the palatal aspect than on the buccal aspect of the extraction socket (Shimizu et al. 1998). The conclusions of the Shimizu et al. study revealed that bone formation and bone resorption take place at distinct sites, but the processes are closely related and coupled so that they take place adjacent to one another (Shimizu et al. 1998).

A historic study of male rats evaluated a healing mandibular molar extraction socket by histologic, radiographic, and histometric methods at various time points (Guglielmotti & Cabrini 1985). The histologic findings from the above study demonstrated that at 0 days, the socket was filled with blood coagulum and surgical debris, at 7 days, the internal and lingual crest of the socket showed signs of resorption, at 14 days, the bone surfaces showed intense bone activity and at 30 days, the socket was filled with new bone and active osteoblasts were predominantly located on the alveolar ridge. This study evaluated the H&E stained socket at 40X magnification.

A more recent study evaluated male mature rats who were subjected to mandibular molar extraction by histometric analysis at 3, 7, 10, and 14 days following extraction (Giorgetti et al. 2012). The control group underwent only mandibular molar extraction with no intervention or treatment and experienced an increase in mineralized tissue and a decrease in nonmineralized tissue at the fundus of the socket between 7 and 14 days (Giorgetti et al. 2012). In this study, new bone formation was evident at 7 and 14 days and was seen as bone trabeculation in the extraction socket.

METHODS AND MATERIALS

Pilot Study

Prior to the core study, a pilot study was undertaken to refine the extraction and defect creation techniques, evaluate the effectiveness and repeatability of the current study's measurement techniques, become familiar with the protocol, and confirm that there is bone loss in the extraction site compared to the contralateral side at a period of 28 days, or 4 weeks, following the surgical procedure. Four retired-breeder Sprague Dawley rats (Harlan Teklad, Madison, WI) were used as a pilot study group. Rats were acclimated prior to experimental procedures for one week and were treated and housed in the University of Nebraska Medical Center College of Dentistry Animal Facility, Lincoln, NE, under approval of the University of Nebraska Medical Center Institutional Animal Care and Use Committee (IACUC #14-080-10-FC). Retired breeder rats were chosen to eliminate the effect of growth on the alveolar bone changes and to standardize the metabolic activities. Each rat was weighed prior to any procedure. The rats were all placed in a surgical group with a 28-day follow-up period planned. Adequate anesthesia was administered by inhalation of isoflurane, followed by a local anesthetic injection of 0.2 cc of 3% carbocaine in 1:20,000 neo-cobefrin into the right facial vestibule as it demonstrated effectiveness in previous rat studies (Killeen et al. 2012). In minor surgeries, this anesthesia method has proven effective in the maxilla.

Extraction of the maxillary right first molar was accomplished using a modified dental carver (1/2 Hollenback carver, Hu-Friedy, Chicago, IL, USA) to incise the gingival attachment and a modified explorer (2 Explorer, Hu-Friedy, Chicago, IL, USA) was used to luxate the tooth mesially. During the procedure, a small flap was reflected using the periodontal probe so that 2 mm of facial bone was partially exposed. A standardized bone defect was created using a #6 round dental bur of 1.8 mm diameter under water irrigation and evacuation, to a depth 2 mm

from the cementoenamel junction of the maxillary right second molar. The maxillary left first molar served as the unmanipulated control for the study. The surgical flap was closed using cyanoacrylate adhesive (PeriAcryl 90, GluStitch Inc, Delta, BC, Canada). A 0.01 mg/kg dose of buprenorphine was administered subcutaneously after the procedure. All animals were euthanized 28 days after the initial surgical procedure and the palates were harvested and placed in 10% formalin for fixation prior to evaluation. All animals were evaluated by μCT and histologic assessment to confirm that bone loss occurred and to identify the appropriate thickness and location for the histologic sections.

Results from the pilot study confirmed the loss of alveolar bone with extraction and surgical defect creation. Loss of alveolar bone on the palatal aspect was more predictable because surgical trauma or harvest frequently caused fracture of the buccal cortical plate. The technique for anesthesia was modified due to right ocular hemorrhage evident in the animals after the procedure, so that the needle was inserted only to a depth of 2 mm and only 0.1 cc of 3% carbocaine in 1:20,000 neo-cobefrin was administered. In addition, isoflurane inhalation anesthesia was adequate, with no animals requiring the intramuscular ketamine/xylazine injection.

There was often communication between the socket and the maxillary sinus upon evaluation of the pilot group; therefore, a #4-round bur with a 1.4 mm diameter was proposed to create the surgical defect and remove residual roots. The pilot study confirmed that a 28 day period was sufficient to see alveolar bone changes, and that interim periods would serve as an opportunity to evaluate morphologic, biochemical, and histologic changes. Time periods of 0 days, 7 days, 14 days, and 28 days were used because of the ability to evaluate the healing process over time by μCT and histological analysis.

Core Study

Fifty mature (10 to 12 month old) retired-breeder female Sprague Dawley rats were chosen for this study (Harlan Teklad, Madison, WI). The core study was split into two parts: Part I consisted of 33 rats and Part 2 consisted of 17 rats. The rats were allowed to acclimate for one week prior to the procedure. All animals were treated and housed at the University of Nebraska Medical Center College of Dentistry Animal Facility under the supervision of the Institutional Animal Care and Use Committee (IACUC #14-080-10-FC), and the study was conducted in accordance with the Helsinki Declaration of 1975, as revised in 2013.

Groups

Rats were divided into six groups: Groups 1-4 were designated to Part 1 of the core study and Groups 5-6 were designated to Part 2 (Table 1) of the core study. All extractions were done on the maxillary right first molar. Groups 1-4 received extraction and surgical defect creation only. Group 1 was euthanized by CO_2 asphyxiation immediately after the extraction and surgical defect creation (day 0), Group 2 was anesthetized, sockets created, then euthanized at 7 days, Group 3 was anesthetized, sockets created, then euthanized at 14 days, and Group 4 was anesthetized by inhalation and sockets created and were sampled for socket fluid at 7 days, 14 days, 28 days and euthanized at 28 days. Groups 5 and 6 were treated like Group 4 with the extraction, defect creation, socket fluid samples at 7 days, 14 days, and 28 days; however, two modifications were made: Group 5 sockets were grafted with a slurry of bovine bone mineral matrix small granules (BMM, Geistlich, Bio-Oss, Princeton, NJ, USA) and packed into the socket prior to the surgical wound being closed using cyanoacrylate adhesive (PeriAcryl 90, GluStitch Inc, Delta, BC, Canada), and Group 6 sockets were grafted with approximately 0.2 mg simvastatin absorbed to BMM (BMM+SIM) conjugate slurry packed into the socket prior to the surgical wound being closed with cyanoacrylate adhesive. For all groups, the left maxillary right

molar served as the unmanipulated control. All groups had at least 8 specimens, and groups 4 and 6 had 9 specimens due to extra animals being delivered to the facility.

Anesthesia/Euthanasia

Anesthesia was induced by placing the rats into an anesthesia induction chamber with 1-4% isoflurane/100% O_2 (1 to 3 L/min). The animal's pattern of breathing was used to determine the depth of anesthesia. Following removal from the incubation chamber, a nose cone was placed over the rat's nose and 0.5 to 2% isoflurane/100% O_2 (0.5 to 1.0 L/min) was used to maintain anesthesia during the procedures. Local anesthesia was achieved by local infiltration into the right maxillary vestibule adjacent to the first molar of 0.1 cc of 3% carbocaine in 1:20,000 neo-cobefrin with the needle inserted to a depth of 2mm. All animals were weighed following anesthesia induction and prior to all procedures to monitor weight gain or loss. Following the anesthesia, injections, and extraction, the rats were monitored until awake and normal movement resumed. After the surgical procedure, Group 1 was euthanized immediately by CO_2 asphyxiation and decapitation, Group 2 was euthanized at 7 days, Group 3 was euthanized at 14 days, and Groups 4-6 were euthanized at 28 days. The palates and maxillary alveolus were separated from the rest of the skull and placed in 10% formalin for storage prior to µCT analysis.

Graft Preparation and Application

Part 2 of the study consisted of evaluation of the pharmacomanipulation of the socket as an intervention for bone preservation. This portion of the study was completed to determine if a bovine bone mineral matrix graft (BMM) with or without a simvastatin-pyrophosphate conjugate shown to stimulate bone formation in experimental periodontitis, can stimulate bone formation. BMM was selected as the graft material based on its biocompatibility, its osteoconductive properties, and its widespread use as a grafting material in dentistry (Darby et

al. 2008). The graft material was supplied in a small granule size (0.25- to 1.0-mm particle size) and it was absorbed to a simvastatin-pyrophosphate conjugate. Preparation of 1.5 mg simvastatin (SIM)-pyrophosphate (PPi) conjugated bone graft per 0.1 g BMM involved 1 g bovine-derived bone mineral particles, BMM, (BioOss®, Geistlich Pharma North America, Inc.) incubated with 5 ml (SIM-PPi) solution (10 mg/ml) in a tube rotator at room temperature for 20 minutes. The unbound SIM was removed and quantified by calculating the amount of SIM-PPi in the supernatant after centrifugation at 3000 rpm for four cycles at 5 minutes per cycle, after which the free SIM remaining in the supernatant was removed by pipette. The concentration of SIM-PPi in the supernatant was determined by measuring ultraviolet absorbance at 238 nm. The usable BMM+SIM-PPi conjugate with 1.5 mg simvastatin per 0.1 g BMM bone graft small grains was obtained after lyophilization for 24 hours. The BMM+SIM-PPi conjugate was stored on dry ice prior to use to eliminate any risk of degradation. At the time of extraction and graft placement, it was determined that the particles were too large for the small bone defect, so further crushing of the particles was accomplished by mortar and pestle and only 0.01 g of graft material was placed in the defect. One half of the animals in Part 2 of the study received only the BMM graft, but the extraction, defect creation, grafting methods, post-operative care, and evaluation methods were consistent regardless of the type of graft placed. The graft materials were hydrated in sterile deionized water for ease of placement. The extraction defect and graft material were covered with cyanoacrylate adhesive in the same fashion as in Part I. Placement of cyanoacrylate cement was repeated one week later during socket fluid sample collection to aid in the retention of the graft material.

Evaluation Methods

I. µCT Measurements

Evaluation of bone changes was done by µCT analysis. Studies have found that extraction in rats leads to alveolar bone morphologic changes that can be assessed by tomograms and three-dimensional imaging (Alikhani et al. 2016). Each maxilla was scanned with a high-resolution system (SkyScan 1172, Bruker microCT, Kontich, Belgium) with the x-ray tube voltage at 70 kV, the current at 141 µA, with a 5 mm-thick aluminum filter, for a fixed exposure time of 580 ms. The images were reconstructed into a 3D-structure with a pixel size of 8.71 um. The x-ray projections were obtained in multiple frames with each rotation at a 0.7˚ interval with a scanning angular rotation of 180˚ and an average of five frames for each rotation.

Two software programs were used to first orient the 3D images (DataViewer, Bruker microCT, Kontich, Belgium) and then a second software program was used to obtain the linear and volumetric measurements (CTAn, Bruker microCT, Kontich, Belgium). All specimens were initially oriented on three axes in the DataViewer software using the orientation lines (red, blue, green), corresponding to the three planes (Figure 1). The image orientation was manipulated for a coronal slice to measure the buccal and palatal alveolar bone and for a sagittal slice to measure the interproximal bone height.

The coronal images were used that captured the best internal anatomy of mesial canals of the maxillary second molar, aligned with the line of best fit through the buccal and palatal cementoenamel junctions (CEJ) parallel to the horizontal orientation lines. The red line was centered through mesial canals of the maxillary second molar in the “transaxial” image as designated by the software, the blue line was oriented down the long axis of the tooth in “coronal” image, and the green line was aligned as the line of best fit through the buccal and palatal CEJ in the “sagittal” image (Figure 1). The buccal bone height was from the mid-socket

by first finding the μCT slice that represented the first time the mesial aspect of M2 was visible and then advancing into the socket 0.557 mm to the point that reproducibly represented the area of interest, then the bone height was measured by recording the distance from the most superior and lateral aspect to the buccal alveolar crest (Figure 2). Additionally, the width of the buccal cortical plate was measured from the superior and lateral aspect and advancing in 0.25 mm increments to the alveolar crest and then measuring the perpendicular width. The height and width of the palatal bone was measured using the same method as the buccal bone height on the same slice from the μCT data but from the most superior and mesial aspect that corresponded to the alveolar process of the maxilla. To measure total width, the mid-socket slice was used and the measurement was obtained by identifying the perpendicular line of greatest width buccal to palatal to the point 1.25 mm crestal from the most superior and lateral point of the buccal cortical plate. The socket total area was recorded from the same mid-socket slice and tracing the outline of all of the radiopaque area including the alveolar bone and tooth structure when present on the control side.

For the sagittal view to evaluate the alveolar bone height mesial and distal to the maxillary second molars, the image was oriented in the DataViewer software using the orientation lines so that the green line intersected the palatal canals of the teeth present, the blue red line was placed equidistant mesial-distally between the palatal roots of the maxillary second molar, and the blue line was oriented as a line of best fit through the mesial and distal CEJ of the maxillary second and third molars (Figure 3). Using μCT and the measurement software (CTAn, Bruker microCT, Kontich, Belgium), the loss of vertical bone height was assessed from the CEJ to the crestal bone adjacent to the periodontal ligament space on the mesial and distal aspects of the maxillary second molars. The amount of interproximal bone loss was recorded on the mesial and distal aspect of M2 by tracing a line from the CEJ to the ABC parallel

to the root structure and recording the linear distance until the most crestal portion of alveolar bone present (Figures 4 and 5).

The bone volume and density parameters of bone quality were also measured in the palatal crest areas using an image from the coronal slice. The region of interest (ROI) was determined by aligning the ROI rectangle to the most cervical location where a standard rectangular box (0.261 x 0.450 x 0.340 μm) could be placed (Figure 6). The ROI was then analyzed for the volumetric and bone quality measurements for the following parameters: mean bone mineral density (BMD), bone volume (BV), bone volume (BV)/trabecular volume (TV) or fraction of mineralized tissue in the ROI, and bone surface (BS)/trabecular volume (TV) for bone surface density (BSD).

II. Histological Analysis

Following analysis by μCT, the specimens were decalcified using a 5% formic acid solution for at least 2 weeks at 4˚C. Each was then processed, blocked, and coronally sectioned for hematoxylin and eosin staining for conventional histological examination. At the palatal alveolar crest, the inflammatory infiltrate area, cell types and bone surface osteoblast/osteoclast presence were measured. At lower magnification (40x), the palatal area was captured using a light microscope and digital camera/software (ProgRes CapturePro; JENOPTIK Optical Systems, Jena, Germany). All specimens were initially interpreted by the primary investigator masked to experimental group and secondly by a masked experienced pathologist and any disagreements in the scoring were resolved by a masked third party. A qualitative assessment of the predominant inflammatory cell type present and relative degree of inflammation were made using a light microscope and the following scale modified from Kristensen et al. (2008), the inflammation as rated 0 to 3. The scoring criteria in the current study was defined as follows: 0 = no inflammatory cells present, no inflammation; 1 = few,

scattered inflammatory cells present, mild inflammation; 2 = multiple clearly present inflammatory cells present, moderate inflammation; 3 = massive presence of inflammatory cells, severe inflammation (Figure 7). Additionally, a qualitative assessment regarding the stage of inflammation was also made in the same manner and scored as either acute, mixed acute and chronic, or chronic, based on the predominant cell types present with acute inflammation characterized by neutrophilic infiltrate and chronic inflammation characterized by a predominantly lymphocytic infiltrate (Farb et al. 1999) (Figure 8). Histopathologic scoring for research is common and specimens are commonly grouped based on microscopic similarities of generalized properties for ease of comparison. Using the 40x magnification view, the general area of inflammatory infiltrate was evaluated. Roughly 600,000 μm of connective tissue area adjacent to the palatal crest was outlined and the internal area of inflammatory infiltrate was outlined and the percentage of inflammatory infiltrate was calculated (Figure 9). Measuring the relative activity of the bone surface in the palatal alveolar crest region was done using higher magnification (100x) to detect specific cells of bone turnover, osteoblasts and osteoclasts, on the bone surface. Osteoblasts were identified by containing one plump nucleus and found in a single layer on the bone surface, osteoclasts were identified as the cells with a multinuclear appearance adjacent to Howship's lacunae, and quiescent surface was any bone surface area that was not undergoing bone turnover (Figure 10). Roughly 4000 μm of bone surface was analyzed and the relative proportions of that surface area that were lined by osteoblasts and osteoclasts were reported (Figure 11).

III. ELISA

Socket fluid absorption samples were taken at weeks 1, 2, and 4 using an absorbent paper strip (Periopaper, IDE Interstate, Amityville, NY, USA). However, the healing process prevented consistent samples after the first week of healing. The samples were frozen at -80˚C

until all samples were collected so the measurements could be obtained at one time. The paper strips were eluted in 250 µL of PBS solution for 1 hour prior to following the protocol for the PGE_2 ELISA monoclonal kit (Cayman Chemical, Ann Arbor, MI) and rat albumin ELISA kit (Innovative Research, Inc., Novi, MI) according to manufacturer instructions. The PGE_2 samples were run at undiluted and 1:10 dilutions and the plate was read at the recommended 405 nm wavelength. The albumin samples were run at undiluted, 1:10 dilutions, and 1:100 dilutions and the plate was read at the recommended 450 nm wavelength. PGE_2 levels were divided by the albumin level to standardize the relative amounts of PGE_2 present due to the variability in the quantity of socket fluid sample collected.

IV. Statistical Analysis

A power analysis was conducted and demonstrated that 8 rats were needed to show greater than 30% increase in alveolar bone growth 80% of the time when testing at the 5% level of significance using various doses for simvastatin, an anti-inflammatory and bone anabolic agent which was the pharmaceutical intervention tested. Each group contained at least 8 rats and additional animals were added to groups 4 and 6 for a total of 9 rats in those groups because extra animals were sent during animal delivery. Specimens were coded by animal number and measured by one examiner without knowledge of group designation. The same examiner repeated these measurements on 10% of the original specimens 2 weeks after initial measurement. Analysis of variance was utilized for intergroup comparisons for all clinical measurements from the treatment and control sides at different postoperative time intervals. The difference in the measurements from the treatment side (right) after operation against the control side (left) from the same animal was computed. The one-sample t-test was used to evaluate whether significantly different values between the treatment side and the control side of the same animal existed between the experimental group and the corresponding intra-rat

control. The Spearman correlations were calculated to measure the correlation between the clinical measurements of bone loss and the inflammatory measurements. Differences between groups were analyzed using the Kruskal-Wallis test for non-parametric and non-normally distributed data. Results were reported as mean ± standard deviations, with the exception of the PGE_2 data which were reported as mean ± standard error, and considered significant when p values were ≤ 0.05. When significant differences were found among groups ($p \leq 0.05$), pairwise comparisons between groups were analyzed using the Wilcoxon rank sum non-parametric method and p-values were adjusted using the Bonferroni method for multiple comparisons. The intra-class correlation coefficients (ICC) and its 95% confidence interval based on two-way random effects model and single measurements calculated assessed the reliability of the measurements.

RESULTS

Part 1

The weight of the animals (Table 4) among groups was not different and no significant weight was lost in any group. No animals died prematurely during Part I of the core study and all animals tolerated the procedures well. Figure 12 demonstrates an intraoral view of the extraction to healing at 28 days. The images demonstrate size of the maxillary right first molar, the configuration and divergence of the five roots, the defect after the round bur was used to remove interradicular bone and residual roots, and the clinical evidence of the collapse of the alveolar ridge in the area of the missing tooth.

I. µCT Linear Measurements

The results for the µCT linear measurements for the mid-buccal ridge width, buccal ridge height, mid-palatal ridge width, palatal ridge height, interproximal height of bone mesial to M2 adjacent to the extraction socket, and interproximal bone distal to M2 are summarized in Figures 13-16. Differences in linear measurements demonstrated that extraction-associated bone loss was evident on buccal, palatal, and interproximal bone, and on palatal bone width both among the time points and from extraction to control side. Radiographic changes day 0 to 28 are seen in Figure 17. The mid-buccal width demonstrated no significant differences, but there was extreme variability in the recorded values (Figures 18 and 19). The buccal height demonstrated statistically significant loss between 7 and 28 day extraction sites and statistically significant loss at 14 days between the extraction and control sites (Figure 14). The mid-palatal width demonstrated statistically significant losses between extraction sites at days 7 and 28, 14 and 28, and 0 and 28 healing time periods, and statistically significant losses at the extraction compared to the control sites at 28 days (Figure 15). The palatal height demonstrated statistically significant losses at the extraction sites between days 0 and 28 and between the

extraction and control sites at 0 (slight difference), and more loss at 14 and 28 days (Figure 16). The progression of palatal bone loss was evident radiographically when evaluating representative sections at the time periods from 0 day to 28 days (Figure 17). The interproximal bone on the distal aspect of the socket, mesial to M2, demonstrated statistically significant bone loss on the extraction site between 0 and 28 days and between the extraction and control sites at 7, 14, and 28 days (Figure 18). As expected, there was no loss of interproximal bone on the distal aspect of M2 where the periodontal tissue was not manipulated (Figure 19). There were no differences in the control groups for parameters measured at the various time points (Figures 18 and 19). The progression of bone loss was evident radiographically when evaluating the time periods from 0 day to 28 days (Figure 20).

Measurements were repeated in 10% of samples and results for the mixed model analysis of variance to determine intra-examiner variability by calculating the intra-class correlation revealed that there was good to excellent reproducibility with all values and are summarized in Tables 2 and 3. Overall, the variability between animals was much greater than variability within the same animal (observations by the examiner) based on the calculated values. The data reported from the extraction sites all had excellent reproducibility as the ICC was 0.978 or above with the exception of good reproducibility of the 1.25 mm buccal width with an ICC of 0.844 and the 1.25 mm palatal width with an ICC of 0.882. Due to the reproducibility of the buccal and palatal width at 1.25 mm from the reference point, those measurements were referenced for the width of the buccal and palatal alveolar bone.

II. µCT Volumetric Measurements

Means of volumetric measurements are summarized in Figures 21 and 22. The µCT volumetric measurements that produced statistically significant differences among various groups were mean bone mineral density (BMD) and bone surface density (BSD). Palatal ridge

BMD increased in both grafted sites compared to immediately post-extraction and after 28 days. BSD increased in the BMM+SIM ridge compared to no graft or BMM alone at 28 days. There were no differences in the control groups at the various time points.

III. Histological Analysis

The histological results of parameters for quantifying and qualifying the inflammatory response adjacent to the palatal alveolar crest are reported in Figures 23 and 24. Compared to the untreated control, day 7, day 14, and day 28 all demonstrated a statistically significant increase in infiltration density of inflammatory cells (Figure 23). The degree of inflammation demonstrated a statistically significant increase between the untreated control and day 7, day 14, and day 28 measurements (Figure 24). The degree of inflammation was decreased in both grafting material groups.

Evaluating the palatal alveolar crest for cellular indicators of bone turnover, there were significant differences in the percentage of bone surface occupied by osteoblasts and osteoclasts (Figures 25 and 26). Compared to the untreated control, day 7, day 14, and day 28 all demonstrated a statistically significant increase in the percentage of osteoblasts at the bone surface and another statistically significant increase was present between 7 and 28 days. The percentage of osteoclasts at the bone surface also produced statistically significant increases between the untreated control and day 7, day 14, and day 28. Both grafting materials demonstrated a decrease in the percentage of osteoclasts at 28 days compared to ungrafted sites.

IV. ELISA

There were no significant differences in the adjusted level of PGE_2 in any of the time periods from Part 1 of the study (data not shown).

Part 2

For Part 2, the weight of the animals among groups (Table 4) was not different and no significant weight was lost in any group. No animals died prematurely during Part 2 of the study and all animals tolerated the procedures well. Figure 12 represents clinical views of the grafted sites from extraction to healing at 28 days.

I. µCT Linear Measurements

The results for the µCT linear measurements for the Part 2 specimens' mid-buccal ridge width, buccal ridge height, mid-palatal ridge width, palatal ridge height, loss of bone mesial to M2 adjacent to the extraction socket, interproximal bone distal to M2, total ridge width, and total ridge area are summarized in Figures 14, 16, 18, 19, 29 and 30. There was a statistically significant loss in palatal height between the extraction sites at day 0 and day 28 BMM, day 0 and day 28 BMM+SIM, and extraction and control sites at both graft intervention groups BMM and BMM+SIM (Figure 16). The interproximal bone on the mesial aspect of M2 demonstrated statistically significant decreases between the day 28 untreated extraction group and the day 28 BMM+SIM group and between the extraction and control groups for both day 28 BMM and day 28 BMM+SIM groups (Figure 18). There was no statistically significant change in the height of the buccal alveolar bone or in the loss of interproximal bone on the distal aspect of M2, shown in Figure 14 and 18, respectively. The total width of the ridge showed statistically significant increases between the untreated day 28 and day 28 BMM and the untreated day 28 and day 28 BMM+SIM groups, as well as between the day 28 BMM+SIM experimental and control groups (Figure 29). The final linear µCT measurement that demonstrated statistically significant differences was the recorded total ridge area where an increase was noted between the day 0 and day 28 BMM+SIM, and untreated day 28 and day 28 BMM+SIM groups (Figure 30). The progression of buccal and palatal bone changes were evident radiographically when comparing

representative sections of the untreated day 28 group, the day 28 BMM group, and the day 28 BMM+SIM group (Figure 31). Similarly, changes were also evident in the same groups when viewing the sagittal sections for interproximal bone changes (Figure 32).

II. μCT Volumetric Measurements

The μCT volumetric measurements results that produced statistically significant differences among various groups were mean bone mineral density (BMD) and bone surface density (BSD), summarized in Figures 21 and 22. The statistically significant differences were noted as increases in mean BMD at the extraction sites between untreated day 0 and day 28 BMM, untreated day 0 and day 28 BMM+SIM, untreated day 14 and day 28 BMM+SIM, untreated day 28 and day 28 BMM, and untreated day 28 and day 28 BMM+SIM (Figure 21). The BSD demonstrated statistically significant increases at the extraction sites between untreated day 28 and day 28 BMM+SIM and between day 28 BMM and day 28 BMM+SIM (Figure 22). There were no differences noted between the extraction and control sites for the Part 2 groups.

II. Histological Analysis

Evaluating the histologic results demonstrated statistically significant differences in parameters for inflammation and in bone surface cells present, summarized in Figures 23 and 24. There was a statistically significant decrease in the inflammatory infiltrate density in the palatal alveolar crest adjacent to extraction sites between untreated day 28 and day 28 BMM+SIM (Figure 23). The degree of inflammation showed statistically significantly decreases in the extraction sites between day 7 and day 28 BMM, day 14 and day 28 BMM+SIM, day 28 and day 28 BMM, day 14 and day 28 BMM+SIM, and day 28 and day 28 BMM+SIM (Figure 24).

Percentage of osteoblasts and osteoclasts on the bone surface of the palatal alveolar crest adjacent to the extraction sites differences are summarized in Figures 25 and 26. There was no statistically significant difference in the percentage of osteoblasts on the bone surface in

Part 2 (Figure 25); however, the percentage of osteoclasts on the bone surface showed a statistically significant decrease between untreated day 28 and day 28 BMM and between untreated day 28 and day 28 BMM+SIM (Figure 26). The measurement of quiescent bone surface produced a statistically significant increase between extraction groups of the untreated day 28 control and day 28 BMM and between untreated day 28 and day 28 BMM+SIM (Figure 27).

III. ELISA

The results for the levels of PGE_2/albumin ratio are reported in Figure 33. There was a statistically significant difference noted between the PGE_2/albumin levels at day 7 between the untreated and BMM+SIM group.

Correlations

Evaluation of significant concurrent correlations, that is, the correlations between parameters evaluated in the same specimen at the same time point are summarized in Table 5. At day 7, there is a positive correlation between buccal height versus inflammatory infiltrate density ($R = 0.74$, $p = 0.037$), and degree of inflammation ($R = 0.80$, $p = 0.016$), and a negative correlation between BSD and percentage osteoblasts on the bone surface ($R = -0.83$, $p = 0.01$). There were no significant correlations at day 14. Contrary to day 7, the untreated day 28 group demonstrated a negative correlation for palatal height versus inflammatory infiltrate density ($R = -0.78$, $p = 0.013$) and percentage osteoclasts ($R = -0.78$, $p = 0.013$). For the day 28 BMM group, there was a positive correlation between mean BMD and percentage osteoclasts ($R = 0.82$, $p = 0.023$) and a negative correlation between BSD and degree of inflammation ($R = -0.78$, $p = 0.034$). Finally, for the day 28 BMM+SIM group, there was a positive correlation between total ridge width and percentage osteoblasts on the bone surface ($R = 0.71$, $p = 0.047$), and a positive

correlation between the 14 day PGE_2 level and the percentage of osteoclasts on the bone surface ($R = 0.77$, $p = 0.024$).

It appears that increased inflammation is not harmful to bone when the inflammation occurs early (in the first 7 days). However, if the inflammation is persistent (14 days), the increased presence of inflammation and an increase in the number of bone surface osteoclasts is harmful to the volume and quality of bone at later stages of healing. When evaluating grafted sites, an elevated level of PGE_2 early appears to be not harmful to bone area or turnover and is not a pro-inflammatory marker. Finally, the presence of SIM is associated with an increased number of bone surface osteoblasts and the amount of bone width.

Table 1: Experimental Group

Group	n	Day 0	Day 7	Day14	Day 28
1	8	Right side: M1 defect Left side: control Euthanize			
2	8	Right side: M1 defect Left side: M1 control	Euthanize		
3	8	Right side: M1 defect Left side: M1 control		Euthanize	
4	9	Right side: M1 defect Left side: M1 control	Socket fluid	Socket fluid	Socket fluid Euthanize
5	8	Right side: M1 defect + BMM graft Left side: M1 control	Socket fluid	Socket fluid	Socket fluid Euthanize
6	9	Right side: M1 defect + BMM+SIM graft Left side: M1 control	Socket fluid	Socket fluid	Socket fluid Euthanize

Table 2: Agreements among Measurements from Coronal Images

	Left transaxial (ICC, 95% CI)	Right transaxial (ICC, 95% CI)
Mid-Buccal width	0.844 (-0.094, 0.995)	0.978 (0.645, 0.999)
Buccal Height	0.574 (-0.103, 0.983)	0.850 (-0.065, 0.996)
Mid-Palatal width	0.979 (0.666, 0.999)	0.882 (-0.326, 0.997)
Palatal Height	0.964 (0.522, 0.999)	0.829 (-0.105, 0.995)

Table 3: Agreements among Measurements from Sagittal Images

	Left Coronal (ICC, 95% CI)	Right Coronal (ICC, 95% CI)
Distal height	0.983 (0.660, 1.000)	0.997 (0.901, 1.000)
Mesial height	0.993 (0.478, 1.000)	0.999 (0.988, 1.000)

Table 4: Animal Weight

weight	Day 0 group		Day 7 group		Day 14 group		Day 28 group		Day 28 BMM group		Day 28 BMM+SIM group	
	Mean	**SD**	**Mean**	**SD**	**Mean**	**SD**	**Mean**	**SD**	**Mean**	**SD**	**Mean**	**SD**
Day 0	299.00	11.93	337.13	26.74	338.00	19.49	310.56	22.63	312.88	20.46	306.56	25.06
Day 7			329.00	22.85	335.88	13.92	304.89	22.86	308.75	22.17	309.11	20.81
Day 14					333.75	14.36	308.11	24.92	314.50	17.91	313.78	19.78
Day 28							312.33	21.98	314.63	16.09	307.00	20.13

Table 5: Significant Correlations

group	correlations	R value	p value
Day 7	Infiltrate Density and Buccal Height	0.74	0.037
	Degree of Inflammation and Buccal Height	0.80	0.016
	BSD and Osteoblast/perimeter	-0.83	0.01
Day 14	*none*		
Day 28	Infiltrate Density and Palatal Height	-0.78	0.013
	Osteoclast/perimeter and Palatal Height	-0.78	0.013
Day 28 BMM	Degree of Inflammation and BSD	-0.79	0.034
	Osteoclast/perimeter and Mean BMD	0.82	0.023
Day 28 BMM+SIM	Osteoblast/perimeter and Total Ridge Width	0.71	0.047

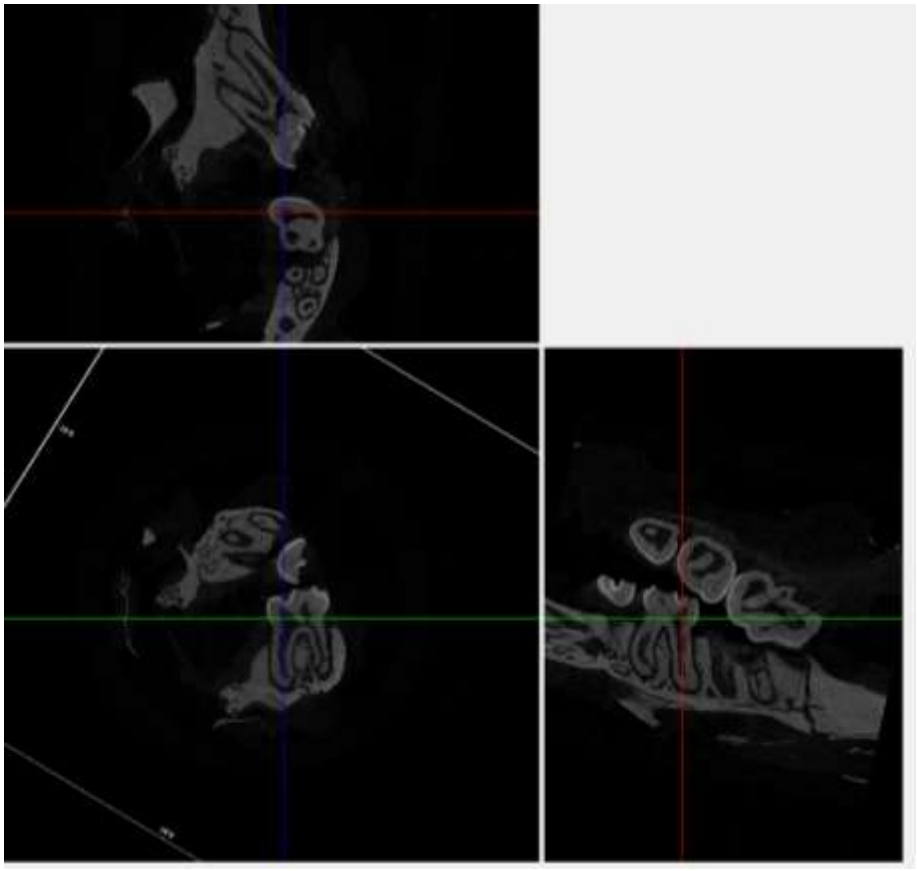

Figure 1: Image orientation for buccal and palatal measurements for Part 1 and 2.
Example of the image in the computer used to orient the 3D images (DataViewer, Bruker microCT, Kontich, Belgium). Note the red, green, and blue orientation lines corresponding to the three planes. The image orientation was manipulated for a coronal slice to measure the buccal and palatal alveolar bone. The coronal section (lower left) was imported into a secondary software used to obtain measurements (CTAn, Bruker microCT, Kontich, Belgium). **Top left:** sagittal view, “transaxial section”. **Bottom left:** superior view, “coronal section”. **Bottom right:** coronal view, “sagittal section”.

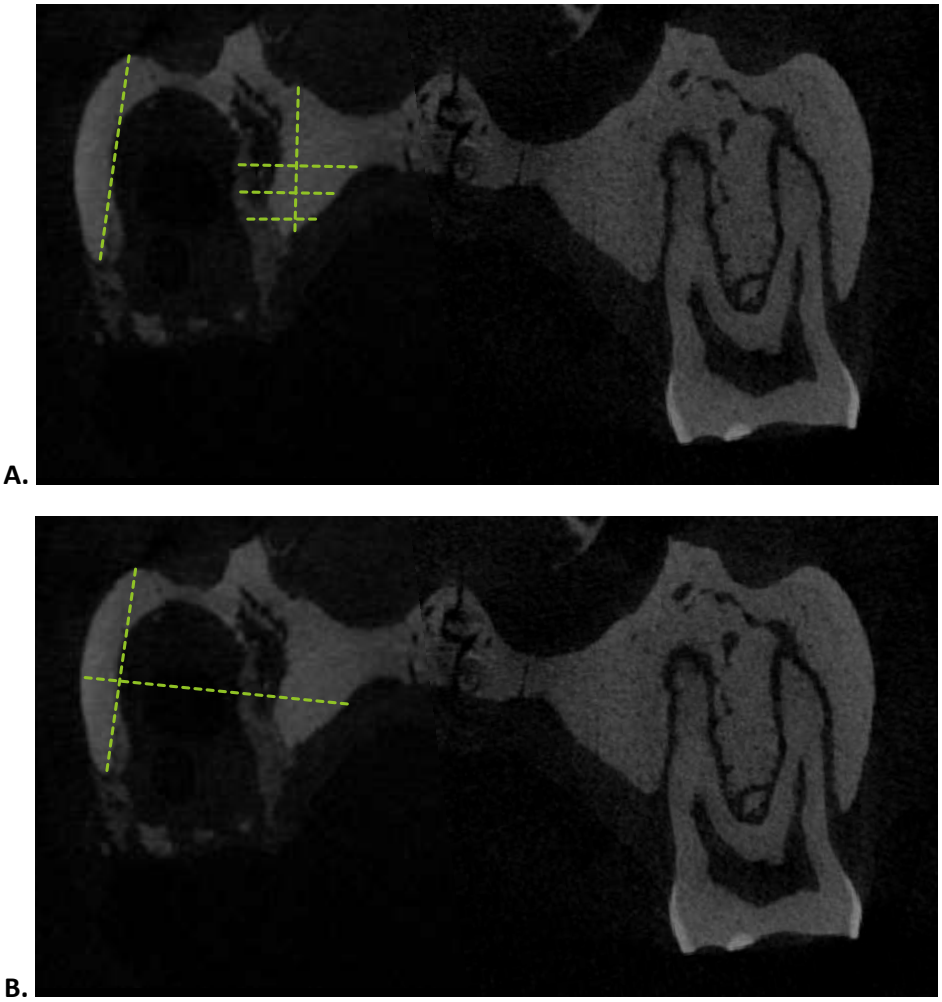

Figure 2: Buccal and palatal measurements for Part 1 and 2.
Example of the image in the software used to obtain measurements (CTAn, Bruker microCT, Kontich, Belgium) for buccal and palatal height and width. **A.** The height and width of the buccal cortical plate was measured from the superior and lateral aspect and advancing in 0.25 mm increments to the alveolar crest and then measuring the perpendicular width. The height and width of the palatal bone was measured from the most superior and mesial aspect that corresponded to the alveolar process of the maxilla. **B.** To measure total width, the mid-socket slice was used and the measurement was obtained by identifying the perpendicular line of greatest width buccal to palatal to the point 1.25 mm crestal from the most superior and lateral point of the buccal cortical plate.

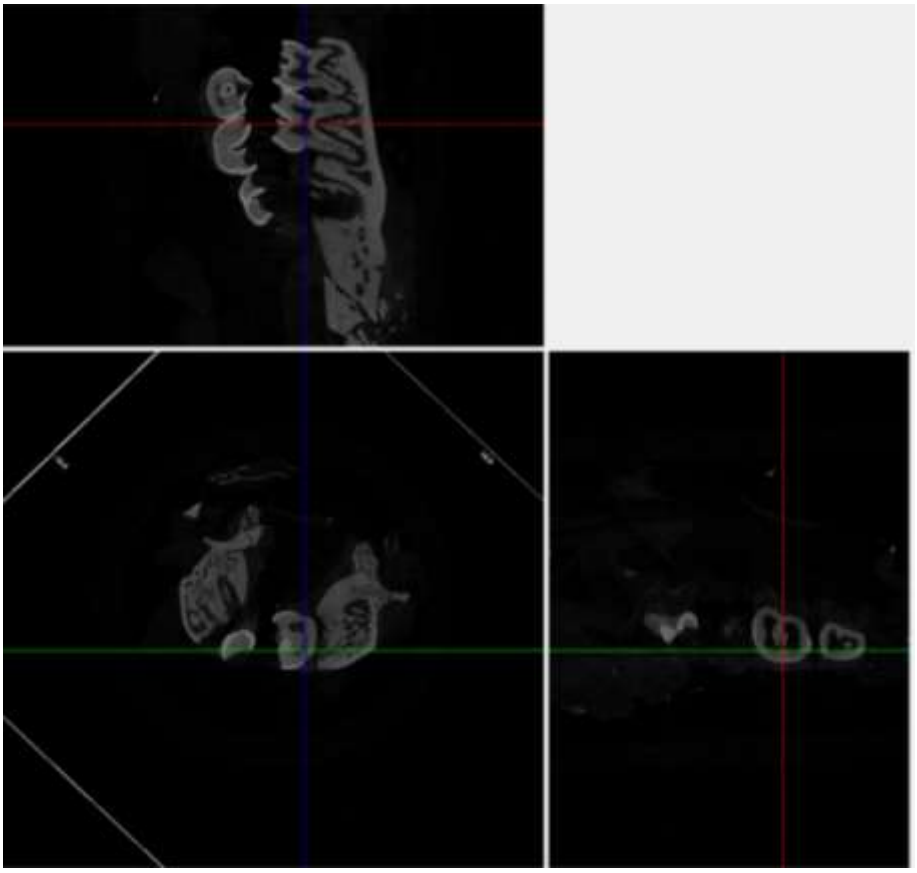

Figure 3: Image orientation for interproximal measurements for Part 1 and 2.
Example of the image in the computer used to orient the 3D images (DataViewer, Bruker microCT, Kontich, Belgium). Note the red, green, and blue orientation lines corresponding to the three planes. The image orientation was manipulated for a sagittal slice to measure the interproximal alveolar bone mesial and distal to M2. The coronal section (lower left) was imported into a secondary software used to obtain measurements (CTAn, Bruker microCT, Kontich, Belgium). **Top left:** sagittal view, "sagittal section". **Bottom left:** superior view, "coronal section". **Bottom right:** coronal view, "transaxial section".

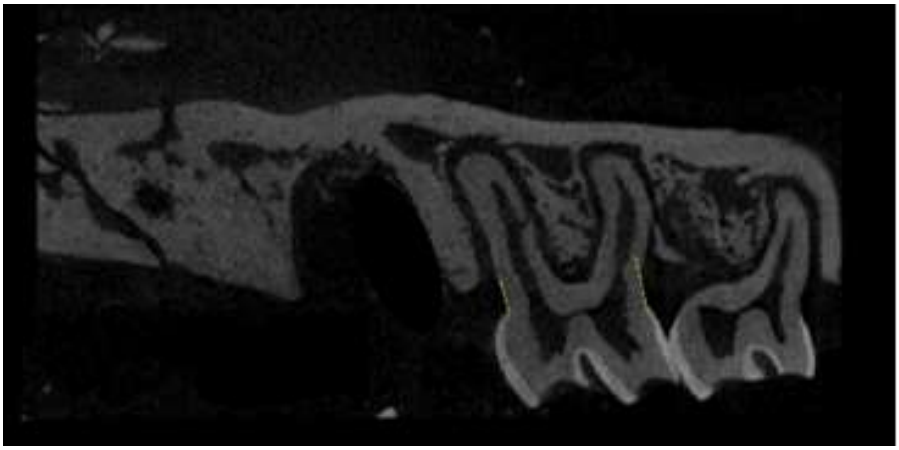

Figure 4: interproximal measurements for Part 1 and 2.
Representative 7 day specimen. Example of the image in the software used to obtain measurements (CTAn, Bruker microCT, Kontich, Belgium) for buccal and palatal height and width. The amount of interproximal bone loss was measured by tracing a line from the CEJ to the ABC parallel to the root structure and recording the linear distance until the most crestal portion of alveolar bone present.

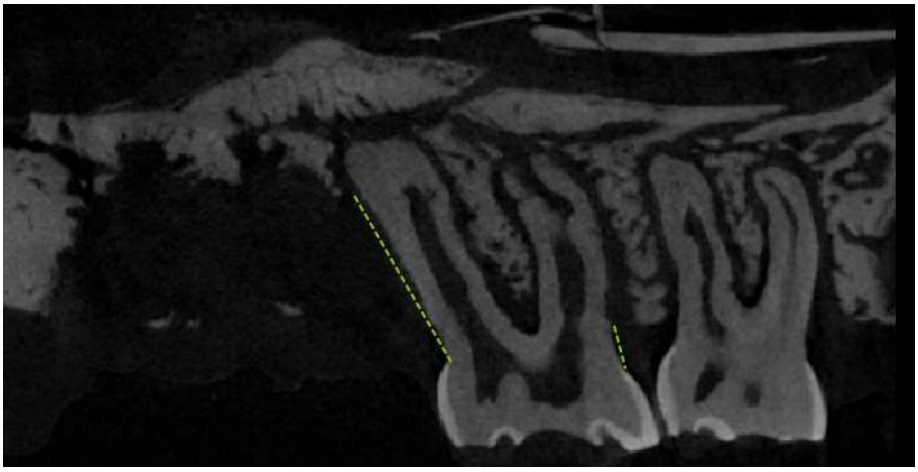

Figure 5: Interproximal measurements for Part 1 and Part 2.
Representative 28 day specimen. Example of the image in the software used to obtain measurements (CTAn, Bruker microCT, Kontich, Belgium) for interproximal bone height. The amount of interproximal bone loss was measured by tracing a line from the CEJ to the ABC parallel to the root structure and recording the linear distance until the most crestal portion of alveolar bone present.

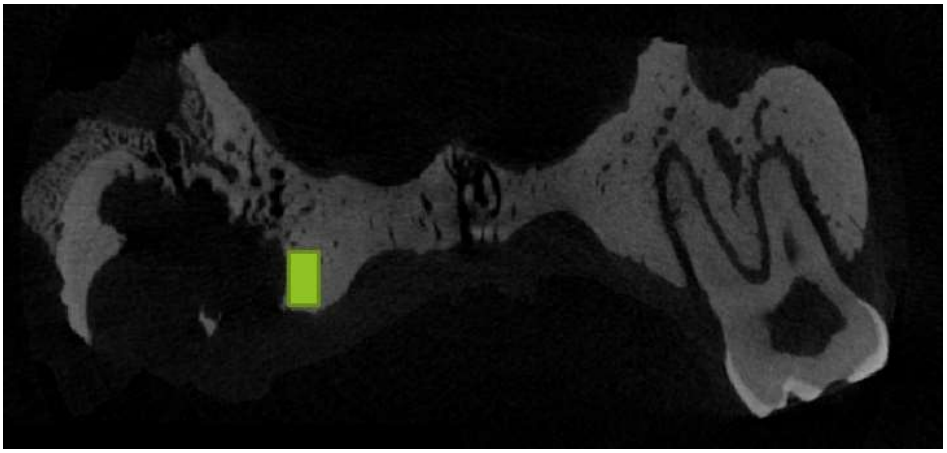

Figure 6: Volumetric measurements for Part 1 and Part 2.
Orientation of the image and definition of the ROI to determine volumetric and density values of bone quality. The ROI was confined to the palatal crest area using an orientation of the most cervical and with the closest approximation to the socket that a standard rectangular box (0.261 x 0.450 x 0.340 µm) could be placed.

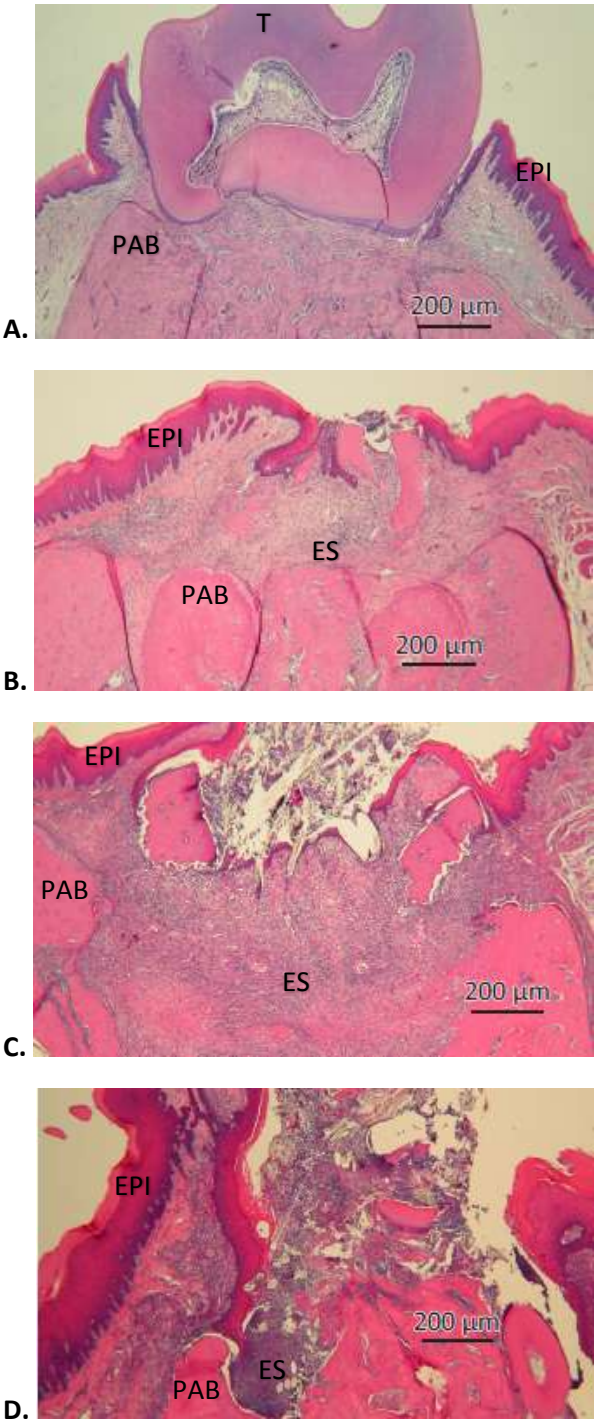

Figure 7: H&E Section for Part 1 and Part 2 inflammation grading. Low magnification.
Representative sections for the qualitative assessment of the relative degree of inflammation using a scale modified from Kristensen et al. (2008). The inflammation as rated 0 to 3. **A.** 0 = no inflammation, no inflammatory cells present, control/left side. **B.** 1 = mild inflammation, few, scattered inflammatory cells present. **C.** 2 = moderate inflammation, multiple clearly present inflammatory cells present. **D.** 3 = severe inflammation, massive presence of inflammatory cells. Note: this specimen was graded as moderate with focally severe inflammation. PAB = palatal alveolar bone. EPI = epithelium. ES = extraction socket base. T = tooth.

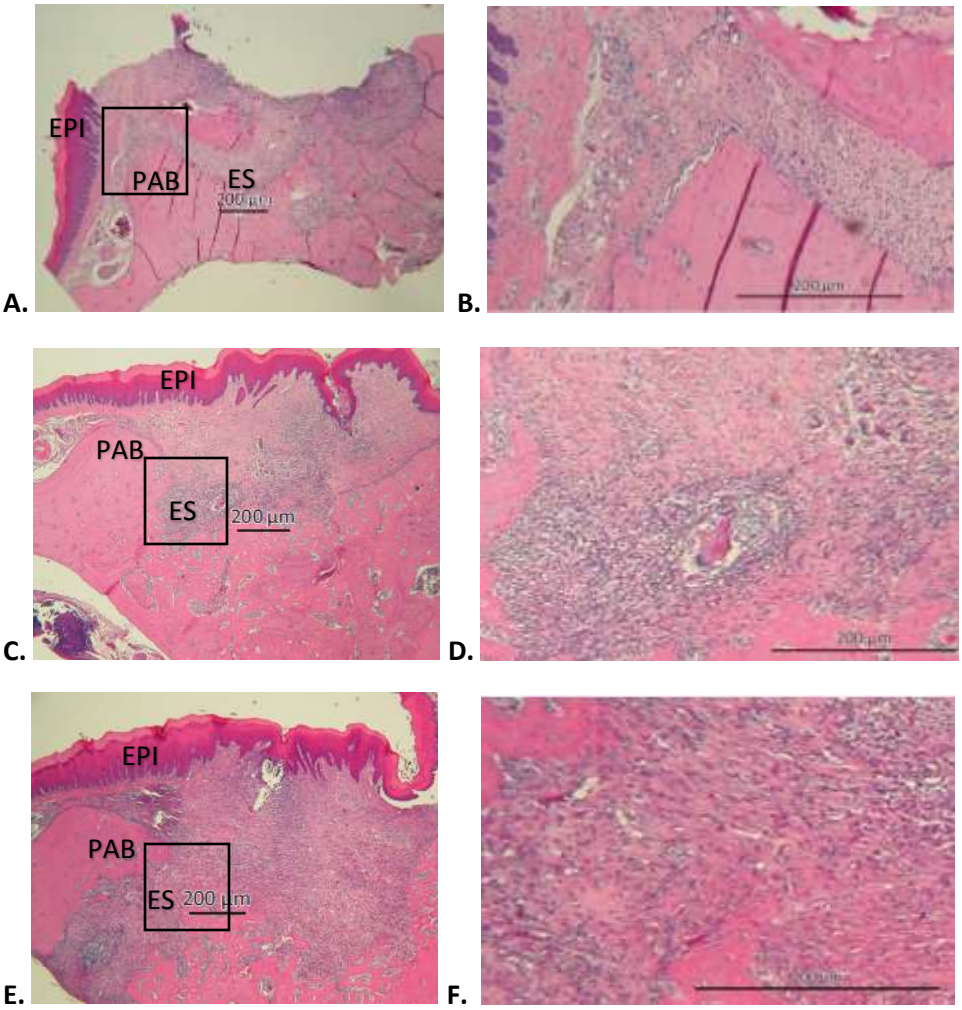

Figure 8: H&E Section for Part 1 and Part 2 inflammation staging. Low magnification. Representative sections for the qualitative assessment of the predominant inflammatory cell type present and a qualitative assessment regarding the stage of inflammation as also made in the same manner and scored as either acute, mixed acute and chronic, or chronic, based on the predominant cell types present The box represents the area of interest and the area of higher magnification. **A.** Acute inflammation characterized by neutrophilic infiltrate. **B.** Higher magnification of acute inflammation. **C.** Mixed acute and chronic inflammation with neutrophilic and lymphocytic infiltrate. **D.** Higher magnification of mixed acute and chronic inflammation. **E.** Chronic inflammation characterized by a predominantly lymphocytic infiltrate. **F.** Higher magnification of chronic inflammation. PAB = palatal alveolar bone. EPI = epithelium. ES = extraction socket base.

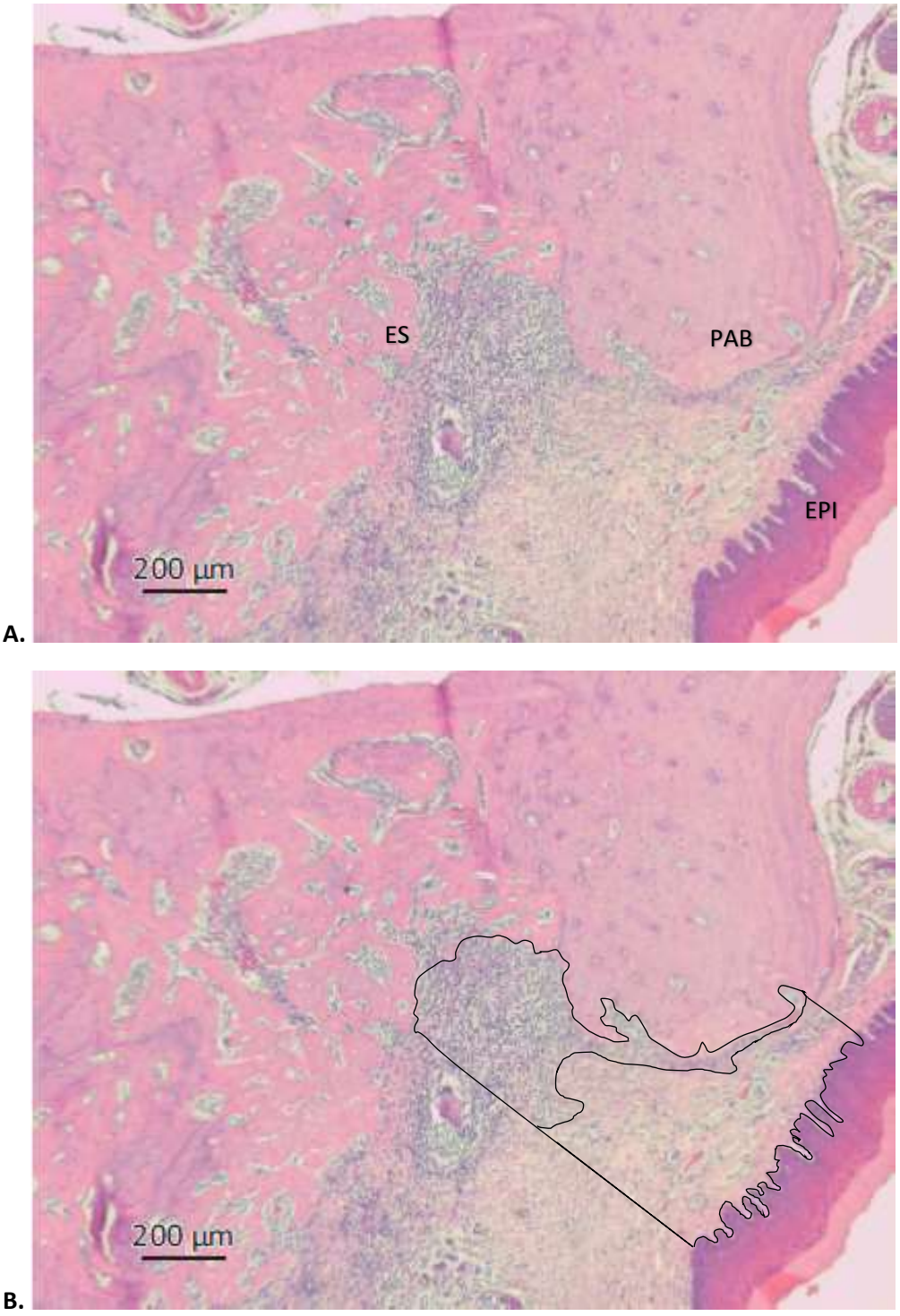

Figure 9: H&E Section for Part 1 and Part 2 inflammatory infiltrate. Low magnification.
Roughly 600,000 µm of connective tissue near the palatal crestal bone area was outlined and the area of inflammatory infiltrate contained within the outer perimeter was recorded. **A.** Raw image. **B.** Image with the traced total area of interest and the area of inflammation outlined. PAB = palatal alveolar bone. EPI = epithelium. ES = extraction socket base.

A.

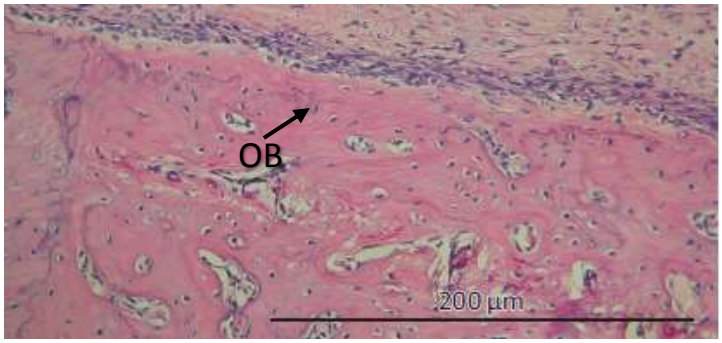

B.

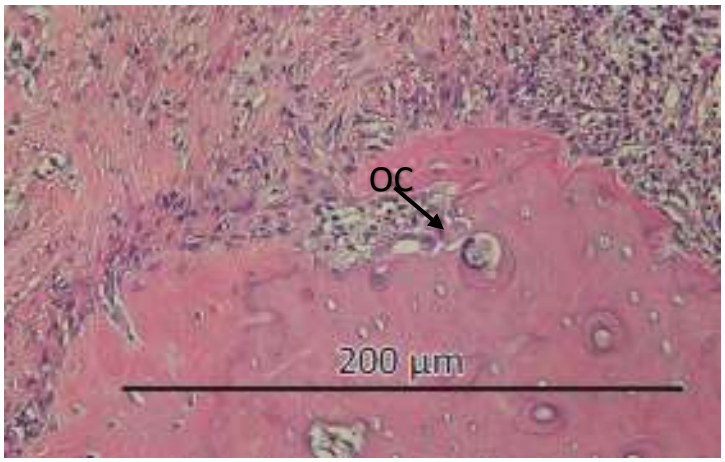

C.

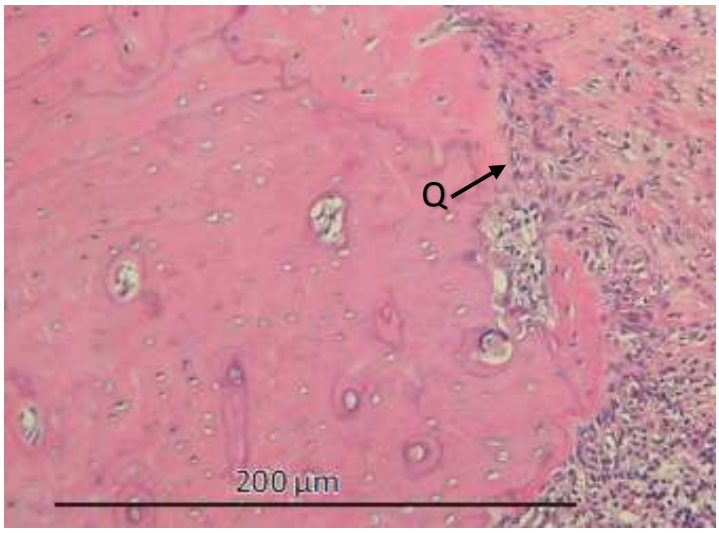

Figure 10: H&E for surface cells. High magnification.
Representative sections demonstrating the osteoblasts and osteoclasts on the bone surface. **A.** Osteoblasts (OB). Note: contain one nucleus and are found in a plump single layer on the surface of the bone. **B.** Osteoclasts (OC). Note: multinuclear appearance and their presence on the surface of accompanied by their resorptive area or Howship's lacunae. **C.** Quiescent surface (Q). Defined as surface not occupied by an active osteoblast or osteoclast.

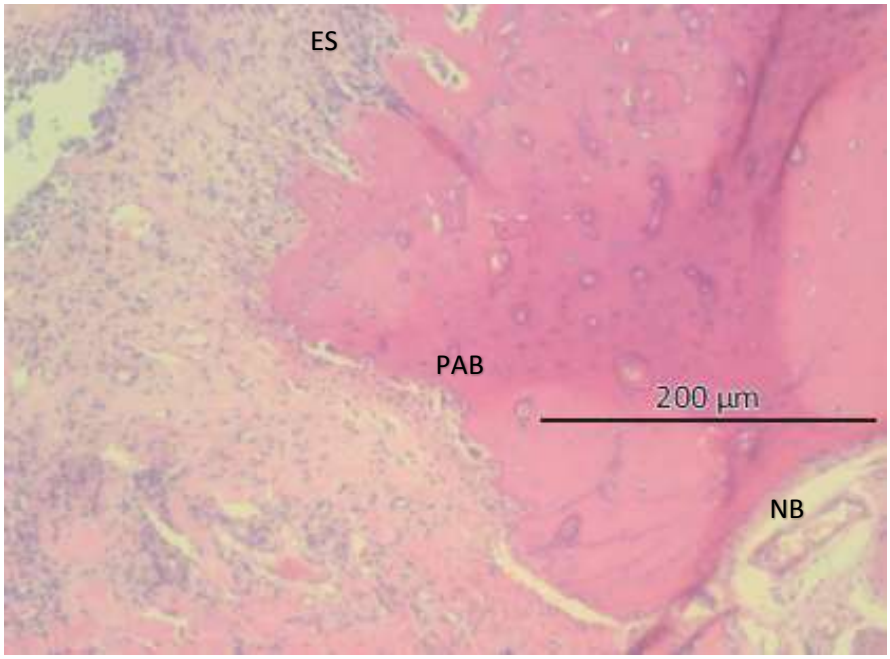

A.

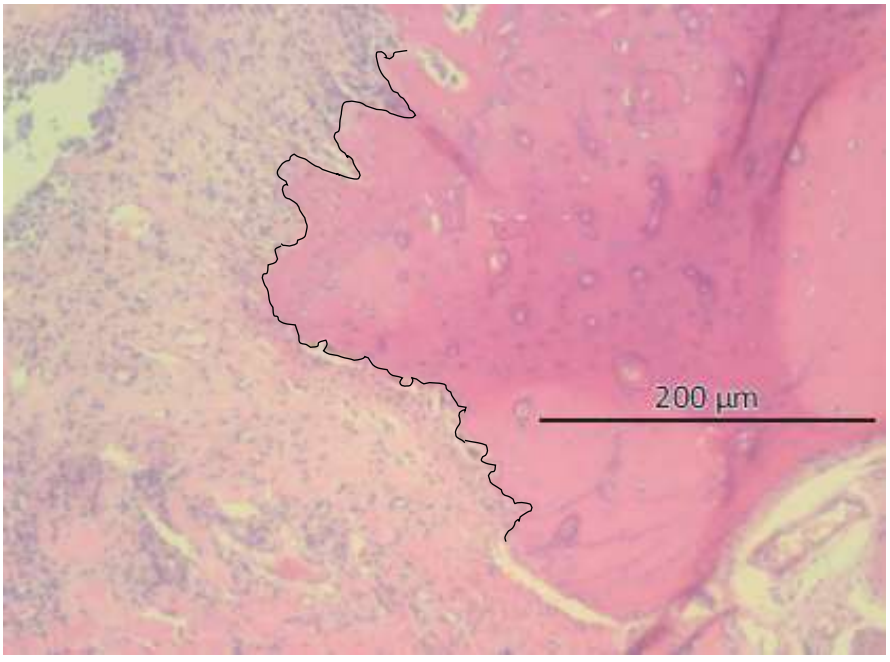

B.

Figure 11: H&E Section for Part 1 and Part 2 bone surface cells. High magnification.
Roughly 4000 µm of palatal crestal bone surface perimeter was outlined and the cumulative perimeter of bone surface area lined by osteoblasts and osteoclasts was recorded and non-osteoblast or osteoclast perimeter (by subtraction of osteoblast and osteoclast perimeter from the total perimeter) was described as quiescent. A. Raw image. B. Image with the total perimeter of bone surface of interest traced and the regions corresponding to osteoblasts and osteoclasts lining the perimeter. PAB = palatal alveolar bone. NB = neurovascular bundle on palatal aspect. ES = extraction socket.

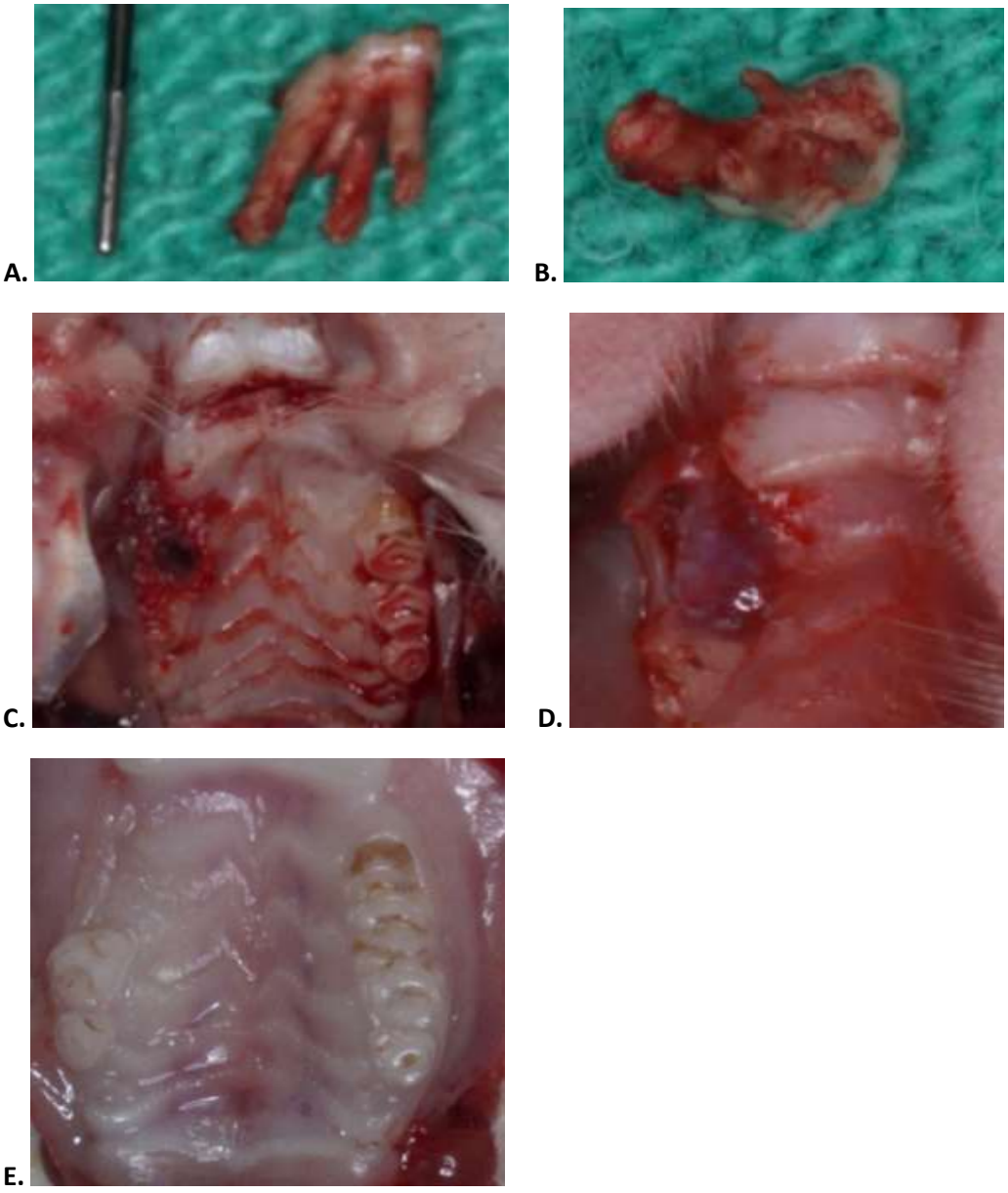

Figure 12: Part 1 Extraction and Healing.
A. Extracted right maxillary first molar with a Marquis color-code probe with 3mm calibrations for size comparison. **B.** Apical view of extracted right maxillary first molar to demonstrate presence and divergence of the 5 roots. **C.** View of the right maxillary molar extraction site and defect. **D.** The extraction site sealed with cyanoacrylate adhesive (PeriAcryl 90, GluStitch Inc, Delta, BC, Canada). **E.** Extraction site after 28 days of healing. Note the evidence of a reduction in the height and width of the alveolar ridge surrounding the socket.

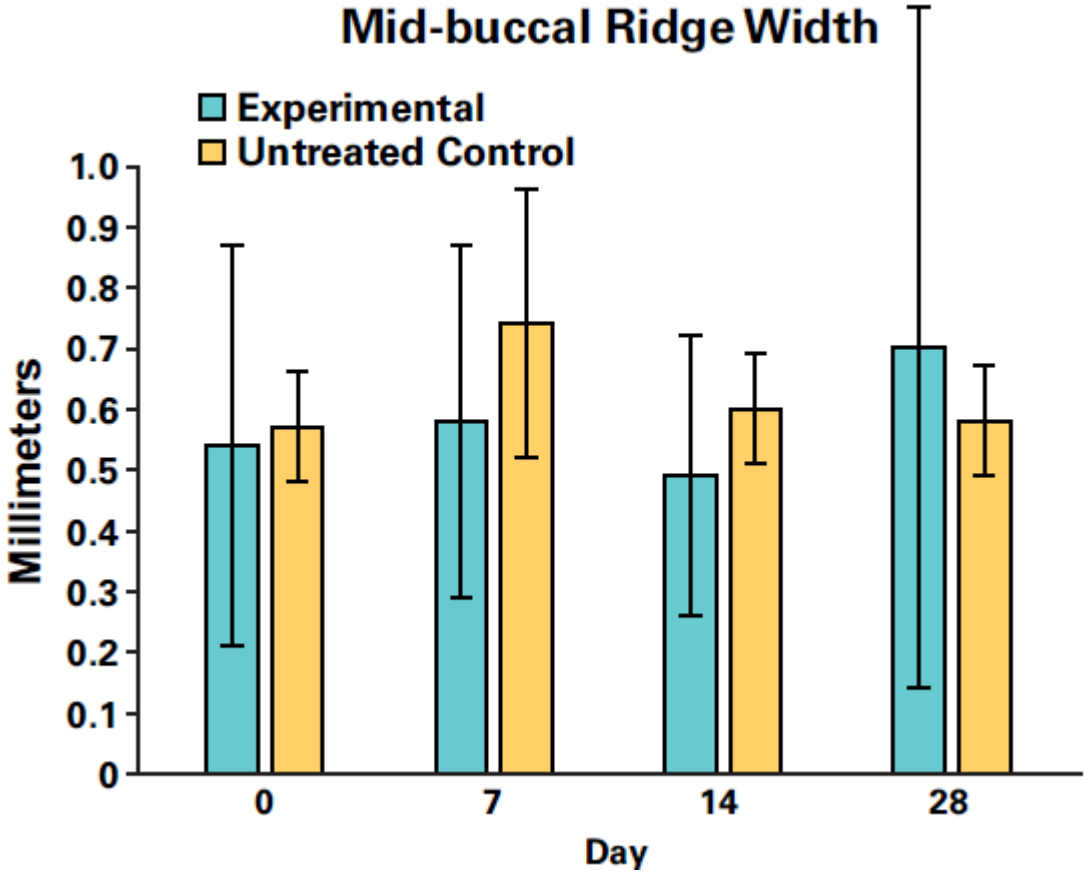

Figure 13: Part 1 Mid-Buccal Width.
Group comparisons and experimental and control for linear measurement of buccal width (mean ± standard deviation). No statistical differences found.

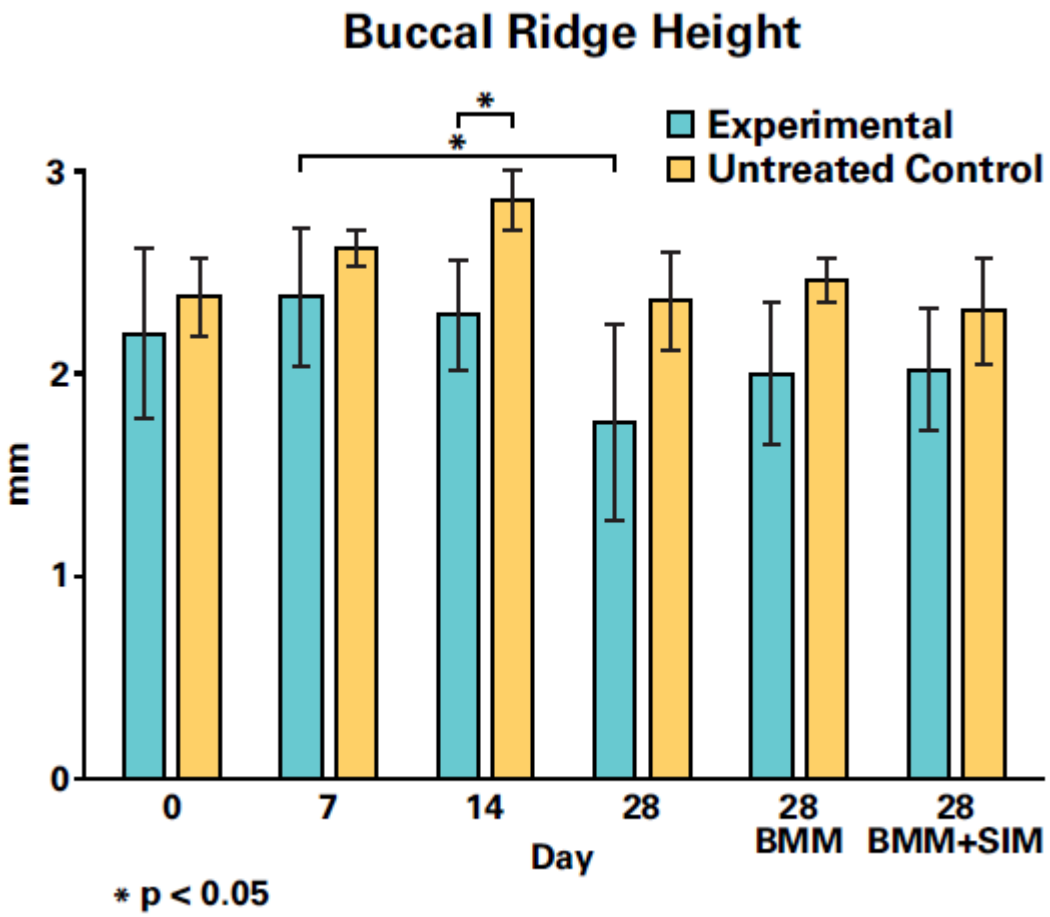

Figure 14: Buccal Height for Parts 1 and 2.
Group comparisons and experimental and control for linear measurement of buccal height (mean ± standard deviation). Statistical differences noted.

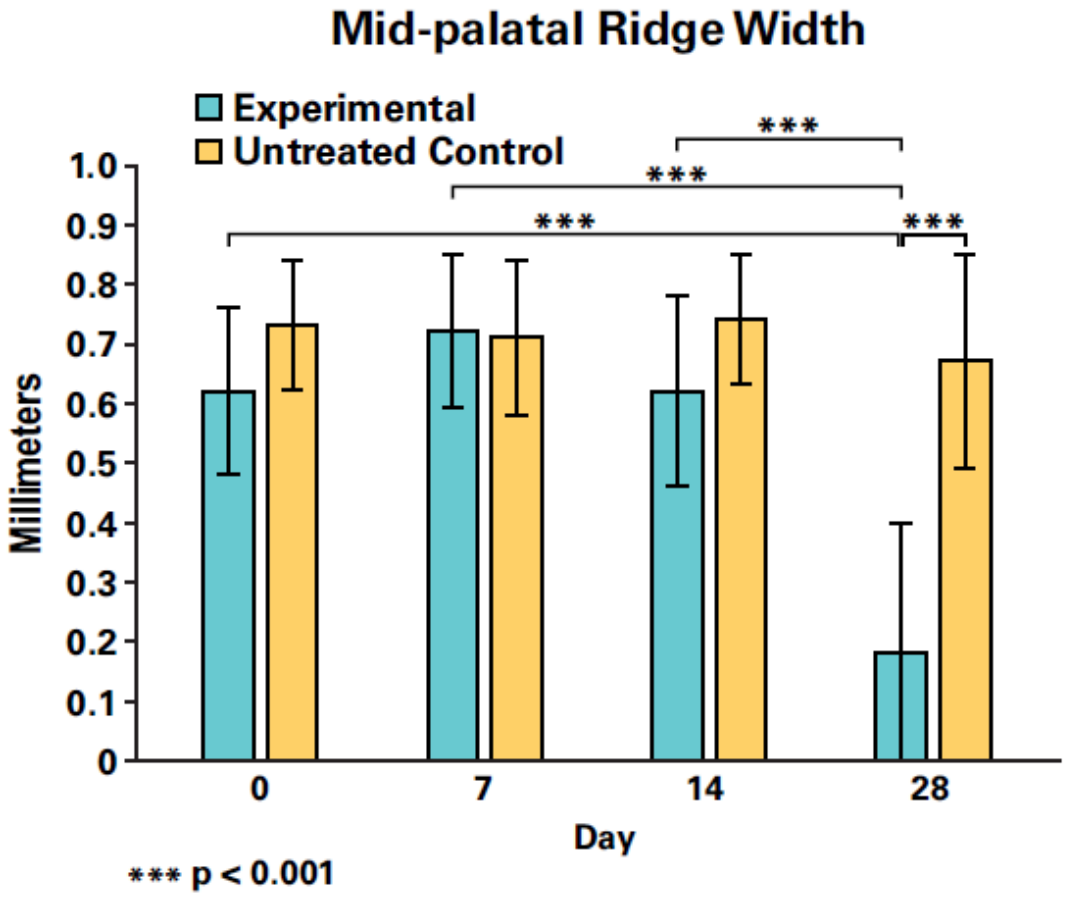

Figure 15: Part 1 Mid-Palatal Width.
Group comparisons and experimental and control for linear measurement of palatal width (mean ± standard deviation). Statistical differences noted.

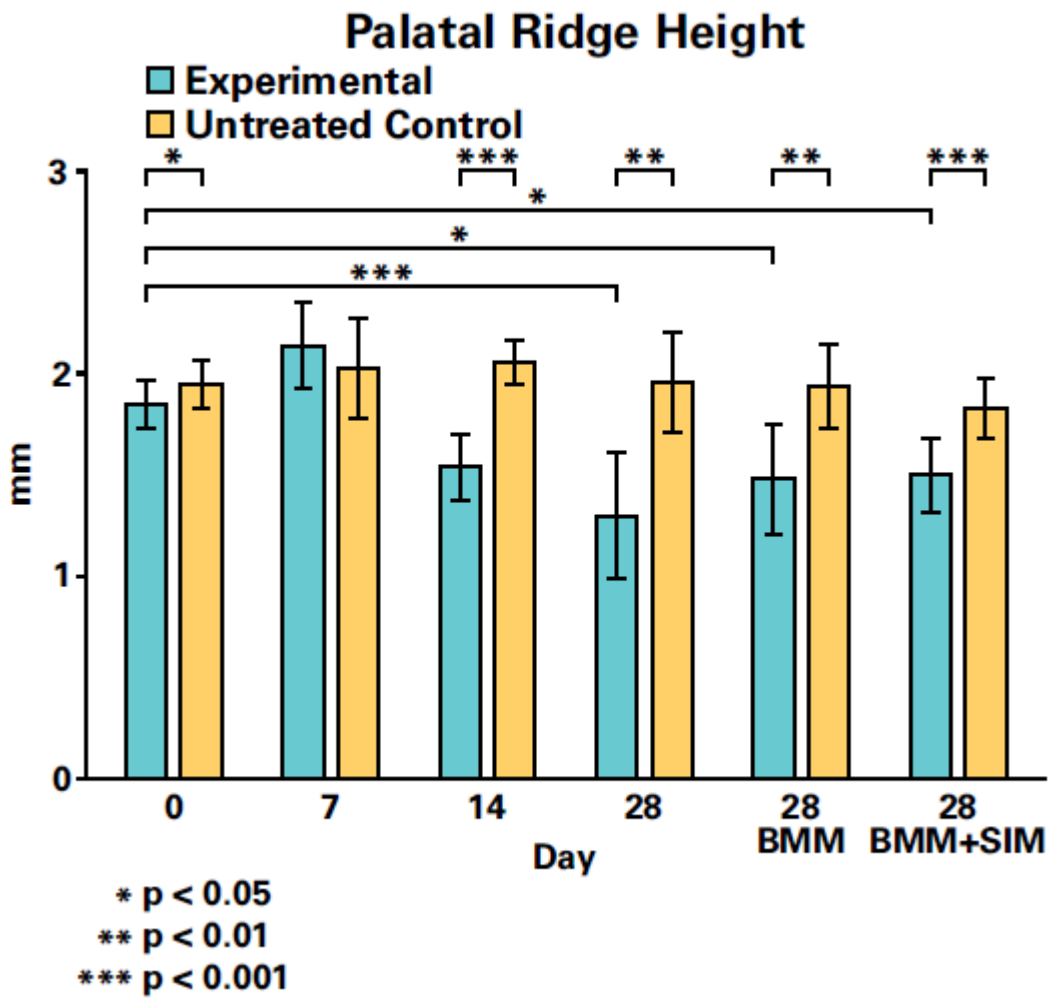

Figure 16: Palatal Height for Parts 1 and 2.
Group comparisons and experimental and control for linear measurement of palatal height (mean ± standard deviation). Statistical differences noted.

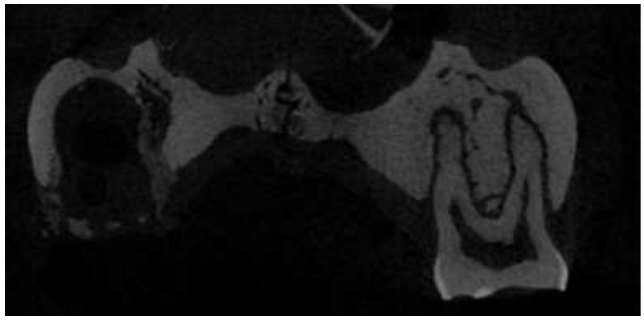

A.

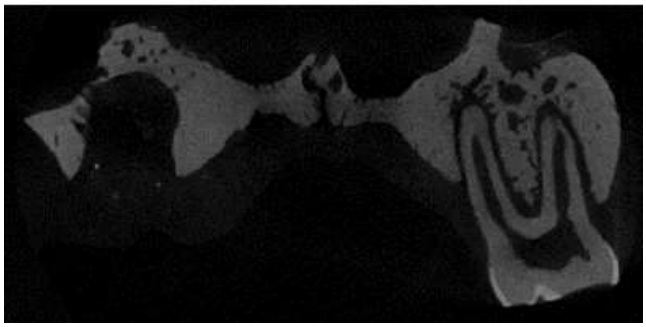

B.

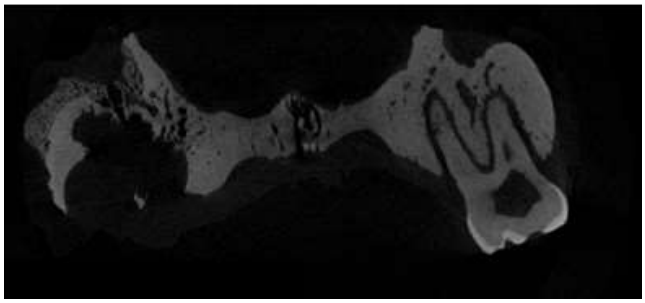

C.

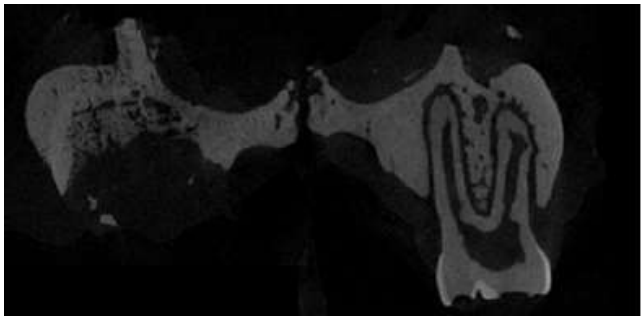

D.

Figure 17: Representative µCT for buccal and palatal bone loss from Part 1.
A. Day 0. B. Day 7. C. Day 14. D. Day 28.

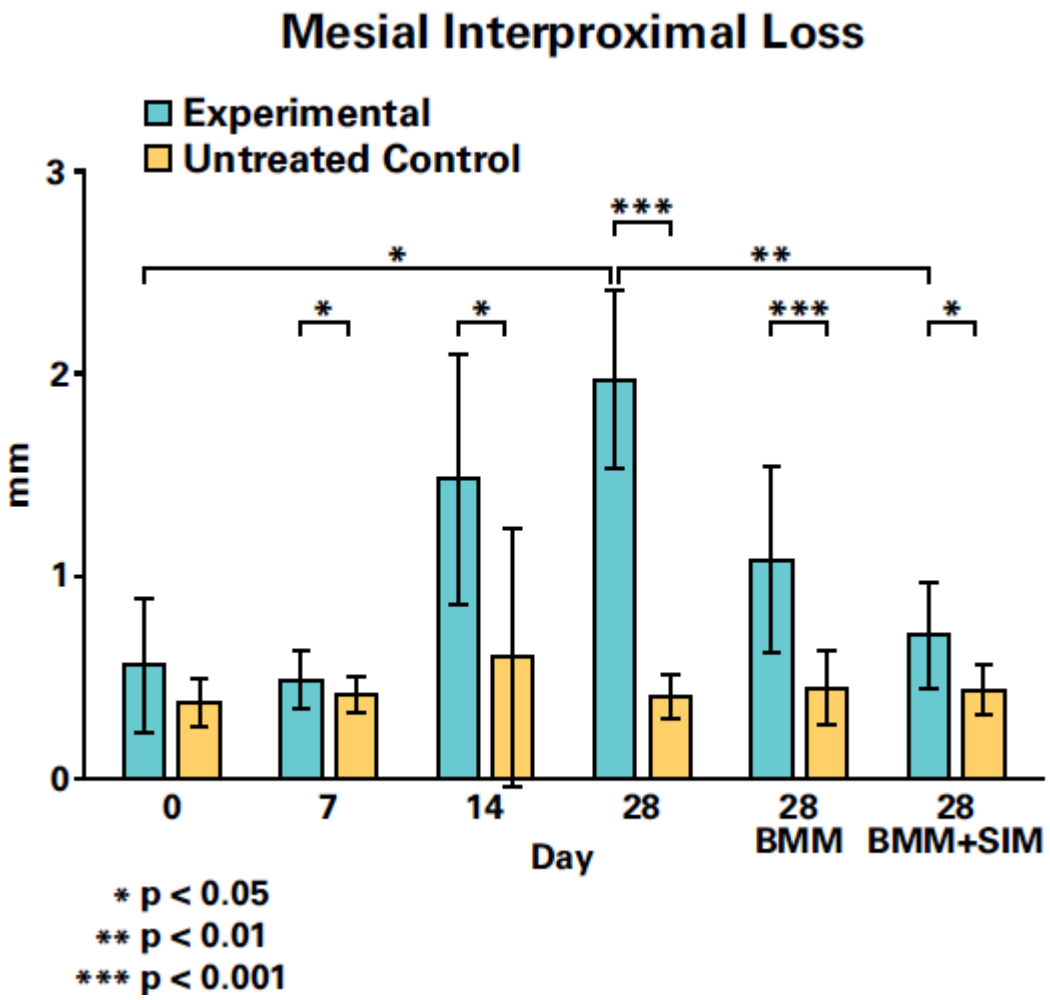

Figure 18: Loss of interproximal bone mesial to M2 for Parts 1 and 2.
Group comparisons and experimental and control for linear measurement of loss of interproximal bone on the mesial aspect of M2, or distal to the extraction socket (mean ± standard deviation). Statistical differences noted.

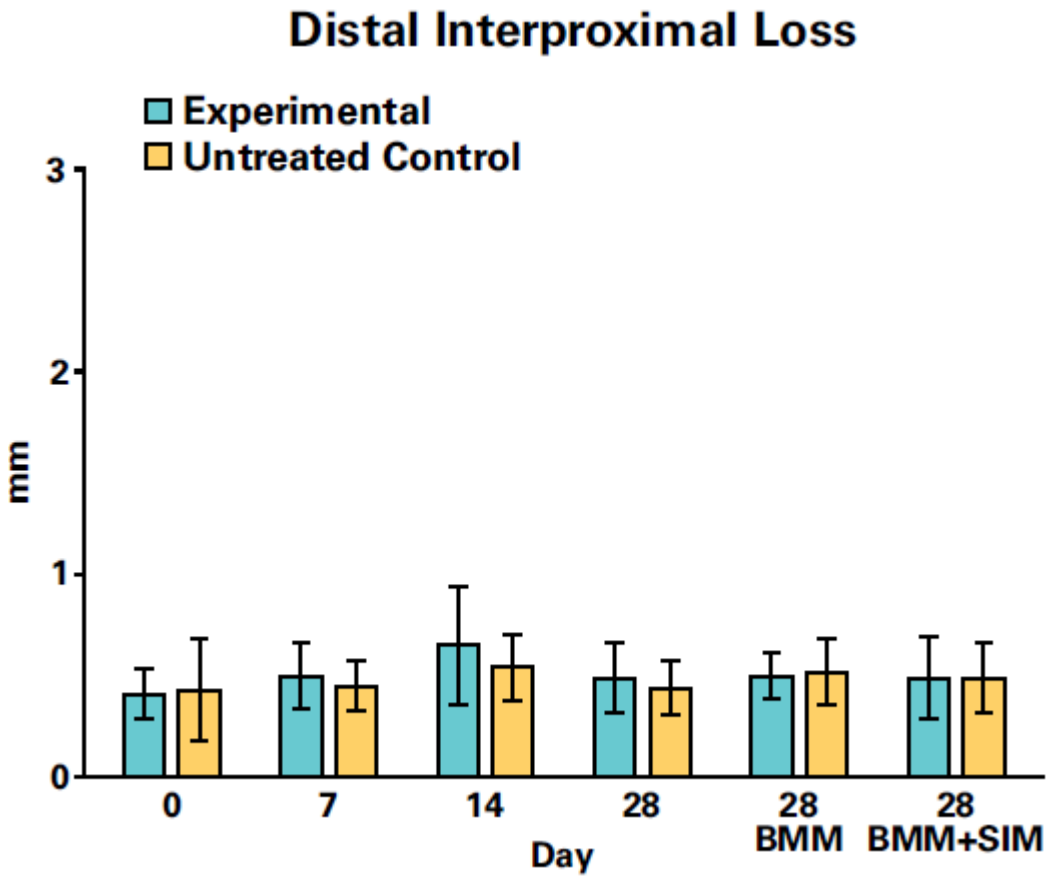

Figure 19: Loss of interproximal bone distal to M2 for Parts 1 and 2.
Group comparisons and experimental and control for linear measurement of loss of interproximal bone on the distal aspect of M2 (mean ± standard deviation). Statistical differences noted.

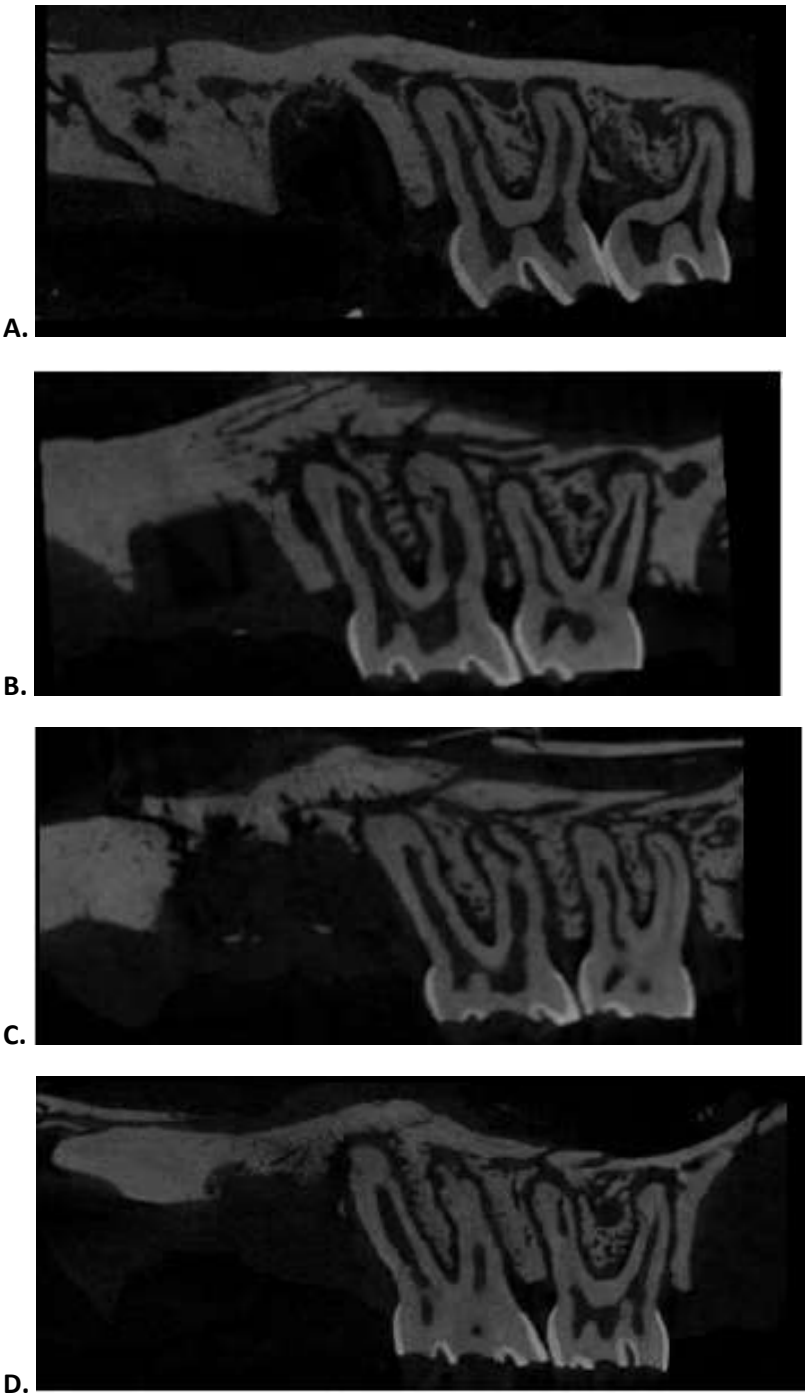

Figure 20: Representative µCT for interproximal bone loss from Part 1.
A. Day 0. B. Day 7. C. Day 14. D. Day 28.

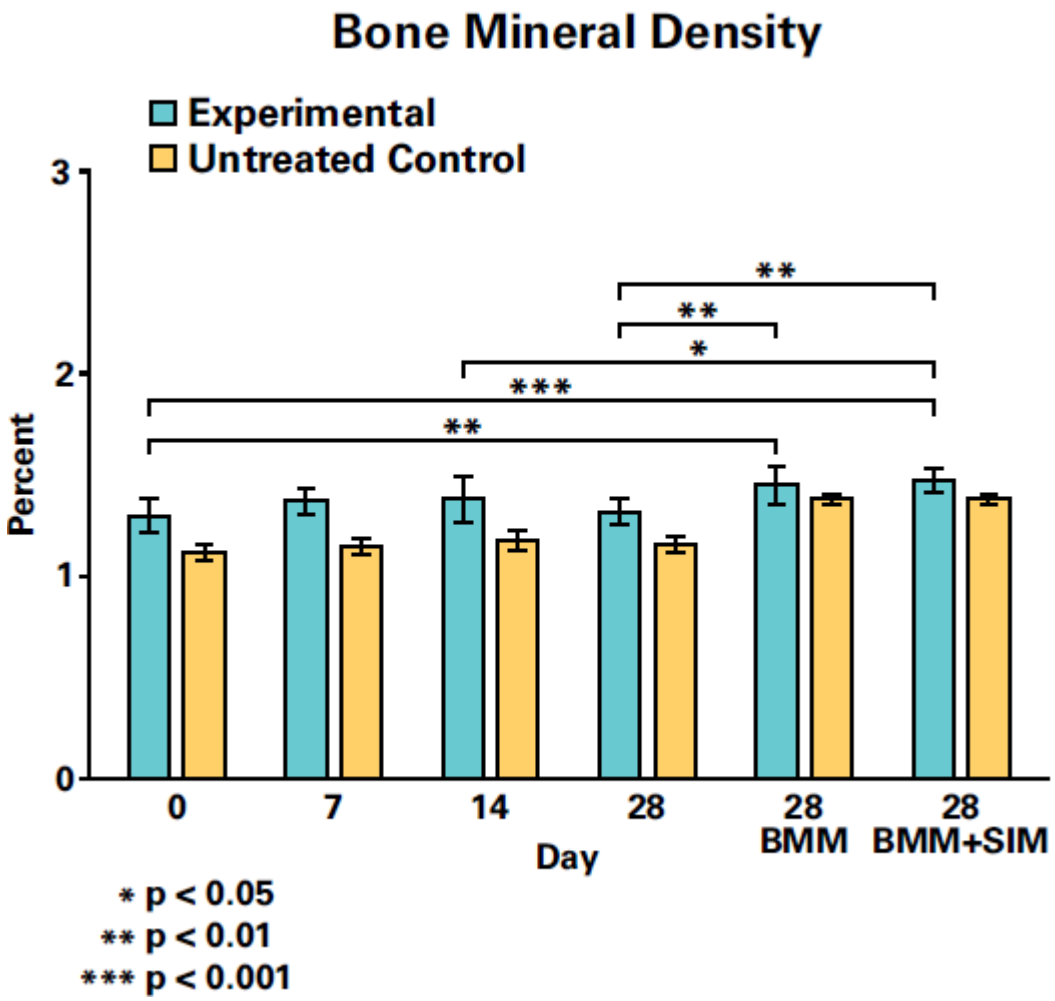

Figure 21: Bone Mineral Density.
Group comparisons and experimental and control for volumetric measurement of mean bone mineral density (mean ± standard deviation). Statistical differences noted.

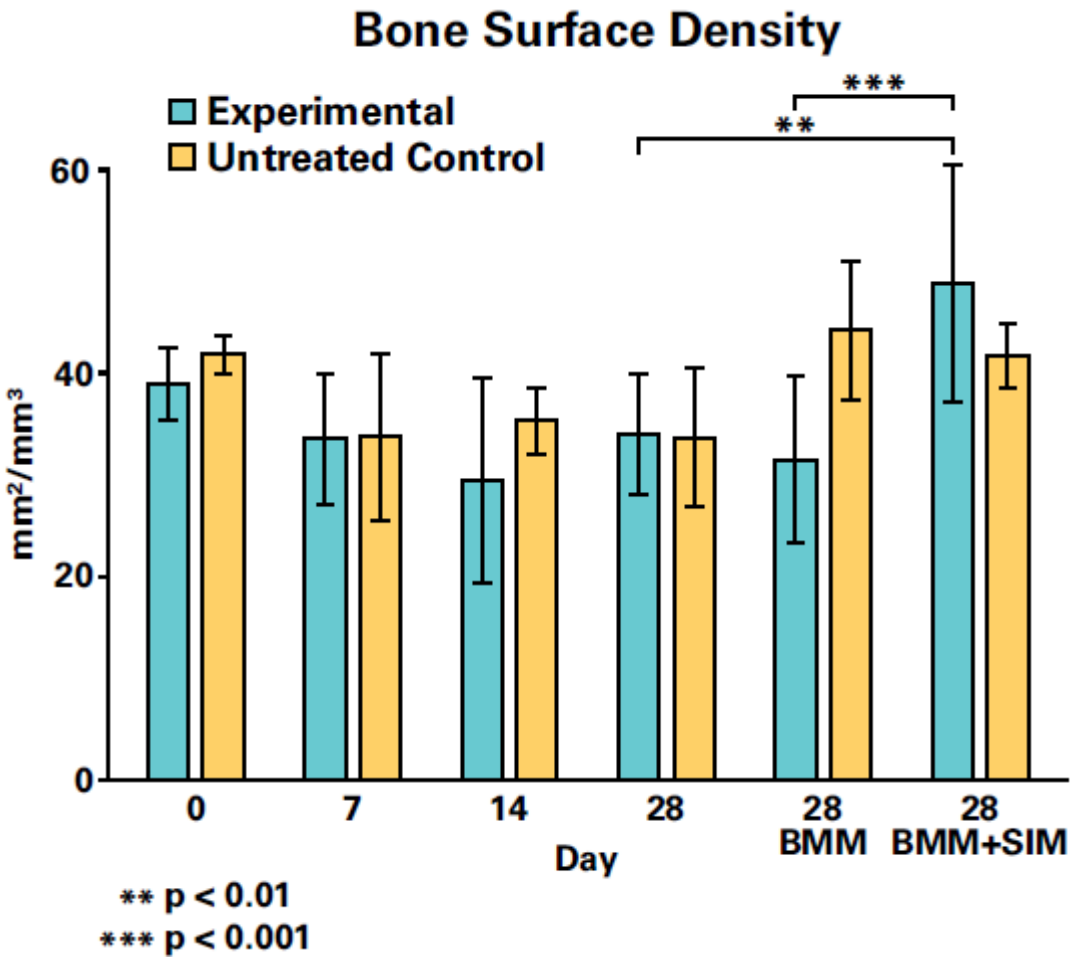

Figure 22: Bone Surface Density.
Group comparisons and experimental and control for volumetric measurement of bone surface density calculated as bone surface (BS)/ trabecular volume (TV) (mean ± standard deviation). Statistical differences noted.

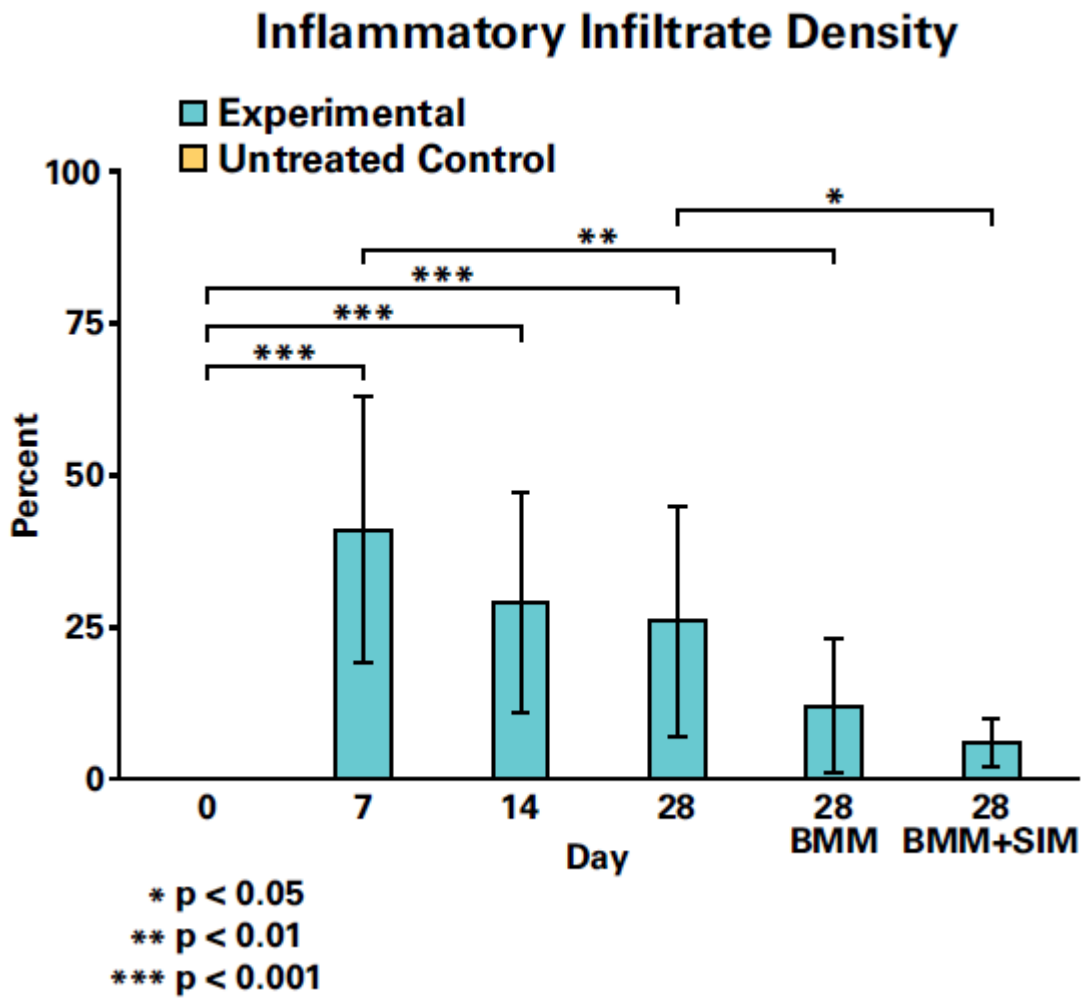

Figure 23: Inflammatory Infiltrate Density.
Group comparisons and experimental and control for histologic measurement of inflammatory infiltrate density (mean ± standard deviation). Statistical differences noted.

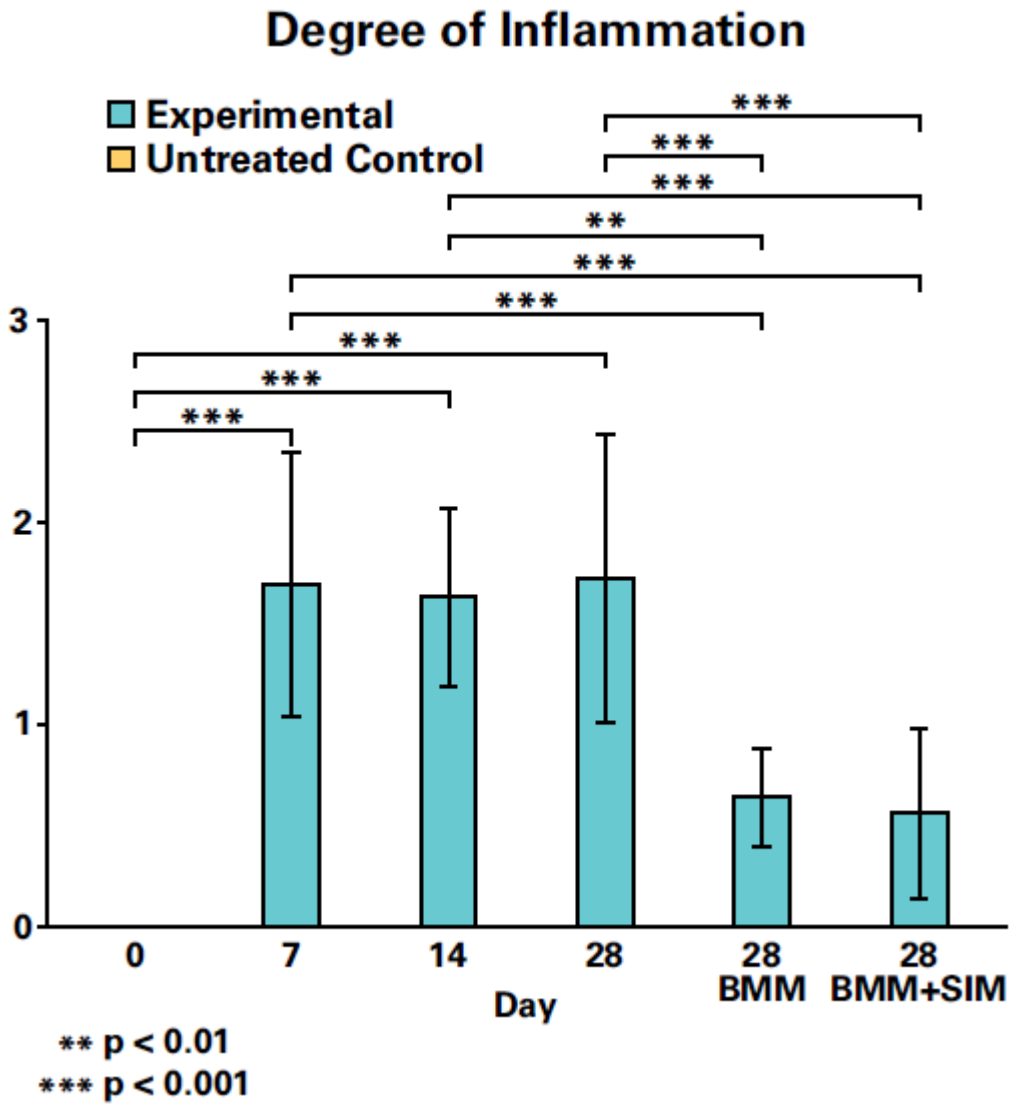

Figure 24: Degree of Inflammation.
Group comparisons and experimental and untreated control for histologic measurement of degree of inflammation (mean ± standard deviation). Statistical differences noted.

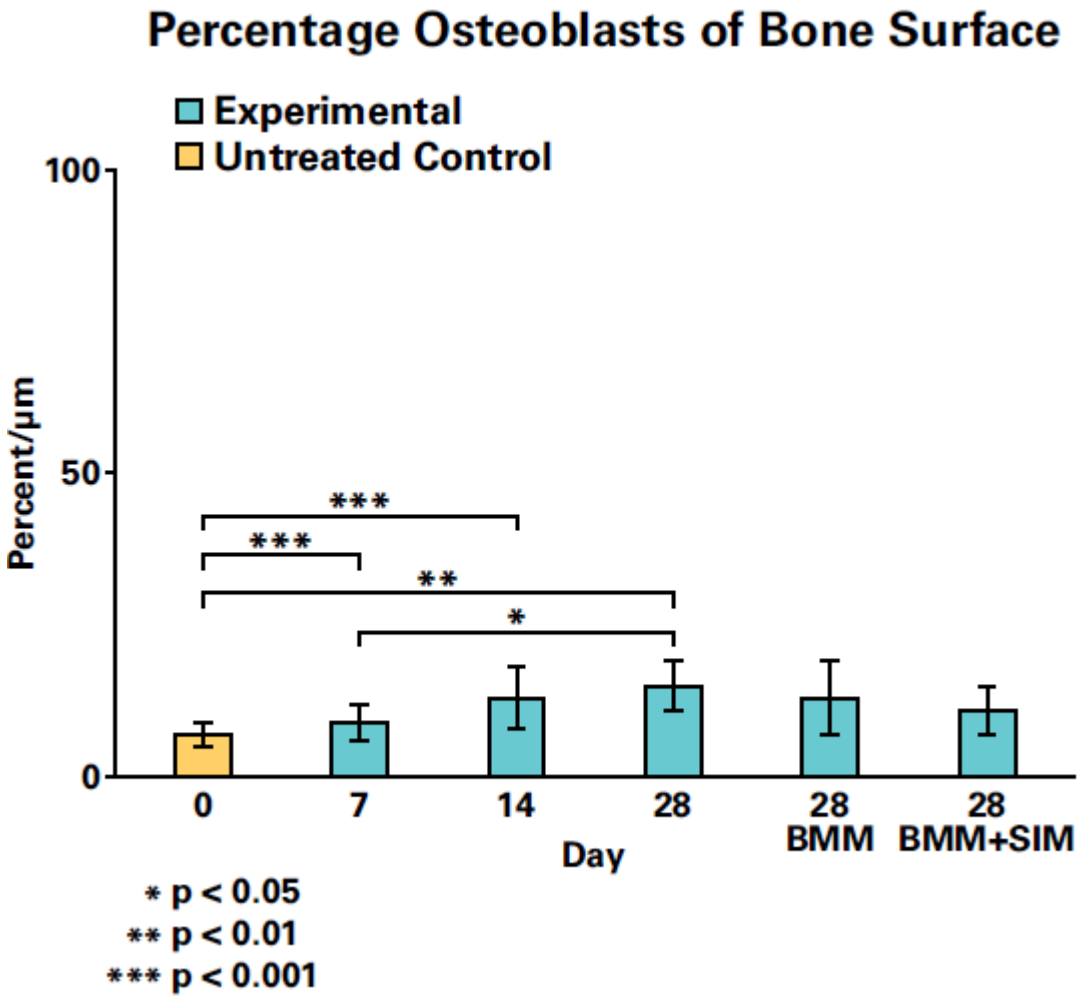

Figure 25: Percentage of Osteoblasts on Bone Surface.
Group comparisons and experimental and untreated control for histologic measurement of percentage of osteoblasts on bone surface (mean ± standard deviation). Statistical differences noted.

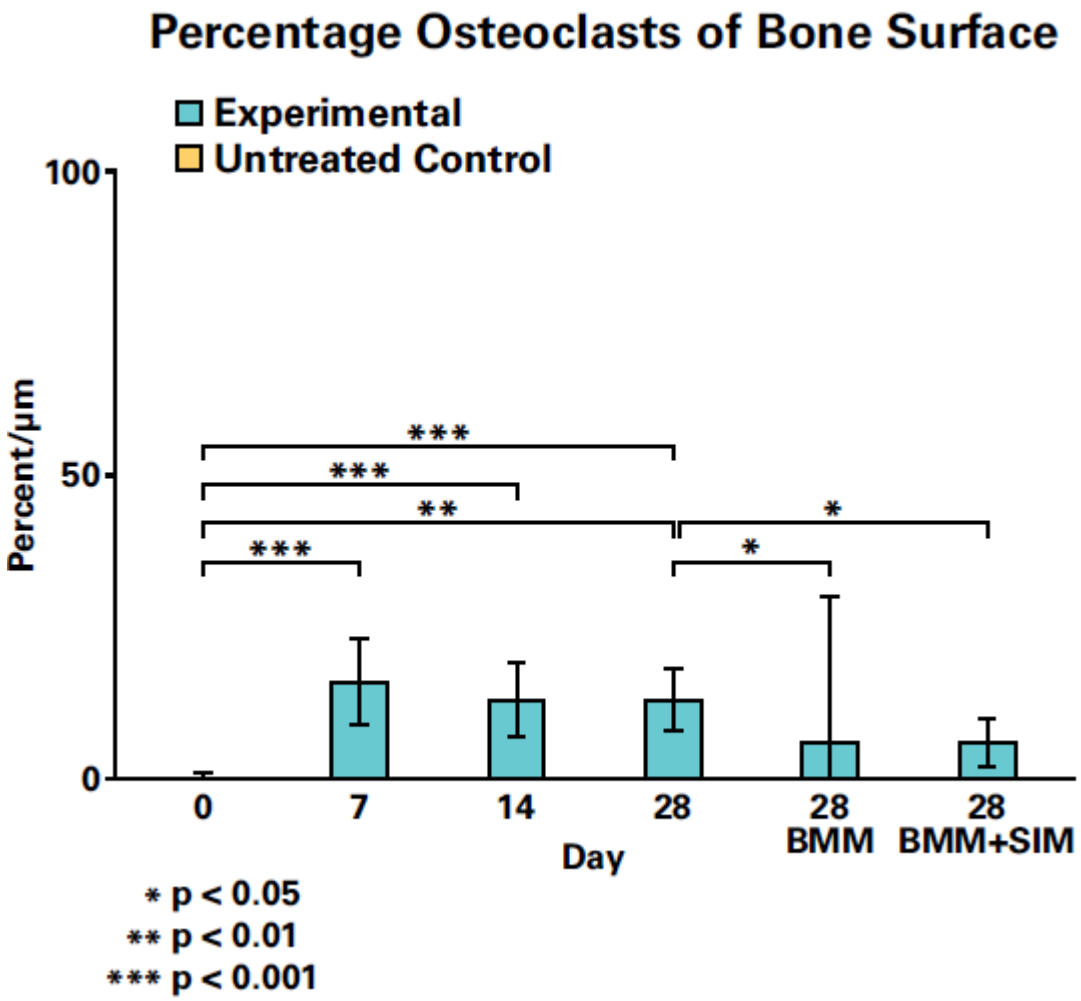

Figure 26: Percentage of Osteoclasts on Bone Surface.
Group comparisons and experimental and untreated control for histologic measurement of percentage of osteoclasts on bone surface (mean ± standard deviation). Statistical differences noted.

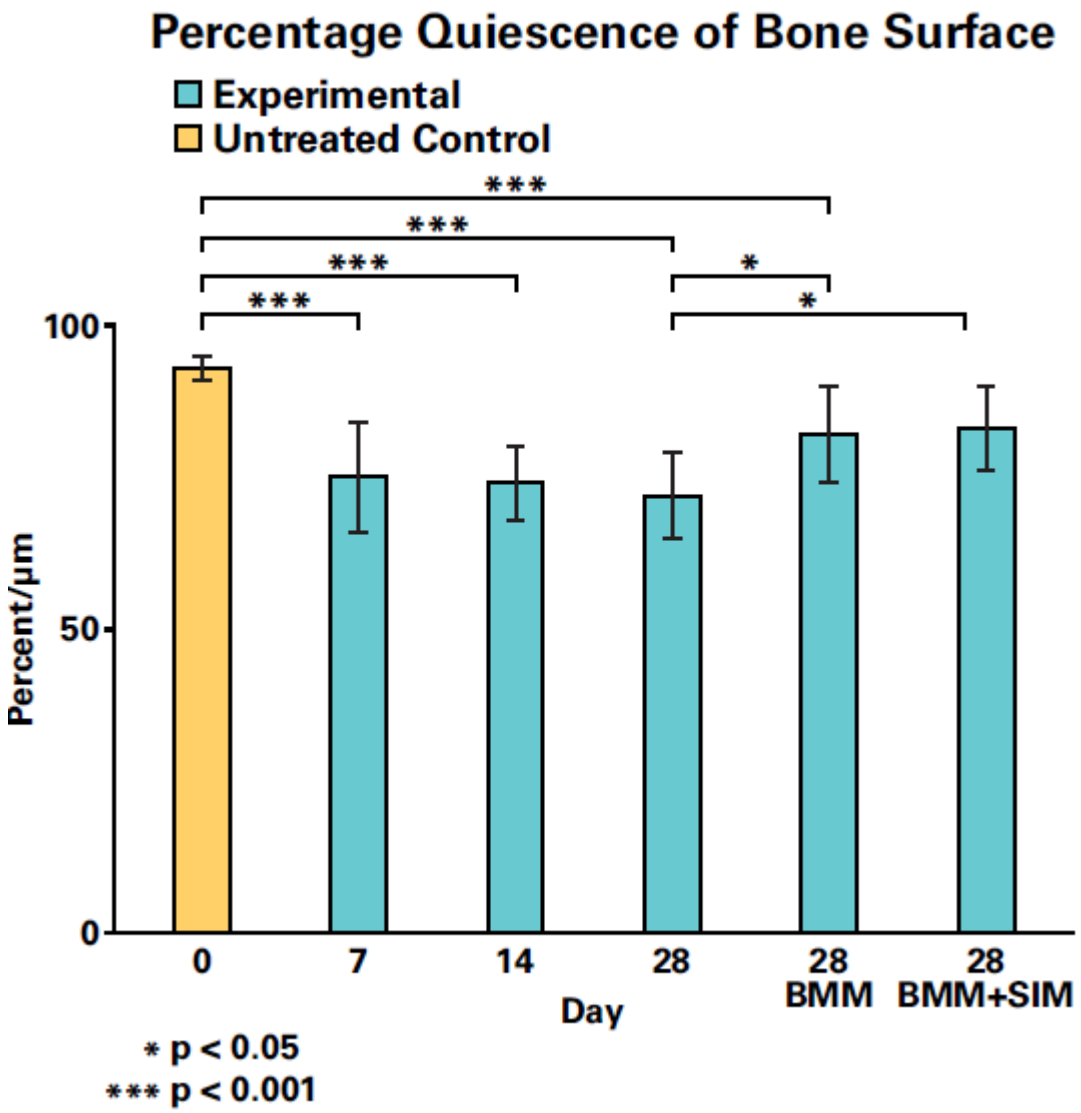

Figure 27: Bone Surface Quiescence.
Group comparisons and experimental and untreated control for histologic measurement of bone surface quiescence (mean ± standard error). Statistical differences noted.

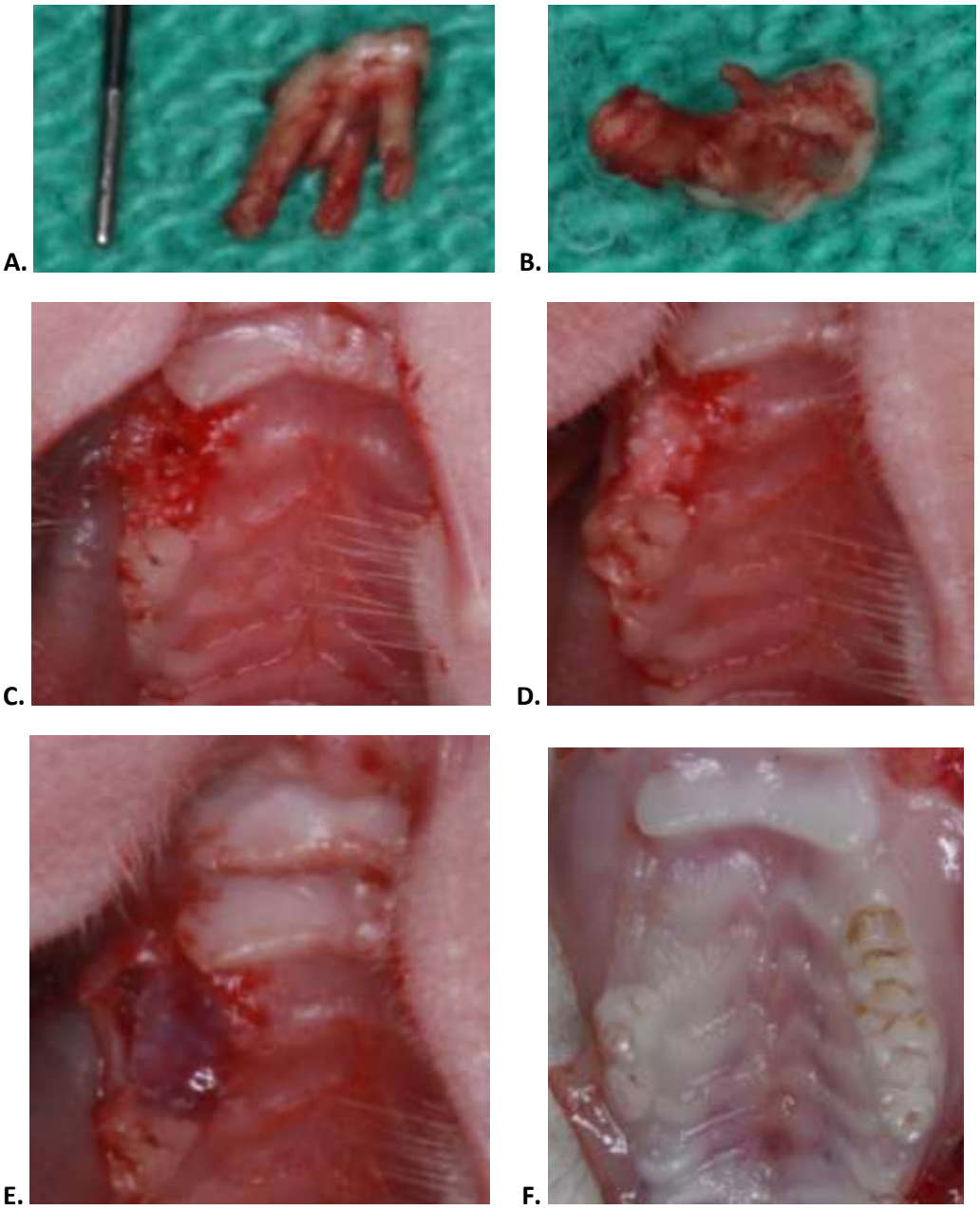

Figure 28: Part 2 Extraction and Healing.
A. Extracted right maxillary first molar with a Marquis color-code probe with 3mm calibrations for size comparison. **B.** Apical view of extracted right maxillary first molar to demonstrate presence and divergence of the 5 roots. **C.** View of the right maxillary molar extraction. **D.** Site grafted with BMM + SIM with 0.01 g of graft material placed in the defect. **E.** The extraction site and graft material sealed with cyanoacrylate adhesive (PeriAcryl 90, GluStitch Inc, Delta, BC, Canada). **F.** The healed, grafted site at 28 days.

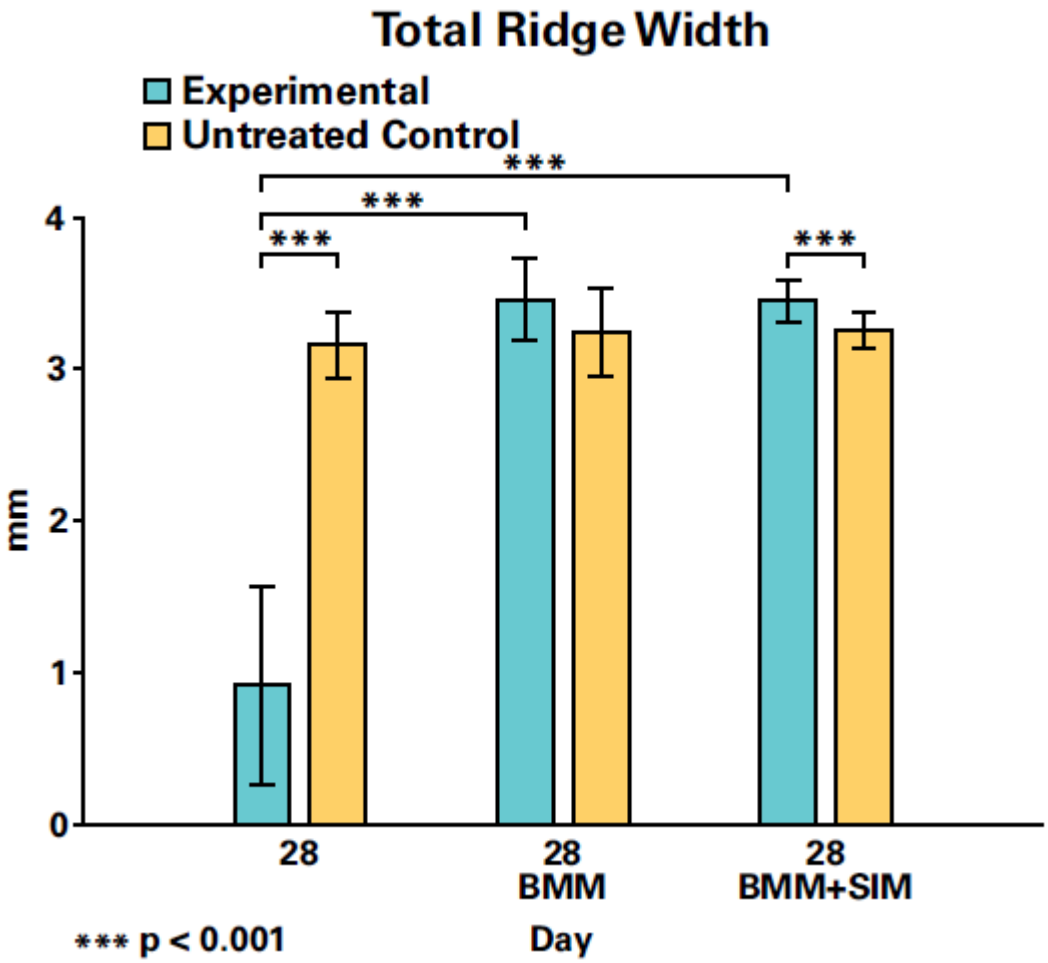

Figure 29: Total Ridge Width.
Group comparisons and experimental and untreated control for µCT linear measurement of total alveolar ridge width (mean ± standard deviation). Statistical differences noted.

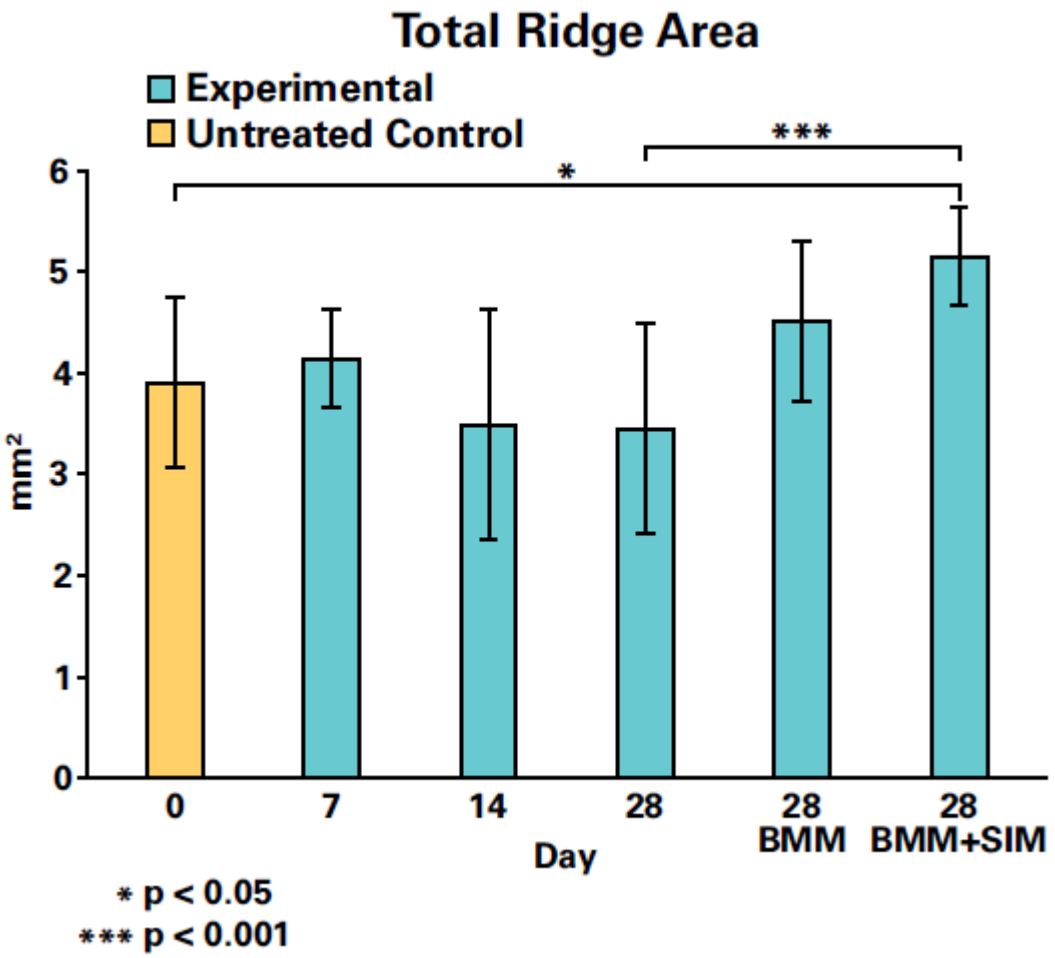

Figure 30: Total Ridge Area.
Group comparisons and experimental and untreated control for µCT measurement of total alveolar ridge area (mean ± standard deviation). Statistical differences noted.

A.

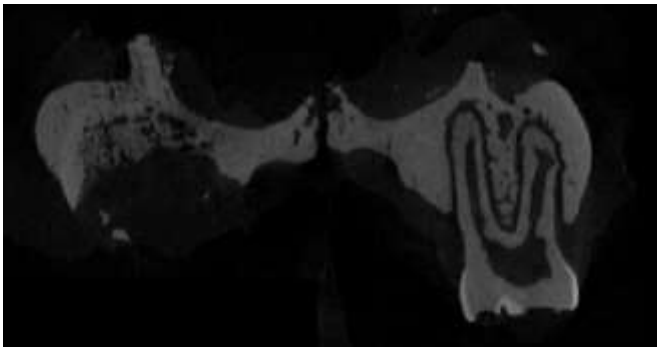

B.

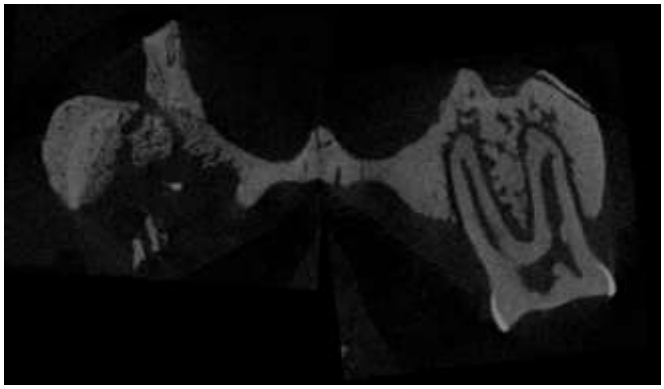

C.

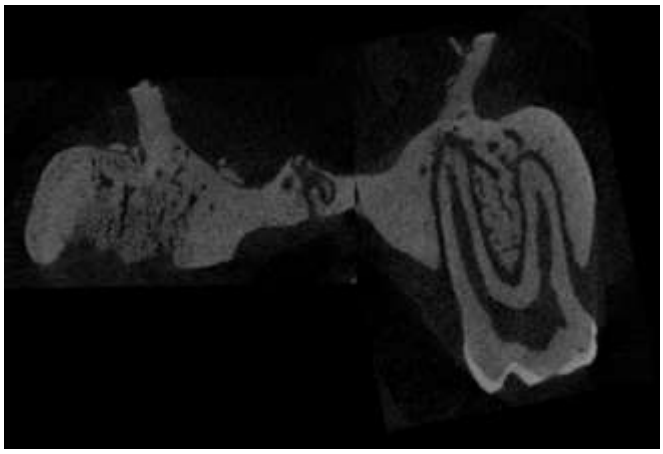

Figure 31: Representative µCT for buccal and palatal bone changes from Part 2.
A. Day 28. **B.** Day 28 BMM. **C.** Day 28 BMM+SIM.

A.

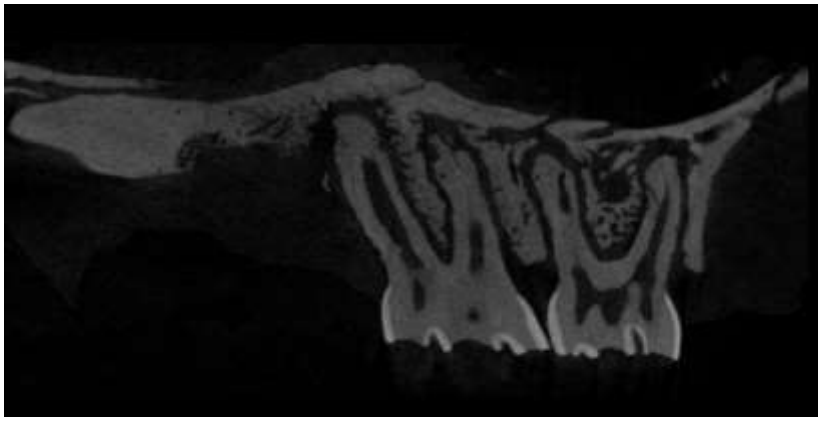

B.

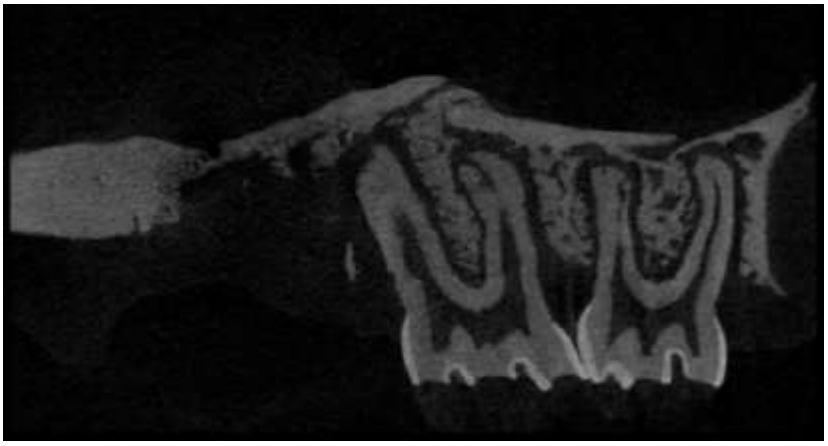

C.

Figure 32: Representative µCT for interproximal bone changes from Part 2.
A. Day 28. **B.** Day 28 BMM. **C.** Day 28 BMM+SIM.

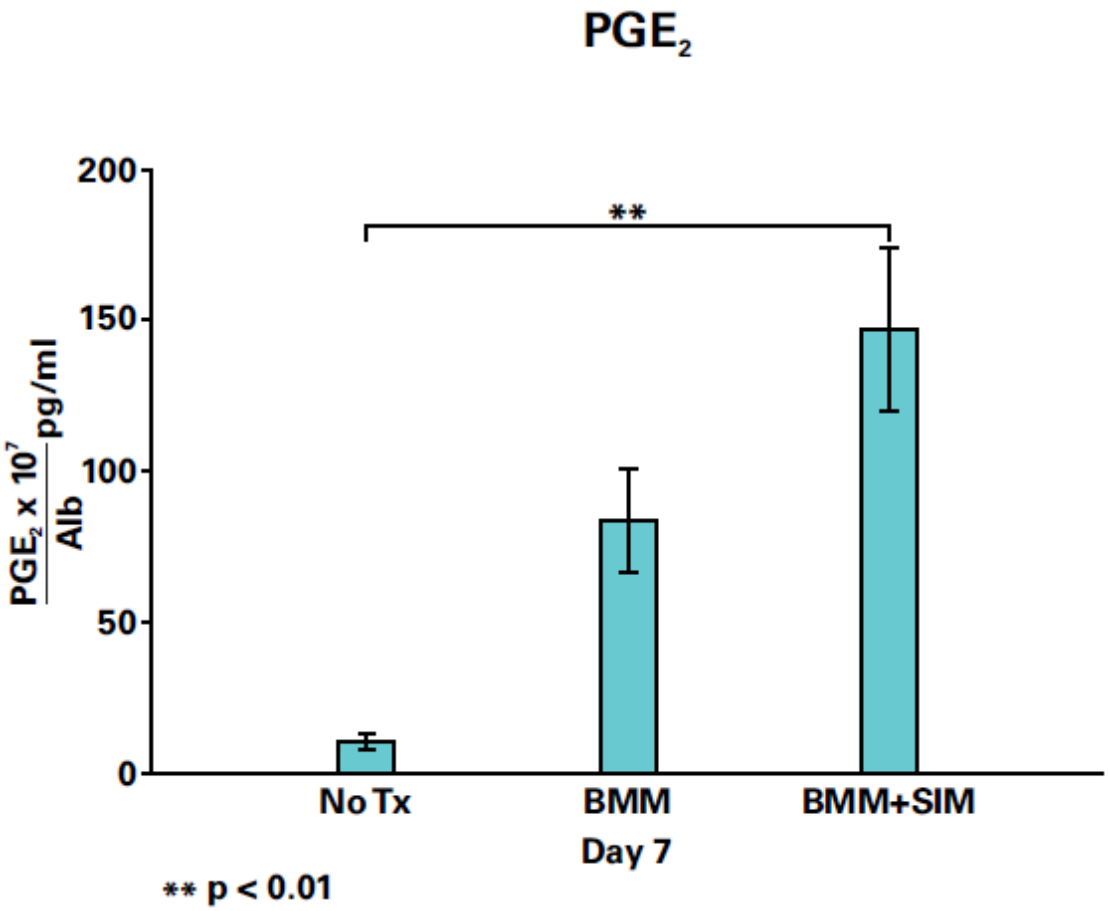

Figure 33: PGE_2/Albumin Ratio from 28 Day Groups.
Group comparisons for all day 28 groups for socket fluid samples at day 7 for ELISA measurement of PGE_2/Albumin Ratio (mean ± standard error). Statistical differences noted.

DISCUSSION

Many fields of dentistry are interested in the preservation of alveolar bone following extraction due to the well-documented changes in bone quality and quantity at the site (Van der Weijden et al. 2009; Sun et al. 2013; Sadeghi et al. 2016) and several techniques and interventions have been proposed to reduce the negative effects of post-extraction conformational changes (Darby et al. 2008; Pagni et al. 2012). Recent studies utilizing μCT in rat extraction studies (Jin et al. 2004; Park et al. 2007) have simply sought to validate the methodology, in contrast to the current study that sought to characterize bone loss measurements against which to compare various interventions and pharmacomanipulations of the extraction sites. The current study was initiated to, first, characterize inflammation and bone loss at the alveolar ridge following extraction in a standardized, cost-effective, rat model, and second, to evaluate possible interventions. In the current study, the unmanipulated physiologic bone quantity and quality changes were quantified to explore the impact of inflammation on the healing process. A proof-of-principle study also was conducted of a grafted socket with or without locally-released simvastatin. Changes were evident in the various dimensions of the alveolar bone in these rats after the 28-day period for both Part 1 and Part 2 of the study. Bone loss was evaluated between groups for linear and volumetric changes by micro computed-tomography (μCT) and the process of inflammation was monitored by histologic and PGE_2 analysis for Parts 1 and 2.

Differences in weight are a valuable method for determining if there is an overall effect on the metabolism and survivability of the animal after treatment with a drug. In Part 1 and Part 2, no animals died and all animals maintained their weight and no statistically significant differences were noted. Overall, there were no changes evident across the time periods in the 28 day groups, demonstrating that there was no adverse reaction to the surgery or the sedation

methods relative to food intake and diet throughout the study. Previous studies of extractions in rats did not report any negative lasting effect of the extractions on the survivability and ability of the animals to thrive (Bodner et al. 1993; Wu et al. 2008).

Historical and more recent studies alike have evaluated the histologic changes and stages of the healing extraction socket in rats (Pietrokovski & Massler 1967; Todo 1968; Kim et al. 2012). The periosteal aspect of the alveolar ridge demonstrated bone turnover and osteoblastic activity in the current study in the same way studies by Pietrokovski & Massler (1967) and Todo (1968) found in previous studies. A study by Kim et al. (2012) identified that normal healing, even in rats, progresses in distinctive phases, consistent with the phases of healing progressing through the inflammatory processes also identified in the current study. The Kim et al. (2012) study evaluated the inflammatory infiltrate and bone surface cells at the periphery of the healing wound and determined that after a rapid acute inflammatory response, that response was noted to diminish at about 10 days when indications of bone turnover and evidence of new bone were coincidently evident. These findings are consistent with the findings from Part 1 where the inflammatory infiltrate density and degree of inflammation decreased to a statistically significant degree between day 7 and day 28. Just as Kim et al. (2012) found bone cells at the surface that indicate bone turnover (osteoblasts and osteoclasts), the current study found that osteoblasts increased between day 7 and day 28 (Figure 25).

In a recent study by Giorgetti et al. (2012) male mature rats subjected to mandibular molar extraction were monitored at distinct time points for histologic evidence of bone changes. Giorgetti et al. (2012) concluded that new bone formation was evident at the later time points, 7 and 14 days after extraction. The study by Giorgetti et al. (2012) used a histometric method for measuring bone morphologic changes that was different than the current study's methods and it evaluated the fundus of the socket. Since loss of alveolar crest height and width is a

critical event post-extraction, often limiting available bone for future implants or prosthesis (Seibert & Salama 1996; Tomlin et al. 2014), study of the alveolar crest is important.

Pietrokovski & Massler (1967) have previously examined the periosteal region of the healing socket and, like the focus of this study, evaluated the region of the alveolar crest for evidence of bone turnover. They found that there was a collapse of the alveolar ridge over the time periods evaluated (1 week, 2 weeks, 4 weeks, 8 weeks) and there was evidence of bone turnover with osteoblastic activity on the palatal aspect of the socket, consistent with the current study's findings. The current study focused on the palatal aspect with the histologic and μCT findings because the palatal ridge was less affected by the extraction procedure than the thin buccal plate which was more likely to be disrupted or fractured. However, when comparing day 0 to controls, it appeared that the simple procedure of extraction resulted in changes in the alveolar bone, either by direct damage by trauma or fracture of alveolar bone or indirect effect from the heat of the rotary instrument (Figure 16). In the current study, it was identified that although some changes were evident at the earlier time points of 7 and 14 days, there were more dramatic changes evident after 28 days for buccal bone height (Figure 14), palatal bone height (Figure 16), interproximal bone height (Figure 18), and total ridge width (Figure 29), corresponding to other studies that demonstrated the effectiveness of using a 28-day study time frame to evaluate alveolar bone changes following interventions (Bodner et al. 1993; Schropp et al. 2003; Wu et al. 2008). The cells on the bone surface became increasingly active towards an appositional process by osteoblastic activity at days 14 and 28 (Figure 25).

A study by Shimizu et al. (1998) evaluated maxillary molar extraction sites by scanning electron microscopy (SEM) and light microscopic analysis and found that there were areas of bone resorption on the buccal and palatal aspects of the extraction site. Consistent with the current study's findings that significant loss of palatal bone height and width occurs (Figure 15

and 16), Shimizu et al. (1998) identified there were more significant areas of resorption on the palatal aspect of the extraction socket. The current study additionally looked at the interproximal bone and found that there is a significant reduction in the alveolar bone height on the distal aspect of the extraction socket, adjacent to M2 (Figure 18). Human studies have substantiated this finding of interproximal bone loss, but no studies in rats have previously quantified the amount of interproximal bone loss. Compared to human studies of healing extraction sockets (Araujo & Lindhe 2005; Avila-Ortiz et al. 2014; Sadeghi et al. 2016), the overall pattern of healing was consistent between those studies and the current study in the rat model by μCT and histologic analysis. In humans, Araujo and Lindhe (2005) identified significant loss of the buccal alveolar bone height and although there is reduction of palatal alveolar bone height, it was not found to be statistically significant. In the current study there was significant loss of both buccal and palatal alveolar height (Figures 14 and 16).

The results from Part 1 concluded that 7 days after extraction, there is a strong acute inflammatory reaction that does not correlate to a measurable loss of buccal bone height (Table 5). Contrary to the findings by Giorgetti et al. (2012), the 14-day period did not demonstrate any significant histologic changes that corresponded to bony contour changes. In the current study evaluating the healing from day 7 to day 28, the inflammatory reaction decreased while the bone loss increased over the same time period (Figures 14, 16, 18, 23, 24 and 29), but inflammation remaining at day 28 was negatively correlated to palatal bone height.

Part 2 of the current study focused on the effect of bone product grafting following extractions both with and without the addition of simvastatin. Grafting has been shown to reduce the loss of alveolar bone height and width in humans (Avila-Ortiz et al. 2014; Sadeghi et al. 2016), and the same results were found in the current study where grafting significantly reduced the loss of interproximal alveolar bone, total ridge area, and total ridge width (Figures

18, 29 and 30). Based on a thorough literature review, grafting extraction sockets with simvastatin in rats has not been previously studied and, thus, comparisons can only be made with previous applications of local simvastatin administration. As simvastatin has proven anabolic in previous applications (Mundy et al. 1999), and rodent studies have demonstrated bone anabolic (Thylin et al. 2002; Stein et al. 2005; Lee et al. 2011) and anti-inflammatory (Funk et al. 2008; George et al. 2013) abilities, this current study sought to identify any differences in bone quality or quantity following extraction that may result from local administration. The doses of simvastatin administered in previous studies (Stein et al. 2005; Lee et al. 2011; George et al. 2013) were much higher (0.5 to 2 mg) than the doses in the graft of the current study (approximately 0.2 mg). This is due to underestimation of the amount of previously prepared BMM+SIM graft material that could be placed in the standardized extraction defect. Even so, an effect was noted for BMM+SIM in increasing bone surface density, decreasing inflammatory infiltrate, and increasing ridge area. Future research with the extraction model in rats will need to test higher doses to be comparable to other studies.

With the grafted extraction sites evaluated at 28 days, there were no previous studies against which to compare the results of the current study, but the findings were that there was significantly less bone loss on the mesial aspect of M2 after 28 days when comparing no intervention to the BMM+SIM group (Figure 18). In the BMM+SIM group, there was less inflammation as measured by the total inflammatory infiltrate density than the untreated socket, but not the BMM alone socket (Figure 23) and a lower degree of inflammation in both grafted groups (Figure 24). Additionally, BMM+SIM resulted in more BSD than BMM alone (Figure 22), but both grafted sockets had increased BMD compared to ungrafted sites (Figure 21). Compared to non-interventions, the graft demonstrated an ability to preserve the ridge width, ridge area, and interproximal ridge height bone lost by extraction, but did not result in

total preservation or regeneration (Figure 16). However, both BMM and BMM+SIM preserved total ridge width, and only BMM+SIM enhanced total ridge width and total area as compared to controls (Figures 28 and 29).

The current study identified that day 7 infiltrate density and degree of inflammation were positively correlated with buccal bone height (Table 5). An apparent unexpected finding at day 7 of Part 1 of the study was the negative correlation between BSD and percentage osteoblasts (Table 5). However, perhaps this is explained by the phenomenon that osteoblasts first lay down an unmineralized secretory product, osteoid, in the apposition of new bone, thus that layer was likely recorded with low BMD by the μCT software. This finding from the current study is consistent with the findings of Bodner et al. (1993) who identified bone formation occurring at 7 and 14 days of healing and bone maturation at 28 days. Differences that can be identified between the work by Bodner et al. (1993) and the current study included the new applications for μCT that the current study utilized, but the histologic methods were consistent.

In the untreated day 28 specimens, there was a negative correlation between infiltrate density and palatal height, and in the 28 day BMM group, there was a negative correlation between degree of inflammation and BSD (Table 5), suggesting that inflammation late in the healing cycle was harmful to bone quality as persistent and uncontrolled inflammation is damaging (Beltran et al. 2015). There was an expected negative correlation between infiltration density and palatal height in the untreated 28 day specimens, but an unexpected positive correlation between mean BMD and percentage of osteoclasts. If percent of osteoclasts is considered a marker of bone turnover, less turnover may lead to more bone density. BMM+SIM was associated with a positive correlation between percentage of osteoblasts and total ridge width.

In assessing the role of PGE_2, a previous study by Lee et al. (2011) showed that higher levels of PGE_2 in the first week of healing enhanced bone growth. In the current study, day 7 PGE_2/Alb levels were significantly higher in BMM+SIM than the untreated sockets (Figure 33). Further studies must be conducted, but the current study supports the premise that high levels of PGE_2/albumin during the first week may promote bone turnover in an anabolic manner, but after that first week, elevated PGE_2 and inflammation may have a less desirable effects on alveolar bone.

CONCLUSIONS

The following conclusions can be made from the results obtained in this study:

1. The principal locations for bone loss following extraction in the current rat model without intervention were on the palatal and interproximal aspects of the site.
2. This model shows promise for testing bone regeneration compounds to prevent crestal bone loss.
3. Higher levels of PGE_2 and a more intense inflammatory reaction early in healing are correlated with more bone quality and quantity.
4. Grafting of the extraction sites demonstrated a reduction in the alveolar bone loss evident after 28 days of healing and BMM+SIM decreased inflammation and enhanced total alveolar ridge width.

The hypothesis of this study was that increased peri-socket inflammation will cause decreased regeneration of bone height and width was not proven. The hypothesis that interventions after extraction, specifically grafting of the defect, will reduce the amount of bone loss was supported.

LITERATURE CITED

Adams, J.E. 1997. Single and dual energy X-ray absorptiometry. *Eur Radiol*. 7:20-31.

Alikhani, M., J.A. Lopez, H. Alabdullah, T. Vongthongleur, C. Sangsuwon, M. Alikhani, S. Alansari, S.M. Oliveira, J.M. Nervina, and C.C. Teixeira. 2016. High-Frequency Acceleration: Therapeutic Tool to Preserve Bone following Tooth Extractions. *J Dent Res*. 95:311-318.

Araujo, M.G., and J. Lindhe. 2005. Dimensional ridge alterations following tooth extraction. An experimental study in the dog. *J Clin Periodontol*. 32:212-218.

Ashman, A. 2000. Ridge preservation: important buzzwords in dentistry. *Gen Dent*. 48:304-312.

Avila-Ortiz, G., S. Elangovan, K.W. Kramer, D. Blanchette, and D.V. Dawson. 2014. Effect of alveolar ridge preservation after tooth extraction: a systematic review and meta-analysis. *J Dent Res*. 93:950-958.

Beltran, S.R., K.K. Svoboda, D.G. Kerns, A. Sheth, and D.J. Prockop. 2015. Anti-inflammatory protein tumor necrosis factor-alpha-stimulated protein 6 (TSG-6) promotes early gingival wound healing: an in vivo study. *J Periodontol*. 86:62-71.

Bodner, L., D. Dayan, D. Rothchild, and I. Hammel. 1991. Extraction wound healing in desalivated rats. *J Oral Pathol Med*. 20:176-178.

Bodner, L., I. Kaffe, M.M. Littner, and J. Cohen. 1993. Extraction site healing in rats. A radiologic densitometric study. *Oral Surg Oral Med Oral Pathol*. 75:367-372.

Bradley, J.D., D.G. Cleverly, A.M. Burns, N.B. Helm, M.J. Schmid, D.B. Marx, D.M. Cullen, and R.A. Reinhardt. 2007. Cyclooxygenase-2 inhibitor reduces simvastatin-induced bone morphogenetic protein-2 and bone formation in vivo. *J Periodontal Res*. 42:267-273.

Clarke, B. 2008. Normal bone anatomy and physiology. *Clin J Am Soc Nephrol*. 3 Suppl 3:S131-139.

Darby, I., S. Chen, and R. De Poi. 2008. Ridge preservation: what is it and when should it be considered. *Aust Dent J*. 53:11-21.

Devlin, H. 2000. Early bone healing events following rat molar tooth extraction. *Cells Tissues Organs*. 167:33-37.

Farb, A., G. Sangiorgi, A.J. Carter, V.M. Walley, W.D. Edwards, R.S. Schwartz, and R. Virmani. 1999. Pathology of acute and chronic coronary stenting in humans. *Circulation*. 99:44-52.

Fine, D.H., H. Schreiner, C. Nasri-Heir, B. Greenberg, S. Jiang, K. Markowitz, and D. Furgang. 2009. An improved cost-effective, reproducible method for evaluation of bone loss in a rodent model. *J Clin Periodontol*. 36:106-113.

Funk, C.D. 2001. Prostaglandins and leukotrienes: advances in eicosanoid biology. *Science*. 294:1871-1875.

Funk, J.L., J. Chen, K.J. Downey, and R.A. Clark. 2008. Bone protective effect of simvastatin in experimental arthritis. *J Rheumatol*. 35:1083-1091.

George, M.D., C.M. Owen, A.L. Reinhardt, P.J. Giannini, D.B. Marx, and R.A. Reinhardt. 2013. Effect of simvastatin injections on temporomandibular joint inflammation in growing rats. *J Oral Maxillofac Surg*. 71:846-853.

Giorgetti, A.P., J.B. Cesar Neto, M.Z. Casati, E.A. Sallum, and F.H. Nociti Junior. 2012. Cigarette smoke inhalation influences bone healing of post-extraction tooth socket: a histometric study in rats. *Braz Dent J*. 23:228-234.

Guglielmotti, M.B., and R.L. Cabrini. 1985. Alveolar wound healing and ridge remodeling after tooth extraction in the rat: a histologic, radiographic, and histometric study. *J Oral Maxillofac Surg*. 43:359-364.

Guo, S., and L.A. Dipietro. 2010. Factors affecting wound healing. *J Dent Res*. 89:219-229.

Hile, D.D., S.T. Sonis, S.A. Doherty, X. Tian, Q. Zhang, W.S. Jee, and D.J. Trantolo. 2005. Dimensional stability of the alveolar ridge after implantation of a bioabsorbable bone graft substitute: a radiographic and histomorphometric study in rats. *J Oral Implantol*. 31:68-76.

Huynh-Ba, G., B.E. Pjetursson, M. Sanz, D. Cecchinato, J. Ferrus, J. Lindhe, and N.P. Lang. 2010. Analysis of the socket bone wall dimensions in the upper maxilla in relation to immediate implant placement. *Clin Oral Implants Res*. 21:37-42.

Jamjoom, A., and R.E. Cohen. 2015. Grafts for Ridge Preservation. *J Funct Biomater*. 6:833-848.

Jensen, S.S., M. Aaboe, E.M. Pinholt, E. Hjorting-Hansen, F. Melsen, and I.E. Ruyter. 1996. Tissue reaction and material characteristics of four bone substitutes. *Int J Oral Maxillofac Implants*. 11:55-66.

Jin, Q., O. Anusaksathien, S.A. Webb, M.A. Printz, and W.V. Giannobile. 2004. Engineering of tooth-supporting structures by delivery of PDGF gene therapy vectors. *Mol Ther*. 9:519-526.

Killeen, A.C., P.A. Rakes, M.J. Schmid, Y. Zhang, N. Narayana, D.B. Marx, J.B. Payne, D. Wang, and R.A. Reinhardt. 2012. Impact of local and systemic alendronate on simvastatin-induced new bone around periodontal defects. *J Periodontol*. 83:1463-1471.

Kim, D.J., J.K. Cha, C. Yang, A. Cho, J.S. Lee, U.W. Jung, C.S. Kim, S.J. Lee, and S.H. Choi. 2012. Changes in periodontium after extraction of a periodontally-involved tooth in rats. *J Periodontal Implant Sci*. 42:158-165.

Kim, Y.K., J.H. Lee, I.W. Um, and W.J. Cho. 2016. Guided Bone Regeneration Using Demineralized Dentin Matrix: Long-Term Follow-Up. *J Oral Maxillofac Surg*. 74:515 e511-519.

Kristensen, K.D., P. Stoustrup, A. Kuseler, T.K. Pedersen, J.R. Nyengaard, E.M. Hauge, and T. Herlin. 2008. Quantitative histological changes of repeated antigen-induced arthritis in

the temporomandibular joints of rabbits treated with intra-articular corticosteroid. *J Oral Pathol Med*. 37:437-444.

Kuroshima, S., R.B. Mecano, R. Tanoue, K. Koi, and J. Yamashita. 2014. Distinctive tooth-extraction socket healing: bisphosphonate versus parathyroid hormone therapy. *J Periodontol*. 85:24-33.

Lee, Y., X. Liu, A. Nawshad, D.B. Marx, D. Wang, and R.A. Reinhardt. 2011. Role of prostaglandin pathway and alendronate-based carriers to enhance statin-induced bone. *Mol Pharm*. 8:1035-1042.

Madden, T.E., and J.G. Caton. 1994. Animal models for periodontal disease. *Methods Enzymol*. 235:106-119.

Moya-Villaescusa, M.J., and A. Sanchez-Perez. 2010. Measurement of ridge alterations following tooth removal: a radiographic study in humans. *Clin Oral Implants Res*. 21:237-242.

Mundy, G., R. Garrett, S. Harris, J. Chan, D. Chen, G. Rossini, B. Boyce, M. Zhao, and G. Gutierrez. 1999. Stimulation of bone formation in vitro and in rodents by statins. *Science*. 286:1946-1949.

Nevins, M., M. Camelo, S. De Paoli, B. Friedland, R.K. Schenk, S. Parma-Benfenati, M. Simion, C. Tinti, and B. Wagenberg. 2006. A study of the fate of the buccal wall of extraction sockets of teeth with prominent roots. *Int J Periodontics Restorative Dent*. 26:19-29.

Pagni, G., G. Pellegrini, W.V. Giannobile, and G. Rasperini. 2012. Postextraction alveolar ridge preservation: biological basis and treatments. *Int J Dent*. 2012:151030.

Park, C.H., Z.R. Abramson, M. Taba, Jr., Q. Jin, J. Chang, J.M. Kreider, S.A. Goldstein, and W.V. Giannobile. 2007. Three-dimensional micro-computed tomographic imaging of alveolar bone in experimental bone loss or repair. *J Periodontol*. 78:273-281.

Pietrokovski, J., and M. Massler. 1967. Ridge remodeling after tooth extraction in rats. *J Dent Res*. 46:222-231.

Pietrzak, W.S. 2006. The hydration characteristics of demineralized and nondemineralized allograft bone: Scientific perspectives on graft function. *J Craniofac Surg*. 17:120-130.

Pinholt, E.M., G. Bang, and H.R. Haanaes. 1991. Alveolar ridge augmentation in rats by Bio-Oss. *Scand J Dent Res*. 99:154-161.

Pountos, I., T. Georgouli, G.M. Calori, and P.V. Giannoudis. 2012. Do nonsteroidal anti-inflammatory drugs affect bone healing? A critical analysis. *ScientificWorldJournal*. 2012:606404.

Preston, R.D., T.A. Meinberg, J.B. Payne, M.J. Schmid, H.M. Lee, L.M. Golub, D.B. Marx, and R.A. Reinhardt. 2007. Inflammatory mediator release following bone grafting in humans: a pilot study. *J Clin Periodontol*. 34:797-804.

Ricciotti, E., and G.A. FitzGerald. 2011. Prostaglandins and inflammation. *Arterioscler Thromb Vasc Biol*. 31:986-1000.

Sadeghi, R., M. Babaei, S.A. Miremadi, and F.M. Abbas. 2016. A randomized controlled evaluation of alveolar ridge preservation following tooth extraction using deproteinized bovine bone mineral and demineralized freeze-dried bone allograft. *Dent Res J (Isfahan)*. 13:151-159.

Schreiner, H., K. Markowitz, M. Miryalkar, D. Moore, S. Diehl, and D.H. Fine. 2011. Aggregatibacter actinomycetemcomitans-induced bone loss and antibody response in three rat strains. *J Periodontol*. 82:142-150.

Schropp, L., and F. Isidor. 2008. Timing of implant placement relative to tooth extraction. *J Oral Rehabil*. 35 Suppl 1:33-43.

Schropp, L., A. Wenzel, L. Kostopoulos, and T. Karring. 2003. Bone healing and soft tissue contour changes following single-tooth extraction: a clinical and radiographic 12-month prospective study. *Int J Periodontics Restorative Dent*. 23:313-323.

Seibert, J.S., and H. Salama. 1996. Alveolar ridge preservation and reconstruction. *Periodontol 2000*. 11:69-84.

Shimizu, M., T. Sasaki, A. Ishihara, R. Furuya, and T. Kawawa. 1998. Bone wound healing after maxillary molar extraction in ovariectomized aged rats. *J Electron Microsc (Tokyo)*. 47:517-526.

Skoglund, A., P. Hising, and C. Young. 1997. A clinical and histologic examination in humans of the osseous response to implanted natural bone mineral. *Int J Oral Maxillofac Implants*. 12:194-199.

Stein, D., Y. Lee, M.J. Schmid, B. Killpack, M.A. Genrich, N. Narayana, D.B. Marx, D.M. Cullen, and R.A. Reinhardt. 2005. Local simvastatin effects on mandibular bone growth and inflammation. *J Periodontol*. 76:1861-1870.

Steiner, G.G., W. Francis, R. Burrell, M.P. Kallet, D.M. Steiner, and R. Macias. 2008. The healing socket and socket regeneration. *Compend Contin Educ Dent*. 29:114-116, 118, 120-114 passim.

Struillou, X., H. Boutigny, A. Soueidan, and P. Layrolle. 2010. Experimental animal models in periodontology: a review. *Open Dent J*. 4:37-47.

Su-Gwan, K., K. Hak-Kyun, and L. Sung-Chul. 2001. Combined implantation of particulate dentine, plaster of Paris, and a bone xenograft (Bio-Oss) for bone regeneration in rats. *J Craniomaxillofac Surg*. 29:282-288.

Sun, Z., S.W. Herring, B.C. Tee, and J. Gales. 2013. Alveolar ridge reduction after tooth extraction in adolescents: an animal study. *Arch Oral Biol*. 58:813-825.

Tan, W.L., T.L. Wong, M.C. Wong, and N.P. Lang. 2012. A systematic review of post-extractional alveolar hard and soft tissue dimensional changes in humans. *Clin Oral Implants Res*. 23 Suppl 5:1-21.

Thylin, M.R., J.C. McConnell, M.J. Schmid, R.R. Reckling, J. Ojha, I. Bhattacharyya, D.B. Marx, and R.A. Reinhardt. 2002. Effects of simvastatin gels on murine calvarial bone. *J Periodontol*. 73:1141-1148.

Todo, H. 1968. Healing mechanism of tooth extraction wounds in rats. I. Initial cellular response to tooth extraction in rats studied with 3H-thymidine. *Arch Oral Biol*. 13:1421-1427.

Tomlin, E.M., S.J. Nelson, and J.A. Rossmann. 2014. Ridge preservation for implant therapy: a review of the literature. *Open Dent J*. 8:66-76.

Trombelli, L., R. Farina, A. Marzola, L. Bozzi, B. Liljenberg, and J. Lindhe. 2008. Modeling and remodeling of human extraction sockets. *J Clin Periodontol*. 35:630-639.

Van der Weijden, F., F. Dell'Acqua, and D.E. Slot. 2009. Alveolar bone dimensional changes of post-extraction sockets in humans: a systematic review. *J Clin Periodontol*. 36:1048-1058.

Wood, R.A., and B.L. Mealey. 2012. Histologic comparison of healing after tooth extraction with ridge preservation using mineralized versus demineralized freeze-dried bone allograft. *J Periodontol*. 83:329-336.

Wu, Z., C. Liu, G. Zang, and H. Sun. 2008. The effect of simvastatin on remodelling of the alveolar bone following tooth extraction. *Int J Oral Maxillofac Surg*. 37:170-176.

Yang, H., H. Pan, F. Yu, K. Chen, G. Shang, and Y. Xu. 2015. A novel model of bisphosphonate-related osteonecrosis of the jaw in rats. *Int J Clin Exp Pathol*. 8:5161-5167.

Yugoshi, L.I., M.A. Sala, L.G. Brentegani, and T.L. Lamano Carvalho. 2002. Histometric study of socket healing after tooth extraction in rats treated with diclofenac. *Braz Dent J*. 13:92-96.

Part 1: Linear Measurements, Coronal Section, Control Side

Specimen	Group	Buccal height	Palatal height	At 1.25 Buccal Width	At 1.25 Palatal width	Total ridge width
A	**8**	2.525	2.151	0.000	0.728	3.356
AA	**8**	2.534	2.351	0.461	0.933	3.092
AB	**6**	2.736	2.174	0.000	0.96	
AC	**4**	2.552	1.926	0.666	0.776	
AD	**2**	2.178	1.785	0.542	0.682	
AE	**8**	2.324	1.783	0.721	0.697	3.23
AF	**6**	2.527	1.943	0.668	0.639	
AG	**4**	2.665	1.946	0.802	0.566	
AH	**2**	2.166	1.893	0.525	0.733	
AI	**8**	2.145	1.915	0.470	0.478	3.092
B	**6**	2.62	2.014	0.528	0.773	
C	**4**	2.588	1.94	0.566	0.702	
E	**2**	2.489	2.092	0.595	0.805	
F	**8**	2.284	1.838	0.524	0.442	2.957
G	**6**	2.469	2.202	0.716	0.767	
H	**4**	2.555	2.076	0.598	0.659	
J	**2**	2.657	1.946	0.552	0.772	
K	**8**	1.858	1.51	0.611	0.5	2.745
L	**6**	2.716	1.897	0.620	0.606	
M	**4**	2.517	1.872	1.246	0.662	
N	**2**	2.194	2.005	0.567	0.836	
O	**8**	2.405	1.858	0.539	0.741	3.285
P	**6**	2.688	2.1	0.635	0.653	
Q	**4**	2.719	1.952	0.683	0.707	
R	**2**	2.528	2.112	0.597	0.74	
S	**8**	2.583	2.067	0.666	0.922	3.446
T	**6**	2.382	2.098	0.606	0.77	
U	**4**	2.602	1.905	0.721	0.565	
V	**2**	2.387	1.893	0.422	0.5	
W	**8**	2.574	2.166	0.641	0.595	3.252
X	**6**	2.359	2.037	0.450	0.756	
Y	**4**	2.762	2.628	0.606	1.028	
Z	**2**	2.469	1.836	0.744	0.795	

Part 1: Linear Measurements, Sagittal Section, Control Side

specimen	group	CEJ to ABC	
		distal to m2	mesial to m2
A	8	0.523	0.288
AA	8	0.527	0.54
AB	6	0.612	0.556
AC	4	0.379	0.338
AD	2	0.319	0.289
AE	8	0.283	0.448
AF	6	0.393	0.313
AG	4	0.48	0.547
AH	2	0.447	0.296
AI	8	0.45	0.441
B	6	0.442	0.423
C	4	0.308	0.381
E	2	0.32	0.339
F	8	0.614	0.296
G	6	0.421	0.418
H	4	0.569	0.372
J	2	0.262	0.587
K	8	0.379	0.427
L	6	0.487	2.165
M	4	0.381	0.331
N	2	0.289	0.254
O	8	0.515	0.465
P	6	0.628	0.386
Q	4	0.508	0.483
R	2	0.337	0.364
S	8	0.205	0.243
T	6	0.465	0.353
U	4	0.639	0.553
V	2	0.454	0.387
W	8	0.479	0.553
X	6	0.887	0.214
Y	4	0.321	0.353
Z	2	1.036	0.523

Part 1: Volumetric Measurements, Coronal Section, Control Side

specimen	group	area			mean BMD	BV/TV	BS/TV
		total	buccal	palatal			
A	**8**	7.84	3.383	3.869	1.11671	65.7891	41.38127
AA	**8**	6.613	2.705	4.028	1.17527	57.72435	35.54262
AB	**6**	7.92	3.477	4.483	1.08628	43.08351	35.39414
AC	**4**	7.049	3.424	3.346	1.08695	93.25035	21.1727
AD	**2**	6.228	2.784	3.581	1.13969	51.85294	41.2296
AE	**8**	6.306	3.23	3.034	1.22079	20.6322	26.32053
AF	**6**	6.937	3.627	3.687	1.17235	76.7359	31.620
AG	**4**	7.117	3.777	3.675	1.19818	58.35974	37.52249
AH	**2**	6.069	2.863	3.338	1.09317	53.07115	44.45661
AI	**8**	6.406	2.888	3.804	1.15283	94.02531	22.03968
B	**6**	6.786	3.405	3.543	1.22474	53.09267	39.52559
C	**4**	7.118	3.578	3.734	1.20892	53.89536	43.01934
E	**2**	7.343	3.289	3.863	1.09949	57.74211	39.0343
F	**8**	5.738	2.798	3.594	1.14042	77.86151	33.80791
G	**6**	6.958	3.529	3.471	1.19407	31.4720	35.36546
H	**4**	7.313	3.237	3.917	1.12855	77.9356	28.81457
J	**2**	7.167	3.087	3.861	1.18304	59.04615	41.87589
K	**8**	4.372	2.37	1.913	1.14587	56.3327	42.05986
L	**6**	7.437	3.523	3.753	1.13683	84.69045	30.03729
M	**4**	4.297	2.529	1.841	1.14886	76.61471	34.52171
N	**2**	6.35	2.72	3.408	1.13917	43.9010	42.59031
O	**8**	6.502	2.955	3.473	1.1476	79.38857	28.66463
P	**6**	7.296	3.537	3.648	1.20868	72.49805	36.31784
Q	**4**	7.767	3.882	3.848	1.11996	91.94018	24.07935
R	**2**	6.835	3.373	3.518	1.08157	65.64642	41.56635
S	**8**	7.109	3.213	4.055	1.16158	61.67461	35.33547
T	**6**	6.849	2.917	4.013	1.18700	74.25245	35.51578
U	**4**	7.451	3.561	3.772	1.15947	61.69712	40.43564
V	**2**	6.615	3.224	3.706	1.18082	45.96094	39.57756
W	**8**	7.307	3.935	3.648	1.22018	46.98005	38.16429
X	**6**	6.492	2.778	3.835	1.22799	51.52551	39.09945
Y	**4**	8.506	3.684	4.709	1.13631	42.44360	40.54568
Z	**2**	6.805	3.318	3.491	1.07431	50.37372	44.33213

Part 1: Linear Measurements, Coronal Section, Experimental Side

specimen	group	Buccal height	Palatal height	At 1.25 Buccal Width	At 1.25 Palatal Width	Total ridge width
A	**7**	0.958	1.082	0	0	0.16
AA	**7**	2.146	1.075	1.594	0	1.867
AB	**5**	2.292	1.42	0.851	0.72	
AC	**3**	2.056	2.358	0.306	0	
AD	**1**	1.379	1.803	0.074	0.629	
AE	**7**	2.053	1.542	0.494	0.45	0.857
AF	**5**	2.109	1.34	0.471	0.543	
AG	**3**	2.715	1.948	0.61	0.789	
AH	**1**	2.056	1.744	0.505	0.666	
AI	**7**	2.149	0.919	0.828	0	0.828
B	**5**	2.337	1.626	0.581	0.491	
C	**3**	2.651	2.08	0.848	0.63	
E	**1**	2.366	2.039	0.702	0.713	
F	**7**	1.031	1.961	0	0.454	0.639
G	**5**	2.47	1.515	0.787	0.635	
H	**3**	2.224	1.943	0.649	0.655	
J	**1**	2.55	1.868	0.436	0.762	
K	**7**	1.741	1.384	0.772	0.392	0.762
L	**5**	2.203	1.433	0.305	0.397	
M	**3**	2.332	1.917	0.625	0.937	
N	**1**	2.274	1.837	0.624	0.78	
O	**7**	2.164	1.249	1.401	0	2.118
P	**5**	2.726	1.84	0.418	0.915	
Q	**3**	2.628	2.134	0.456	0.764	
R	**1**	2.343	1.932	0.831	0.519	
S	**7**	1.559	1.153	0.305	0	0.369
T	**5**	2.402	1.618	0.339	0.713	
U	**3**	2.634	2.462	1.011	0.552	
V	**1**	1.917	1.922	0.106	0.451	
W	**7**	2.035	1.373	0.916	0.364	0.699
X	**5**	1.807	1.538	0.189	0.523	
Y	**3**	1.772	2.289	0.117	0.702	
Z	**1**	2.738	1.662	1.027	0.4	

Part 1: Linear Measurements, Sagittal Section, Experimental Side

specimen	group	CEJ to AC	
		distal to m2	mesial to m2
A	7	0.368	2.375
AA	7	0.491	1.812
AB	5	0.755	0.544
AC	3	0.421	0.504
AD	1	0.249	0.526
AE	7	0.262	1.912
AF	5	0.494	1.916
AG	3	0.32	0.688
AH	1	0.537	0.456
AI	7	0.697	2.438
B	5	0.521	1.87
C	3	0.425	0.359
E	1	0.537	0.396
F	7	0.814	1.151
G	5	0.29	1.637
H	3	0.653	0.5
J	1	0.476	0.508
K	7	0.396	2.451
L	5	1.224	0.524
M	3	0.37	0.353
N	1	0.359	1.367
O	7	0.37	1.889
P	5	0.828	1.461
Q	3	0.654	0.65
R	1	0.326	0.552
S	7	0.473	1.551
T	5	0.408	1.783
U	3	0.741	0.568
V	1	0.279	0.343
W	7	0.494	2.1841
X	5	0.669	2.13
Y	3	0.391	0.332
Z	1	0.494	0.349

Part 1: Volumetric Measurements, Coronal Section, Experimental Side

specimen	group	area			mean BMD	BV/TV	BS/TV
		total	buccal	palatal			
A	**7**	2.556	1.81	0.597	1.33434	68.45437	36.21995
AA	**7**	5.133	4.19	0.996	1.26473	75.74670	32.94163
AB	**5**	5.215	2.495	2.516	1.31239	70.16788	35.63164
AC	**3**	3.695	1.104	2.78	1.47243	29.76055	27.01848
AD	**1**	3.255	1.315	1.938	1.39417	54.59972	38.56248
AE	**7**	3.723	1.842	2.233	1.34674	58.60679	36.95086
AF	**5**	2.237	0.861	1.54	1.35034	97.28516	21.22989
AG	**3**	4.491	1.906	2.56	1.32309	95.55072	25.3470
AH	**1**	3.612	1.713	1.821	1.27179	71.97186	40.89362
AI	**7**	3.015	1.716	1.48	1.24302	64.50633	39.16527
B	**5**	3.705	1.886	2.02	1.17187	91.19432	20.54619
C	**3**	4.833	2.57	2.01	1.42778	49.43133	33.68933
E	**1**	5.121	2.419	2.886	1.16602	79.04828	35.20235
F	**7**	2.302	1.545	0.736	1.36653	49.11255	29.6530
G	**5**	4.581	1.928	2.703	1.46287	51.10664	41.46869
H	**3**	4.685	1.802	2.706	1.31222	74.60048	26.77056
J	**1**	3.213	1.291	2.061	1.25151	39.72706	43.14048
K	**7**	3.451	1.702	1.763	1.40183	50.37701	38.09159
L	**5**	2.752	0.647	2.006	1.42190	97.97055	17.30113
M	**3**	3.804	1.652	2.089	1.36674	55.64728	41.81488
N	**1**	4.262	1.676	2.512	1.31857	65.95352	38.45656
O	**7**	4.692	2.428	2.162	1.21818	94.57144	20.55683
P	**5**	3.968	1.417	2.35	1.37582	93.55088	22.27349
Q	**3**	3.873	1.713	2.19	1.4138	41.65096	37.56404
R	**1**	4.446	1.943	2.452	1.27542	32.62973	35.75925
S	**7**	2.176	1.371	0.671	1.31893	63.19286	33.66956
T	**5**	3.122	0.961	2.111	1.43727	66.37437	39.82204
U	**3**	3.594	1.512	1.8	1.32482	46.30391	35.79151
V	**1**	2.646	1.859	0.617	1.36152	50.77540	44.07769
W	**7**	4.017	1.999	1.947	1.37811	52.65591	38.59748
X	**5**	1.948	0.7	1.313	1.51326	65.20213	37.6842
Y	**3**	4.142	1.324	2.678	1.34044	66.60489	40.41352
Z	**1**	4.617	2.772	2.114	1.36920	61.62941	43.73693

Part 1: Histologic Measurements, Coronal Section, Experimental Side

specimen	group	area of infiltrate	um^2	infiltrate/um^2	degree inflamm	OC/perimeter	OB/perimeter	quiescent/ perimeter
A	7	98775	631279	0.156468	1.5	0.16103138	0.2198978	0.61907079
AA	7	225343	632593	0.356221	2	0.24321682	0.1510633	0.60571987
AB	5	198831	656204	0.303002	2	0.19554031	0.1009556	0.70350404
AC	3	211822	592828	0.357308	1	0.22862823	0.1227634	0.64860835
AD	1				0			
AE	7	101097	692234	0.146045	1	0.0779805	0.1317171	0.79030242
AF	5	91082	618394	0.147288	1	0.05006258	0.1341677	0.81576971
AG	3	372760	572736	0.650841	2.5	0.14681934	0.0801527	0.77302799
AH	1				0			
AI	7	208133	567634	0.366668	3	0.16662522	0.1288237	0.70455111
B	5	118270	497969	0.237505	1	0.11604692	0.2233591	0.66059396
C	3	382768	625424	0.612014	1.5	0.27329341	0.1166467	0.61005988
E	1				0			
F	7	81579	602718	0.135352	1.5	0.08746356	0.1389699	0.77356657
G	5	67322	709221	0.094924	1.5	0.12434062	0.094951	0.78070836
H	3	86580	604906	0.14313	1	0.16888459	0.1282361	0.70287926
J	1				0			

Part 1: Histologic Measurements, Coronal Section, Experimental Side

specimen	group	area of infiltrate	um^2	infiltrate/um^2	degree inflamm	OC/perimeter	OB/perimeter	quiescent/ perimeter
K	7	98321	609122	0.161414	0.12935	0.12935203	0.1629594	0.70768859
L	5	278528	498441	0.558798	0.08093	0.08093742	0.1118628	0.80719981
M	3	175839	611152	0.287717	0.18191	0.18191109	0.0636178	0.75447113
N	1				0			
O	7	98060	575747	0.170318	0.07944	0.07944036	0.1041024	0.8164572
P	5	321345	623493	0.515395	0.18300	0.18300498	0.1208165	0.6961785
Q	3	178118	616305	0.28901	0.08233	0.08233533	0.0688623	0.8488024
R	1				0			
S	7	420117	600383	0.699748	0.12365	0.12365328	0.1192458	0.75710088
T	5	233649	624682	0.374029	0.21680	0.21680019	0.0791454	0.70405438
U	3	461759	636373	0.725611	0.09903	0.0990368	0.077303	0.82366016
V	1				0			
W	7	93734	616631	0.15201	0.11922	0.1192239	0.2037273	0.67704876
X	5	71134	651805	0.109134	0.11007	0.11007321	0.1694017	0.72052512
Y	3	111669	516496	0.216205	0.09932	0.09932498	0.042189	0.85848602
Z	1				0			

Part 1: PGE_2 Measurements, Experimental Side

specimen	group	day 7 PGE2	day 7 Alb	PGE2x10^2 /Alb	day 14 PGE2	day 14 Alb	PGE2x10^2 /Alb	day 28 PGE2	day 28 Alb	PGE2x10^2 /Alb
A	**7**	914.847	4602.250	19.878	180.098	3336.350	5.398	22.477	331.165	6.787
AA	**7**	674.940	2137.050	31.583	429.413	5412.300	7.934	25.962	35.650	72.825
AE	**7**	311.564	3443.950	9.047	471.750	1137.280	41.481	53.985	46.750	115.476
F	**7**	849.454	5788.350	14.675	277.435	6346.000	4.372	91.844	2255.450	4.072
K	**7**	749.364	42000.000	1.784	729.600	21118.600	3.455	40.437	158.850	25.456
O	**7**	540.121	42000.000	1.286	347.079	42000.000	0.826	22.610	23.505	96.192
S	**7**	989.344	42000.000	2.356	570.376	25333.200	2.251	11.335	495.965	2.285
W	**7**	914.847	42000.000	2.178	443.228	11122.200	3.985	37.366	43.435	86.026

Part 1: Weight Measurements

specimen	group	weight (g)			
		0 day	7 day	14 day	28 day
A	**7**	324	314	320	336
AA	**7**	337	338	344	344
AB	**5**	329	329	325	
AC	**3**	310	311		
AD	**1**	276			
AE	**7**	283	279	281	282
AF	**5**	338	322	319	
AG	**3**	342	323		
AH	**1**	288			
AI	**7**	311	298	300	307
B	**5**	369	351	346	
C	**3**	357	334		
E	**1**	307			
F	**7**	286	287	292	290
G	**5**	345	344	345	
H	**3**	308	304		
J	**1**	306			
K	**7**	305	301	321	309
L	**5**	359	350	348	
M	**3**	334	343		
N	**1**	299			
O	**7**	296	276	274	292
P	**5**	335	349	349	
Q	**3**	350	344		
R	**1**	313			
S	**7**	303	314	300	319
T	**5**	312	319	318	
U	**3**	384	369		
V	**1**	305			
W	**7**	350	337	341	332
X	**5**	317	323	320	
Y	**3**	312	304		
Z	**1**	298			

Part 2: Linear Measurements, Coronal Section, Control Side

specimen	group	Buccal height	Palatal height	Total ridge width
1	12	2.298	1.865	3.383
2	10	0	2.139	2.584
3	12	2.466	1.964	3.222
4	10	2.412	1.757	3.281
5	12	1.675	1.744	3.228
6	10	2.41	1.946	3.224
7	12	2.265	1.594	3.357
8	10	2.561	1.855	3.478
9	12	2.542	2.11	3.269
10	10	2.455	1.55	3.406
11	12	2.463	1.829	3.256
12	10	2.61	2.079	3.287
13	12	2.346	1.8	3.386
14	10	2.269	2.004	3.474
15	10	2.487	2.197	3.223
16	12	2.444	1.752	3.402
17	12	2.324	1.775	3.034

Part 2: Linear Measurements, Sagittal Section, Control Side

specimen	group	CEJ to AC	
		distal to m2	mesial to m2
1	12	0.762	0.413
2	10	0.451	0.416
3	12	0.643	0.69
4	10	0.364	0.436
5	12	0.421	0.528
6	10	0.436	0.475
7	12	0.553	0.331
8	10	0.845	0.359
9	12	0.351	0.404
10	10	0.611	0.851
11	12	0.653	0.505
12	10	0.436	0.25
13	12	0.306	0.436
14	10	0.641	0.289
15	10	0.407	0.491
16	12	0.409	0.326
17	12	0.276	0.354

Part 2: Volumetric Measurements, Coronal Section, Control Side

specimen	group	area			mean BMD	BV/TV	BS/TV
		total	buccal	palatal			
1	12	6.329	3.103	3.248	1.40117	57.5731	45.84361
2	10	5.102	3.402	1.882	1.39402	51.15794	46.74146
3	12	6.449	2.772	3.743	1.40258	63.9758	37.50658
4	10	6.123	2.886	3.126	1.40601	42.25889	39.3351
5	12	5.398	2.448	2.913	1.38282	62.85683	42.6149
6	10	6.379	3.184	3.205	1.36139	55.3298	44.1857
7	12	5.861	2.661	3.276	1.37875	53.47056	44.56749
8	10	7.066	3.297	3.908	1.37672	65.44681	40.13952
9	12	7.175	3.239	3.743	1.36055	34.97243	40.01729
10	10	5.996	2.994	2.837	1.38986	68.05284	38.18254
11	12	6.684	3.425	3.381	1.34022	72.71868	36.81418
12	10	6.805	3.378	3.649	1.35889	60.2007	40.6264
13	12	6.162	2.891	3.299	1.38157	52.27509	41.16002
14	10	6.802	3.458	3.263	1.34021	52.46548	45.28456
15	10	6.997	3.489	3.467	1.3772	69.7224	59.16701
16	12	6.487	3.442	3.024	1.39785	59.29264	45.19325
17	12	6.02	2.913	3.269	1.38105	44.57904	41.48087

Part 2: Linear Measurements, Coronal Section, Experimental Side

specimen	group	Buccal height	Palatal height	Total ridge width
1	11	1.787	1.732	3.621
2	9	1.865	1.588	3.425
3	11	1.957	1.708	3.391
4	9	1.492	1.383	3.009
5	11	1.647	1.595	3.418
6	9	2.124	1.905	3.374
7	11	1.904	1.165	3.326
8	9	1.832	1.47	3.325
9	11	2.176	1.618	3.271
10	9	1.981	1.034	3.737
11	11	1.921	1.392	3.59
12	9	1.917	1.599	3.313
13	11	1.953	1.483	3.643
14	9	2.744	1.627	3.832
15	9	2.023	1.202	3.654
16	11	2.152	1.379	3.279
17	11	2.705	1.417	3.476

Part 2: Linear Measurements, Sagittal Section, Experimental Side

specimen	group	CEJ to AC	
		distal to m2	mesial to m2
1	11	0.437	0.607
2	9	0.45	0.716
3	11	0.802	0.604
4	9	0.402	0.865
5	11	0.339	0.611
6	9	0.407	0.904
7	11	0.363	0.728
8	9	0.575	0.864
9	11	0.335	0.469
10	9	0.697	2.055
11	11	0.407	1.013
12	9	0.393	0.714
13	11	0.773	0.54
14	9	0.597	1.067
15	9	0.467	1.424
16	11	0.647	0.58
17	11	0.29	1.273

Part 2: Volumetric Measurements, Coronal Section, Experimental Side

specimen	group	mean BMD	BV	TV	BV/TV	BS/TV
1	11	1.55894	0.03153	0.05336	59.08658	62.87701
2	9	1.40916	0.01684	0.05333	31.58410	26.20168
3	11	1.46077	0.02979	0.05336	55.8235	44.214
4	9	1.51149	0.03811	0.05334	71.44124	27.38097
5	11	1.51077	0.03232	0.05335	60.58481	43.82793
6	9	1.28565	0.03604	0.05335	67.55899	32.34835
7	11	1.44444	0.03298	0.05334	61.83137	67.29622
8	9	1.46405	0.02625	0.05331	49.24345	44.9193
9	11	1.37079	0.02872	0.05333	66.90113	36.02535
10	9	1.3882	0.0479	0.05330	89.85745	26.95086
11	11	1.46486	0.02713	0.05333	50.87565	36.42129
12	9	1.51203	0.03521	0.05336	65.98290	32.63277
13	11	1.50497	0.02968	0.05336	55.62899	44.0692
14	9	1.50056	0.05063	0.05333	94.93382	20.2442
15	9	1.53945	0.02724	0.05329	51.45704	41.42747
16	11	1.48606	0.03268	0.05328	61.34513	44.42881
17	11	1.38359	0.04655	0.05334	87.28354	60.61967

Part 2: Histologic Measurements, Coronal Section, Experimental Side

specimen	group	area of infiltrate	um^2	infiltrate/um^2	degree inflamm	OC/perimeter	OB/perimeter	quiescent/ perimeter
1	11	56269	667090	0.08435	0.5	0.059653	0.156808	0.783539
2	9	103866	681909	0.152317	1	0.051038	0.06655	0.882412
3	11	83790	690823	0.12129	0.5	0.109286	0.189196	0.701519
4	9	86131	654461	0.131606	0.5	0.097206	0.136374	0.76642
5	11	42883	557947	0.076859	1	0.067231	0.108258	0.82451
6	9	15816	471827	0.033521	0.5	0	0.084242	0.915758
7	11	15186	613811	0.024741	1	0.026387	0.070777	0.902836
8	9	9086	653178	0.01391	0.5	0.030723	0.061447	0.90783
9	11	8678	575870	0.015069	0.5	0.045533	0.070032	0.884435
10	9	199025	668758	0.297604	1	0.056155	0.200343	0.743502
11	11	0	667577	0	0	0.033603	0.116978	0.849419
12	9	19153	638380	0.030003	0.5	0.061777	0.129953	0.80827
13	11							
14	9							
15	9	108736	531598	0.204546	0.5	0.099652	0.196283	0.704065
16	11	25604	633747	0.040401	0	0.024444	0.068443	0.907113
17	11	45072	561431	0.080281	1	0.133693	0.095418	0.770889

Part 2: PGE_2 Measurements, Experimental Side

specimen	group	day 7 PGEPGE2	day 7 Alb	PGE2x10² /Alb	day 14 PGE2	day 14 Alb	PGE2x10² /Alb	day 28 PGE2	day 28 Alb	PGE2x10² /Alb
1	11	230.1285	107.1665	214.7392	0	24.675	0			
2	9	257.012	113.192	227.0584	0	13.501	0			
3	11	111.432	192.787	57.80058	6.13	62.8235	9.757495		9.41	
4	9	71.059	129.0565	55.06038	0	17.4145	0		4.5915	
5	11	243.4025	173.0925	140.6199	85.277	96.8885	88.01561			
6	9	271.4645	184.8915	146.8237	65.0275	131.018	49.63249			
7	11	0	146.081	0	0	0.737	0			
8	9	154.3035	226.165	68.22607	202.4135	125.359	161.4671			
9	11	659.233	350.779	187.934	104.522	129.241	80.87372			
10	9	82.351	152.432	54.02475	0	14.513	0			
11	11	0	32.4565	0	0	26.886	0	0	3.011	0
12	9	163.2905	178.3885	91.53645	114.591	2.8585	4008.781	113.679	0.931	12210.42
13	11	94.216	45.894	205.2905	0	13.0335	0			
14	9	0	109.737	0	0	30.6075	0			
15	9	62.1745	231.1305	26.90017	0	4.4395	0			
16	11	165.5865	124.015	133.5213	0	3.2245	0			
17	11	502.445	131.468	382.1805	285.1655	42.629	668.9472			

Part 2: Weight Measurements

specimen	group	weight (g)			
		0 day	7 day	14 day	28 day
1	11	309	319	310	313
2	9	302	300	304	305
3	11	329	313	309	306
4	9	296	287	300	314
5	11	304	296	303	305
6	9	356	343	341	328
7	11	257	266	284	263
8	9	304	298	293	296
9	11	299	317	322	307
10	9	316	314	329	338
11	11	342	336	340	335
12	9	294	285	310	309
13	11	327	330	347	328
14	9	327	340	335	331
15	9	308	303	304	296
16	11	303	300	299	305
17	11	289	305	310	301